THE UNIVERSITY OF CHICAGO

PROBING INDIVIDUAL AND COLLECTIVE MACROPHAGE RESPONSES WITH FLUIDIC FORCE MICROSCOPY

A DISSERTATION SUBMITTED TO
THE FACULTY OF THE DIVISION OF THE PHYSICAL SCIENCES
IN CANDIDACY FOR THE DEGREE OF
DOCTOR OF PHILOSOPHY

DEPARTMENT OF PHYSICS

BY
ELIZABETH J. MULDER

CHICAGO, ILLINOIS
JUNE 2023

To my grandparents: I wouldn't be where or who I am today without you.

TABLE OF CONTENTS

LIST OF FIGURES

LIST OF TABLES

ACKNOWLEDGMENTS

Thank you to all my friends, who have made the last six years so much better, especially Marybeth, Emily W., Pratiti, Sophia, Dan, Tracy, Lucas, Kaeli, Louis, Michael, Claire, Nina, and Emily S. I'm going to miss our regular brunches, game nights, and fun adventures around Chicago. To my family, especially my parents, who encouraged and supported me the whole way through, my cousins Bryan and Jessie, who gave me a place to stay when I was ill, and my sister, Gabi, for being my best friend and lifeline. To my lab-mates, who have made our lab such a kind and supportive place to work. My mentors, Dani, Brittany and Ethan, who taught me so much about being a scientist, and my mentees, Jenny and Sara, who taught me so much about being a mentor. To my advisor, Aaron, who has provided support, advice, patience, guidance, and literally life-saving masks, tests, and air purifiers. To my undergraduate advisor, Joyce, who has kept in touch with me all these years, and is always willing to listen. And to my cat, Ophelia, who makes sure I get up in the morning. Thank you all, I couldn't have done this without you.

Scientific contributions: Dr. Brittany Moser began the FluidFM project and both she and Jenny Delgado worked on developing the FluidFM method with me (chapter 2). Sara Hoggatt is working on the FluidFM single host-pathogen interactions project with me, and she collected the data shown in chapter 6. Samuel Weng and Allen Huff conducted the proteomics analysis shown in chapter 5.

ABSTRACT

Macrophages play a central role in the immune response by monitoring for signs of infection and then initiating a wider response. This immune response needs to be proportionate to the threat; both over-responding and under-responding are potentially dangerous to the body. The number of macrophages that activate, the degree and duration of their responses, and the types of signals they generate may all impact the downstream immune response. However, not all macrophages respond identically even to a uniform stimulus, and macrophages residing in tissues likely encounter localized and/or transient signals to which individual cells may respond differently depending on their context, history, cell state, etc. Within this complex environment, how do macrophages calibrate their individual and collective responses to correctly match their response to the threat? Answering this question is difficult with traditional experimental techniques that either treat an entire culture or isolate cells from their environment. Fluidic Force Microscopy (FluidFM) combines the precision control of Atomic Force Microscopy (AFM) with a pneumatic system capable of delivering picoliter volumes of liquid through a hollow AFM probe. FluidFM stimulation targets cells on their length-scale, allows simultaneous live cell monitoring, preserves environmental context, and gives the user precise control over the location, concentration, and duration of stimulation. Using the FluidFM, I determined the minimum conditions in concentration and time for activation of single macrophages via TLR stimulation, compared single, small group, and whole culture stimulation, and found a dependence on culture density in modulating the group response. I built a model to determine the stimulus gradients produced by FluidFM dispensing and how it related to the spatial limits of the macrophage group response. Lastly, I developed a method to investigate whole pathogen-macrophage interactions with the FluidFM, in order to determine the physical parameters that are necessary to generate an immune response. This research advances our knowledge of how macrophages, singly and collectively, modulate their responses to signs of infection and environmental factors. These regulation strategies

by early-responding cells are one piece of how the whole immune system regulates itself for safe and effective function.

Note: supplementary data and code files from this research can be found online at: DOI10.17632/mfyddz6n8k.1

CHAPTER 1

INTRODUCTION

1.1 Macrophages and the innate immune response

The immune system can be broadly divided into innate and adaptive immunity. The innate immune response targets non-specific markers of infection for a quick, initial response. The adaptive immune response takes longer to ramp up, but engages immunological memory to specifically target and eliminate a threat. Both pieces of the immune system are necessary to effective protection. Early-responding innate immune cells detect pathogen-associated molecular patterns (PAMPs) such as foreign genetic material, or proteins found on the surface of many bacteria. These PAMP signals activate families of receptors called Pattern Recognition Receptors (PRR). One category of PRRs is the Toll-like receptor (TLR) family. TLRs can be found on the outer membrane and endosomal membrane of immune cells, where they can detect PAMPs in their environment, on the surface of pathogens, and in endocytosed material. Activated TLRs cause the innate immune cells to initiate an immune response, by recruiting other immune cells, directly targeting pathogens, killing infected cells, or presenting antigen (pathogenic fragments) to the adaptive immune system for comparison with the adaptive immune memory. In this way, innate immune cells mediate the start of a large immune response to potential threats (Murphy et al. [2012]).

In my research I focused on one type of innate immune cell, macrophages. As one of the early-responding immune cells, macrophages play a key role in creating a proportionate immune response to any signal they detect. Macrophages can be found dispersed throughout the body's tissues. In each niche, these macrophages have adapted and integrated into their environment to perform diverse functions as well as monitor for threats. These macrophages are called tissue resident macrophages.

1.2 Tissue Resident Macrophages

The traditional understanding of resident macrophages is that they primarily keep their resident tissue free of threats and debris, such as pathogens, damaged or dying cells, or other debris that could cause inflammation, through phagocytosis. While this high phagocytic capacity is their defining characteristic, resident macrophages perform diverse functions related to tissue homeostasis and development. Blériot et al. [2020] suggest four categories of factors that influence macrophage identity and function: ontogeny (including intrinsic factors), features of the local environment (such as architecture, or secreted signals), inflammation status of individual macrophages, and time of residence in tissue. Many of these factors still need further investigation in order to untangle how they impact the diverse populations of tissue resident macrophages. But what is clear is that extrinsic factors are as impactful as intrinsic factors in determining macrophage responses to stimuli.

Resident macrophages communities are shaped to suit their environment and function within it. In turn, the resident tissue cooperates with macrophages to perform their immune functions. In the case of highly sessile (stationary) macrophage populations, this communication is essential. Westphalen et al. [2014] found that alveolar macrophages are largely immobile and communicate with epithelial cells to modulate immunity. Bissonnette et al. [2020] describes research wherein alveolar macrophages act in a regulatory manner by removing inhaled particles and apoptotic cells and decreasing overall inflammation in alveolar tissue. Alveolar macrophages communicate with lung epithelial cells in a variety of ways including physical junctions and secreted signals. In a different tissue context, Uderhardt et al. [2019] found that resident macrophages act to regulate inflammation when they cloak microlesions in stromal tissue to prevent neutrophils from doing excessive damage. All three of these examples describe macrophages cooperating with their host tissue to regulate inflammation.

Another key factor in resident macrophage function is their abundance in tissue. Rather

than being replaced by circulating monocytes from the blood, resident macrophages often establish their own populations in tissue from embryonic origins. These populations take on unique characteristics depending on their history and cooperation with the resident tissue cells. The degree to which the population continues to be replenished by blood monocytes varies between tissue sites, and with age and sex. The resident tissue regulates macrophage density via chemical signals that affect their growth and proliferation. Zhou et al. [2018] describe a two cell system *in vitro* by which fibroblasts regulate macrophage density via macrophage colony stimulating factor (CSF1) to maintain a 1:1 ratio of fibroblast and macrophage. One prominent hypothesis is that the availability of CSF1, which is necessary for resident macrophage survival and often present at low levels, acts as a limiting factor on macrophage density in the tissue. Dube et al. [2022] found that resident macrophage density in dermal tissue decreased with age in mice, impacting their ability to assist in wound healing. Thus environmental factors that impact macrophage density, and that density itself, are key to the functioning of the population as a whole.

1.3 Dynamic Signaling

Many cells signal and sense via complex dynamics depending on the temporal behavior of the stimulus and factors in the cellular environment. In particular, most traditional TLR-stimulation experiments mix the agonist into culture media and constantly stimulate the cells for hours. However, in biological context, macrophages may not see such strong, consistent signals. In particular, when looking for a threshold of activation, I needed to consider not just dose, but stimulation time. And I wanted to be able to separate stimulation time (how long the stimulus is applied) from activation time (how long it takes to see an NF$\varkappa$B response, particularly using stimulation times shorter than the activation time.

I only found one previous example in the literature of stimulating macrophages with brief signals. Ashall et al. [2009] showed that pulsed stimulation with TNF generates different

responses depending on the relative frequency of the TNF pulses and NFκB oscillatory response. Thus, when the stimulus is too frequent, the response is lower. macrophages have a recovery period for full response.

I found the concept of dynamic signaling to be useful when thinking about single cell responses to a time-varying stimulus. Purvis and Lahav [2013] describe the various ways information can be encoded in a signal: abundance, identity, modification, location, and how concentration varies with time. It is natural to consider first, when thinking about cell signaling, the type of ligand detected and its abundance. However, other temporal factors like the ligand concentration over time, as well as spatial factors such as the concentration gradient and spatial extent of stimulus, can provide information as well to the target cell. It makes sense that immune cells might incorporate information from multiple factors in determining their response, since they have an important role to play in maintaining the delicate balance of the immune system.

There is evidence that macrophages use dynamic signaling. Zhang et al. [2017] describe how NFκB dynamics encode TNFαdose of the stimulus. DeFelice et al. [2019] further explore how dose encoding arises from an autoregulatory loop in the NFκB circuit. Kellogg et al. [2017] found that macrophages have distinct temporal NFκB responses to distinct TLR agonists. when multiple TLR agonists are present, macrophages do not integrate the response to both, rather they pick one mode of response. this switch-like decision making depends on the timescale of the response to each TLR, individual cell variability, and cross-tolerance mediated by negative feedback. And Nelson and Nelson [2018] found that distinct NFκB response patterns have consequences by impacting gene expression. Thus, dynamic signaling on the part of the NFκB response enables the macorphage to discriminate between ligand type and dose in its response downstream of NFκB.

1.4 Heterogeneity in macrophage responses

Since macrophages have this role as pathogen-detectors, one would expect that they behave relatively consistently given the same stimulus. In bulk, this is true: a population of macrophages has a consistent, population-level response to a uniform stimulus. However, methods that stimulate cells uniformly and measure individual responses have found heterogeneity in single immune cell responses to TLR stimulation. Paszek et al. [2010] found that macrophage heterogeneity lead to population robustness by decreasing sensitivity to parameter perturbations, and decreasing fluctuations in paracrine signaling. By broadening the overall response, any one variation has a decreased impact on the average response. Hughey et al. [2014] similarly described a population invariance arising from single-cell heterogeneities. NF$\varkappa$B oscillations in a population vary cell to cell, and also with stimulus identity and concentration. Some features of the population response varied with stimulus, but the average NF$\varkappa$B oscillation period remained constant across all stimuli. Kalita et al. [2011] constructed a Bayesian model to identify sources of this cell to cell variability in NF$\varkappa$B responses. They found cell geometry, initial NF$\varkappa$B levels, and I$\varkappa$B translation and degradation rates together explained cell to cell differences in NF$\varkappa$B translocation. Thus intrinsic variations in a culture of macrophages leads to heterogeneous responses that overall preserve a consistent group response. But if individual macrophages respond so differently when stimulated together, how do they respond when faced with a signal on the single-cell scale, such as might happen when encountering single pathogens in a tissue context? Few experiments have probed immune cell responses with localized PRR stimulation instead of constant, uniform stimulation.

1.5 Established methods for studying single cell responses

Traditionally, single-cell biology has meant measuring single cell responses in a uniformly-stimulated group, but not necessarily stimulating just one cell, much less one cell in culture. The change from bulk measures of activity to single-cell measures allowed for distinguishing between binary single-cell responses and more gradual population-level changes. It also allows us to measure the large variability in single-cell responses. While this may seem like biological noise, information is encoded in the differences between single cell responses. Like the measuring of single cell responses allows us more insight into individual and population level behavior, single cell stimulation allows us to distinguish between responses that are specific to one cell, and the influence of environmental factors. In order to stimulate just one cell, it is easier to isolate the cell, than to sufficiently localize the stimulus down to a single-cell level. However, isolation loses contextual information from the cell environment, and the disturbance might perturb its state.

We wanted to study single cells within their environmental context. We turned to techniques employed in neurobiology (such as the stimulation of single neurons in a network) for options. Technologies including optogenetics, photocaged molecules, and specialized micropipettes have been used to stimulate individual cells Using optogenetics would allow for light-activated stimulation of TLR receptors directly. Photocaged ligands likewise are light-activated, but would diffuse away from the target cell. Specialized micropipettes used techniques such as hydrodynamically-confined flow to focus chemical stimulation on one area, and allowed for longer stimulation times and more control over the concentration gradient.

Isolating single cells is the most straightforward way of limiting any stimulation ot just one cell. Zhang et al. [2019] use a microfluidic setup that isolates single cells into individual chambers for high-throughput measurements of single-cell readouts. There are advantages to this system, such as the fine control over single-cell conditions and large-scale live-cell readout. However, isolating the macrophages in this way from their culture environment

limits observations of environmental factors and cell to cell communication.

Since we wanted to study not just single cell stimulation in isolation, but single-cell stimulation in the culture environment, my lab has previously explored using photo-caged molecules to locally target TLR stimulation on the single cell level *in vitro* and *in vivo* Ryu et al. [2014, 2017], Stutts and Esser-Kahn [2015]. While we found success with these techniques, immune cell PRR activation requires stimulation from minutes to hours, so we needed a method that can provide sustained stimulation at one precise location. Li et al. [2015].

For sustained stimulation, micropipette systems are a good option. Page et al. [2017] describe a combined stimulation and sensing micropipette system, called "self-referencing scanning ion conductance microscopy - scanning electrochemical microscopy." The probe has two openings, one for dispensing a chemical stimulus, and one for detection of molecules in the local environment. Ainla et al. [2012] review several microfluidic techniques that use hydrodynamically confined flow. These techniques use the physics of fluid flow on small scales to localize a chemical stimulus and prevent mixing and diffusion. The technique we decided to use (Fluidic Force Microscopy) builds upon these micropipette techniques by combining them with the precision control of an AFM (atomic force microscope) system Meister et al. [2009], Guillaume-Gentil et al. [2014]. FluidFM has been used in a variety of contexts to dispense chemical stimuli or whole pathogens Aebersold et al. [2018], Stiefel et al. [2012]. The techniques I used in my thesis build upon this research. In the next chapter I will elaborate on the development of the FluidFM methodology for this work.

CHAPTER 2

TARGETED IMMUNE CELL STIMULATION IN CULTURE WITH FLUIDFM: METHOD DEVELOPMENT

Fluidic Force Microscopy (FluidFM) builds upon micropipette techniques with the addition of an AFM-based controller, that holds and positions the micropipette probe with micrometer precision to ensure accurate levels of agonist are delivered (Meister et al. [2009]). FluidFM technology has been used to measure individual cell responses to local chemical stimulation (Aebersold et al. [2018], Lee et al. [2009]). It allows for sub-millimeter scale perturbations in a cell's environment while preserving the rest of its environmental context, allows for monitoring over the length and timescales relevant to macrophage activation, and gives the user precise control over the location, concentration, and duration of stimulation.

In applying this FluidFM technology to study single immune cell responses, we chose macrophages as a model system. Macrophages play a key role in the early immune response to infection or vaccination by releasing chemical signals to initiate an inflammatory immune response in response to TLR stimulation. Uniform TLR stimulation of macrophages has revealed significant heterogeneity in single immune cell responses (Paszek et al. [2010], Hughey et al. [2014], Lee et al. [2009], Xue et al. [2015]), suggesting the importance of studying individual macrophage stimulation. Macrophages are well suited for use with FluidFM technology: they are adherent, they respond to a soluble ligand dispensed by the FluidFM at low pressures, and the timescales of NF-$\varkappa$B activation and response readily provide clear measurements via fluorescent microscopy of multiple cells ¬allowing for sufficient data-sets for statistical analysis. Using this unique tool and set of experimental conditions, we sought to understand how individual macrophages respond to a local stimulus while surrounded by unstimulated cells. By comparing these values, we report on a role for cell density in determining how individual macrophages mediate a group response.

2.1 Quantitative readout for individual macrophage activation

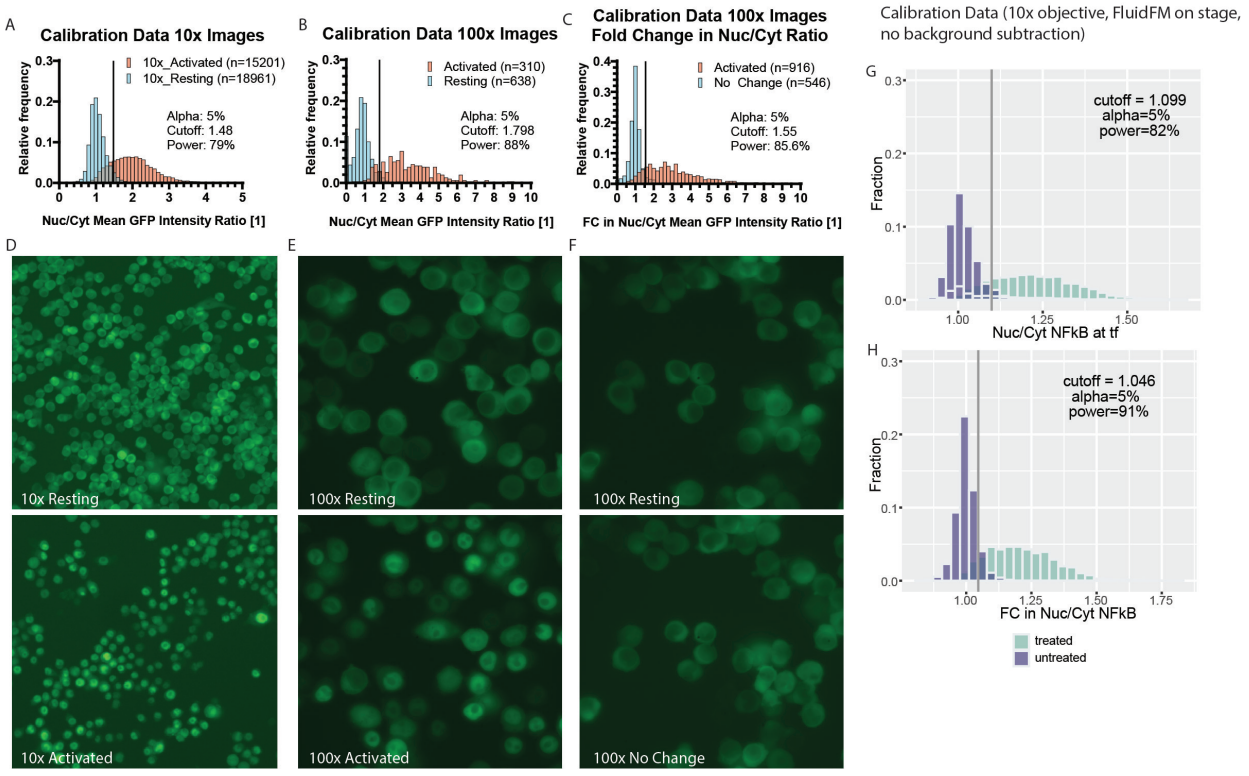

Figure 2.1: Calibration data used to determine activation cutoffs for 10x images of cells (group activation data), and 100x images of cells (single cell targeting data). (A-C, G-H) Histograms of resting and activated populations with activation cutoff shown, annotated with cutoff value "cutoff", percent negative population above cutoff "alpha", and percent positive population above cutoff "power." (D-E) Representative images of calibration data using NFκB reporter cells. (D) 10x images of resting (top) and activated (bottom) cells. (E) 100x images of activated cells before (top) and after (bottom) stimulation. (F) 100x images of resting cells at the start (top) and end (bottom) of a 15-minute incubation.

For our activation readout we used fluorescent NFκB reporter cells gifted to us by the Frasier Lab (Li et al. [2015]). These cells produce GFP-tagged NFκB, which allows us to see the translocation of NFκB from the cytoplasm to the nucleus upon activation of the macrophage. In this way we can measure single-cell activation readouts in the culture.

In order to categorize individual cells as activated or unactivated, we needed a cutoff value for the quantified microscopy data. Since changes to the experimental setup (objec-

tive magnification, presence/absence of the FluidFM controller in the light-path, CellProfiler pipeline parameters) affect the raw intensity values, we needed a cutoff value for each experiment and quantitative parameter used. We imaged resting and highly activated cells under the range of imaging conditions used in the experiments and then quantified these images using the same pipeline as for the corresponding experiment data (Figure 2.1). After quantification, cutoffs were determined to be where 95% of resting cells were below the line and the power of the test is the number of activated cells above the cutoff. Histograms with the cutoff were made in Prism and R. The code for quantification and analysis can be found in appendices D.2 and D.3, respectively.

2.2 FluidFM-compatible culturing conditions

The FluidFM experiments require use of an open cell dish so the probe can be lowered into the cells. We used CO_2 Independent Medium which allows the cells to maintain the proper pH under atmospheric CO_2 conditions. To check that the cells still activated normally when plated in CO_2 Independent Media and incubated at 37°C and atmospheric CO_2 on the microscope, RAW Blue SEAP NFκB reporter cells were plated in 50 mm microscope dishes as for a FluidFM experiment and the next day the media was changed to either DMEM + 10% HIFBS, DMEM + 10% HIFBS + 10 mM HEPES, or CO_2 Independent Media + 10% HIFBS. Half of the dishes in each group were treated with 1 ug/mL R848. Half the dishes with DMEM+HIFBS were placed in the incubator, and all the others were incubated on the microscope (Figure 2.2). Supernatant was taken at 5 hr (about how long a dish would be sitting under those conditions during a FluidFM experiment) and at 20 hr (the recommended time for incubating RAW Blue cells for an assay) and incubated with QUANTI-Blue reagent for colorometric readout of NFκB activity (absorbance at 620 nm). The results showed that the cells in CO_2 Independent Medium activated about the same as those in the incubator (the positive control). The 10 mM HEPES, while often used to

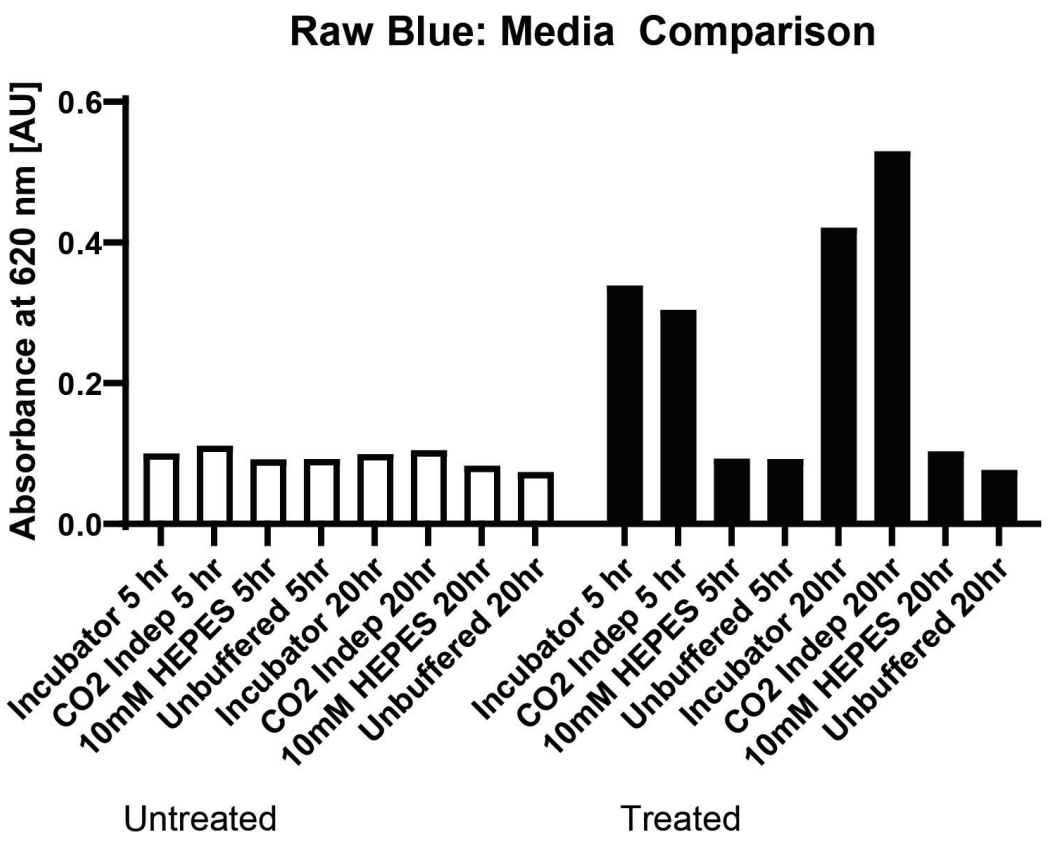

Name	Media	Incubation Conditions	Incubation Time	Result
Incubator 5 hr	DMEM + 10% FBS	5% CO_2 and 37°C	5 hr.	Activated
CO2 Indep. 5 hr	CO2 independent medium + 10% FBS	Atmospheric CO_2 and 37°C	5 hr.	Activated
10 mM HEPES 5 hr	DMEM + 10% FBS + 10 mM HEPES	Atmospheric CO_2 and 37°C	5 hr.	Unactivated
Unbuffered 5 hr	DMEM + 10% FBS	Atmospheric CO_2 and 37°C	5 hr.	Unactivated
Incubator 20 hr	DMEM + 10% FBS	5% CO_2 and 37°C	20 hr.	Activated
CO2 Indep. 20 hr	CO2 independent medium + 10% FBS	Atmospheric CO_2 and 37°C	20 hr.	Activated
10 mM HEPES 20 hr	DMEM + 10% FBS + 10 mM HEPES	Atmospheric CO_2 and 37°C	20 hr.	Unactivated
Unbuffered 20 hr	DMEM + 10% FBS	Atmospheric CO_2 and 37°C	20 hr.	Unactivated
Untreated	--	--	--	Unactivated

Figure 2.2: RAW Blue Assay with RAW Blue NF$\varkappa$B reporter cells, plated in 50 mm microscope dishes and treated with 1 ug/mL R848 for the indicated times. Treatment groups are shown in the table. Each bar is the average of the two replicates.

buffer cells for experiments outside the incubator, did not work well under the experimental conditions needed for FluidFM experiments. The unbuffered cells (negative control) showed similarly low levels of activation, matching the untreated cells.

2.3 FluidFM dispensing characterization

Determination of the concentration of agonist dispensed by the FluidFM The small molecule fluorophore AF488 was dispensed (Figure 2.3A) and its diffusion compared to theoretical prediction from a point source model (described below). I dispensed AF488 under the same conditions as I would the agonist R848 for both single-cell targeting and group stimulation. I imaged the resulting cloud of fluorescent fluorophore at 30 sec intervals for 20 minutes, ending dispensing and removing the probe from the field of view at 15 minutes. In this way I was able to capture the growth and decay of the concentration gradient, as well as its size and shape. I wrote two ImageJ macros to extract the time-behavior of the cloud as well as the intensity vs distance from the dispensing point profile (Appendix D).

To determine concentration of the dispensed fluorophore, reference slides containing 1µL AF488 at varying concentrations, pressed between coverslips with or without a coverslip spacer, were imaged under the same conditions as the dispensing experiment (Figure 2.3B). The area of the spots was measured in ImageJ, and the thickness calculated by dividing the volume by the area. Modal intensity of these reference images, when plotted against the concentration and thickness of the layer of fluorophore imaged, allowed for the calculation of a conversion factor between image brightness and the total amount of fluorophore (Figure 2.3C). We used this conversion factor to plot the predicted intensity profile from the diffusion model, for comparison with the AF488 data (Figure 2.3E). After fitting the model to the data (see below), the diffusion coefficient of AF488 was replaced with that of R848 in order to estimate the relative concentration of R848 dispensed under the same conditions (dispensing over-pressure and probe height) (Figure 2.3H). Both diffusion coefficients were estimated

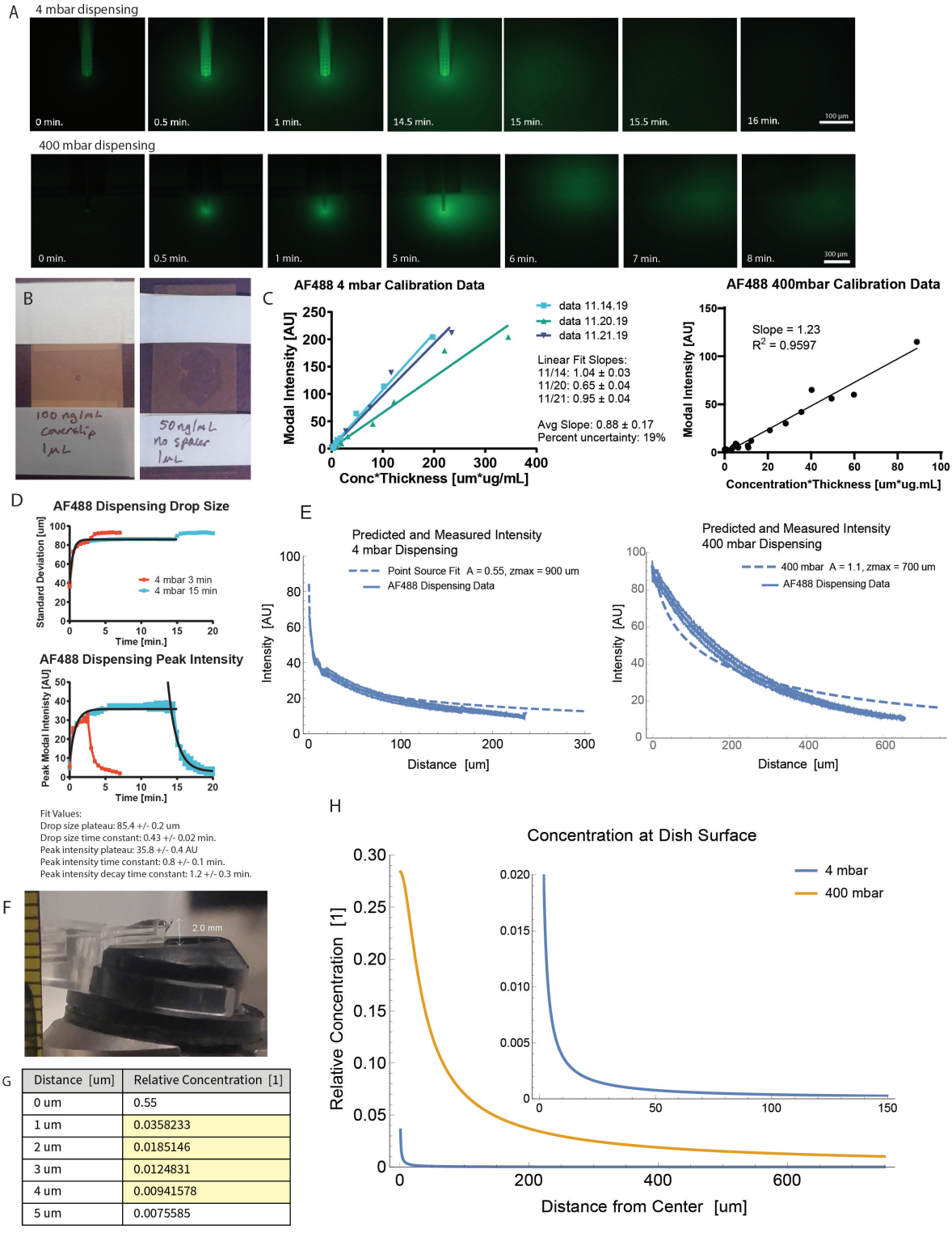

Distance [um]	Relative Concentration [1]
0 um	0.55
1 um	0.0358233
2 um	0.0185146
3 um	0.0124831
4 um	0.00941578
5 um	0.0075585

Figure 2.3: (A) AlexaFluor488 dispensed into water at (top) 4 mbar overpressure (continued)

Figure 2.3: for 15 minutes at 4 microns height or (bottom) 400 mbar overpressure for 5 minutes at 20 microns height. Timepoints relative to start of dispensing, scale bars 100 (top) and 300 (bottom) microns. (B) Reference slides of AF488 solution, compressed between coverslips to create layers of varying concentration and thickness. (C) Modal intensity of the drops in (B), plotted against the product of AF488 concentration and drop thickness, for converting between AF488 concentration and fluorescent intensity. Slides measured under the same imaging conditions as for 4 mbar dispensing (left) and 400 mbar dispensing (right). (D) Peak brightness and standard deviation of AF488 cloud from (A) measured in ImageJ and plotted over time. Exponential curve fits in GraphPad Prism to both parts of the curve give time constants for the rise to equilibrium and decay back to zero. (E) Comparison of predicted (dashed line) and measured (points with error bars) intensity of dispensed fluorophore gradient at equilibrium as a function of distance from the dispensing point. (F) Measurement of the distance between the probe and the window of the probe holder, maximum for the fit parameter "zmax" (see below) (G) Predicted concentration (relative to C_0) for 4 mbar dispensing at 0 – 5 microns from the dispensing point in 3D space. (H) R848 concentration (relative to C_0) at the dish surface versus distance from the center (directly underneath the dispensing point) calculated from the diffusion model for each dispensing condition (4 mbar at 4 µm height and 400 mbar at 20 µm height).

with the SEGWE calculator using the molecular weight of the molecules and the preset values for water at room temperature (for AF488) or 37°C (for R848).

Definitions:

C_0 is the concentration loaded into the probe

V is the dispensing rate in volume/time

D is the diffusion coefficient of the dispensed molecule

k is the conversion factor from integrated concentration to brightness

r is distance from the dispensing point in 3D space

ρ is distance from the dispensing point location in the XY plane

Derive an expression for $C(r)$ from the differential equation of a point source:

Differential equation for steady state diffusion from a constant source:

$$D\nabla^2 C + s = 0 \tag{2.1}$$

A point source at $\vec{r} = 0$ dispensing at a constant rate of mass per time:

$$s = \dot{M}\delta(\vec{r}); \quad \dot{M} = C_0 V \tag{2.2}$$

Differential equation for the point source:

$$D\nabla^2 C + C_0 V \delta(\vec{r}) = 0 \tag{2.3}$$

Solution to the differential equation:

$$C(r) = \frac{C_0 V}{4\pi D r} \tag{2.4}$$

Apply boundary conditions:

Add parameter R to prevent C from going to infinity at $r = 0$:

$$C(r) = \frac{C_0 V}{4\pi D(r + R)} \tag{2.5}$$

Apply the boundary condition $C = C_0$ at $r = 0$ to solve for R:

$$C(0) = C_0 = \frac{C_0}{4\pi D(0 + R)} \Rightarrow R = \frac{V}{4\pi D} \tag{2.6}$$

Final expression for $C(r)$:

$$C(r) = \frac{C_0}{1 + \frac{4\pi D}{V} r} \tag{2.7}$$

Convert to intensity:

$$I(\rho) = \int_{-\infty}^{\infty} k \cdot C(\rho^2 + z^2) dz \tag{2.8}$$

This integral does not converge; can only solve computationally. In order to solve the integral, limits of integration were chosen that match the physical dimensions of the apparatus: the dispensing point was 4 µm above the surface of the coverslip, and the distance from the dispensing point to the top of the water drop (where it contacted the FluidFM instrument) was measured to be 2 mm as shown in (F). So the intensity was predicted computationally as follows:

$$I(\rho) = \int_0^h k \cdot C(\rho^2 + z^2) dz + \int_0^{zmax} k \cdot C(\rho^2 + z^2) dz \tag{2.9}$$

Where h is the height of the probe above the surface of the slide (4 µm in this case) and

$zmax$ is a fit parameter describing the height of the dispensed "cloud" of AF488. The value of $zmax$ is constrained by the height of the water drop (F), and assuming spherical symmetry should be about the same as the radius of the cloud in the x-y plane. The best value fit for $zmax$ (900 µm for 4 mbar dispensing of AF488, and 700 µm for 400 mbar dispensing) is within those parameters.

The point source prediction for $C(r)$, including an overall fit parameter A, is:

$$C(r) = \frac{A \cdot C_0}{1 + \frac{4\pi D}{V} r} \tag{2.10}$$

The parameters $zmax$ and A were fit by minimizing chi-squared for the difference between the dispensing data between 0 and 100 µm distance from the dispensing point and the predicted value for those same points. (In the single cell targeting experiments most cells are within 100 µm of the dispensing point. Including larger distances weighted the distribution too heavily towards the tail, rather than the center where accuracy is most important in order to compute the concentration at the target cell location).

Method (in Mathematica) (more details in Appendix D.1.2):

1. Generate predicted $I(\rho)$ curve for each pair of A and $zmax$ values for $\rho = 0$ to 100 μm
2. Compute χ^2 distance between AF488 dispensing data and the predicted curves
3. Find pair of parameters that have the smallest χ^2 value

Results:

- Best values for 4 mbar dispensing at 4 µm height: $A = 0.55, zmax = 900\mu m$
- Best values for 400 mbar dispensing at 20 µm height: $A = 1.1, zmax = 700\mu m$

Dilution Factor: the "dilution factor" determines the ratio between C_{max}, the concentration at the dish surface below the dispensing point (the target cell position, in single cell targeting experiments), and C_0, the concentration of agonist loaded into the probe.

For group targeting (400 mbar dispensing at 20 µm height), after fitting, the dilution factor was determined to be 0.28.

For single cell targeting (4 mbar dispensing at 4 µm height), the distance between the probe opening and the target cell surface varied due to variation in cell height. This introduced additional uncertainty into the calculation of concentration at the target cell surface. We calculated R848 concentrations from the best fit 4 mbar model for distances 0 to 5 µm from the dispensing point (probe opening).

In the single cell targeting condition, the target cell surface is estimated to be 1-4 µm from the probe opening. The relative concentration of agonist for those distances is shown in the table (highlighted portion). Accounting for this uncertainty, the dilution factor (the relative concentration of agonist at the target cell position compared to the concentration loaded into the probe, C_0) was estimated to be 0.02 ± 0.01. This number was used to estimate R848 concentration for the FluidFM single cell targeting experiments.

2.4 FluidFM protocol overview

Fluidic Force Microscopy allows for the stimulation and monitoring of single cells and small groups of cells in culture

We delivered agonist (Resiquimod, or R848) directly onto target cells in pico-liter volumes using the FluidFM. This technology allowed us to stimulate a single cell within a larger microenvironment composed of unstimulated cells (Figure 2.4). We monitored the cells throughout with live cell fluorescence microscopy.

To assess the macrophage immune response, we employed a commonly used measure of macrophage activation – nuclear translocation of transcription factor NF-κB. In the resting state, NF-κB resides in the cytoplasm, and translocates to the nucleus after TLR activation1. Using the FluidFM (Meister et al. [2009], Aebersold et al. [2018], Dorig et al. [2013], Guillaume-Gentil et al. [2014]), we treated individual RAW264.7 macrophage NF-κB re-

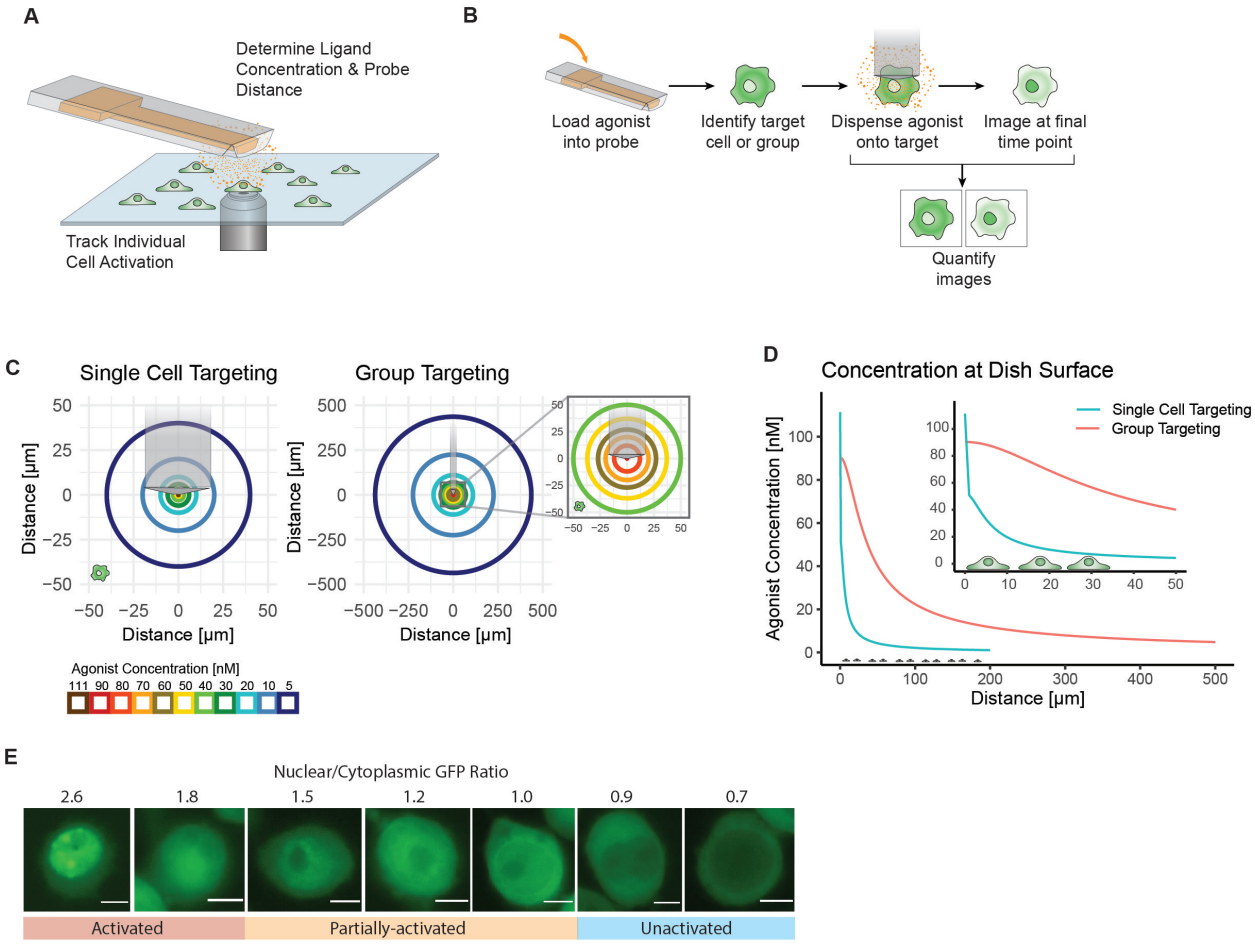

Figure 2.4: (A) Schematic of FluidFM experiment showing probe, cells, and microscope objective. (B) FluidFM experimental workflow (C-D) Single cell and group targeting modes in FluidFM dispensing. Schematic of concentration vs distance shown from an overhead view (C) and side view (D) for the condition where C_{max} is closest to 100 nM for each mode (C_0 = 5.5 μM for single cell targeting and 0.318 μM for group targeting). Cartoon cells shown for scale. (E) Quantified cell images: NF-κB fluorescence, scale bar 5 μm, activation numerical cutoff from calibration data of resting and activated cells under same imaging conditions (Figure 2.1); exact numerical values vary depending on the imaging conditions of the experiment – these values match those used in the single cell targeting experiments (Figures 3.1, 3.3).

porter cells (Li et al. [2015]) in culture with a localized stimulus and monitored the NF-κB response by tracking the translocation of the GFP reporter.

Having established methods for treating and monitoring single cells in culture, we then determined stimulation conditions. Several variables were considered in the design of this study, including cell density, agonist type, agonist concentration, stimulation time, and time at image collection. To simulate physiological macrophage densities, we plated macrophages within the range estimated for tissue-resident macrophages: 500-1000 cells/mm^2, estimated from Li, Germain, and Gerner 2019 (Li et al. [2019]). We also plated macrophages at more confluent densities for comparison (Figure 2.5A,B). For the agonist we selected the TLR7/8 agonist R848 for three reasons. First, R848 dispenses well out of the FluidFM probe without aggregating or clogging. Second, as a small molecule its diffusion could be mathematically modeled for an accurate concentration gradient. Finally, it consistently elicited measurable NF-κB activation in as little as 15 minutes, allowing for rapid collection of single-cell datasets.

Having established a minimum response time (15 min), we then tested shorter stimulation times until we established a minimum stimulation time (3-5 min). We also assayed FluidFM dispensing conditions (flow rate and height) and established two dispensing modes: single cell targeting, and group targeting. We dispensed R848 with stimulation times of 3, 5, and 15 minutes in these two stimulation modes. For single cell activation without making physical contact, we dispensed ligand at a minimal flow rate a few microns above the target cell surface. The ligand then diffused rapidly in the area surrounding the target cell. For group activation, we dispensed ligand at an increased height and flow rate to cover a wider area with a more uniform concentration (Figures 2.4C-D and 2.3).

The concentration of R848 loaded into the probe (C_0) and the position and dispensing rate of the probe together determine the concentration gradient of agonist at the dish surface (Figure 2.4C-D and Figure 2.3H). C_{max} denotes the concentration at the center of the gradient, right below the dispensing point. The concentration of agonist at the position of each

cell is a function of C_0, the dispensing conditions, and the diffusion of the agonist into the surrounding media over time. Diffusion modeling with AlexaFluor488 determined 3 minutes (about three time-constants) to be the minimum time needed for the concentration distribution to reach equilibrium - shorter dispensing times were not used in these experiments (Figure 2.3D).

Lastly, we needed to convert our microscopy images into quantified data for analysis. In each experiment, we imaged the reporter macrophage fluorescence to quantify the NF-κB activation state of each cell before and after stimulation (Figure 2.4B,E, 2.1D-F). We stimulated cells for three or five minutes and imaged before stimulation, at the start of stimulation (time 0), and at 15 minutes after that time. For 15-minute stimulation, the cells were imaged before stimulation, at the start of stimulation, and at 15 and 30 minutes. These time-points reliably captured the response of the target macrophages. We then categorized the single cell responses with calibration data to establish a quantitative activation cutoff and determine the fraction activated for each set of experimental parameters (Figure 2.4E, 2.1A-C,G-H, appendix D.3). A detailed protocol for stimulation with the FluidFM can be found in appendix B.

2.5 Integrating agonist concentration, culture density, and macrophage location and response for analysis

With such multifaceted data, varying sample sizes, and naturally noisy data, it was a challenge to find a clear way to present it. The first challenge was calculating activation in a way that separated natural variance in degree of response from uncertainty in the frequency of response. For this reason I developed the "fraction activated" method and used bootstrap analyses to calculate the uncertainty (see appendix D.4.1 item 4). Secondly, I took inspiration from Aebersold et al. [2018] in designing the plots to display the FluidFM Group Stimulation data in a way that could represent the spatial distribution of both the stimulus

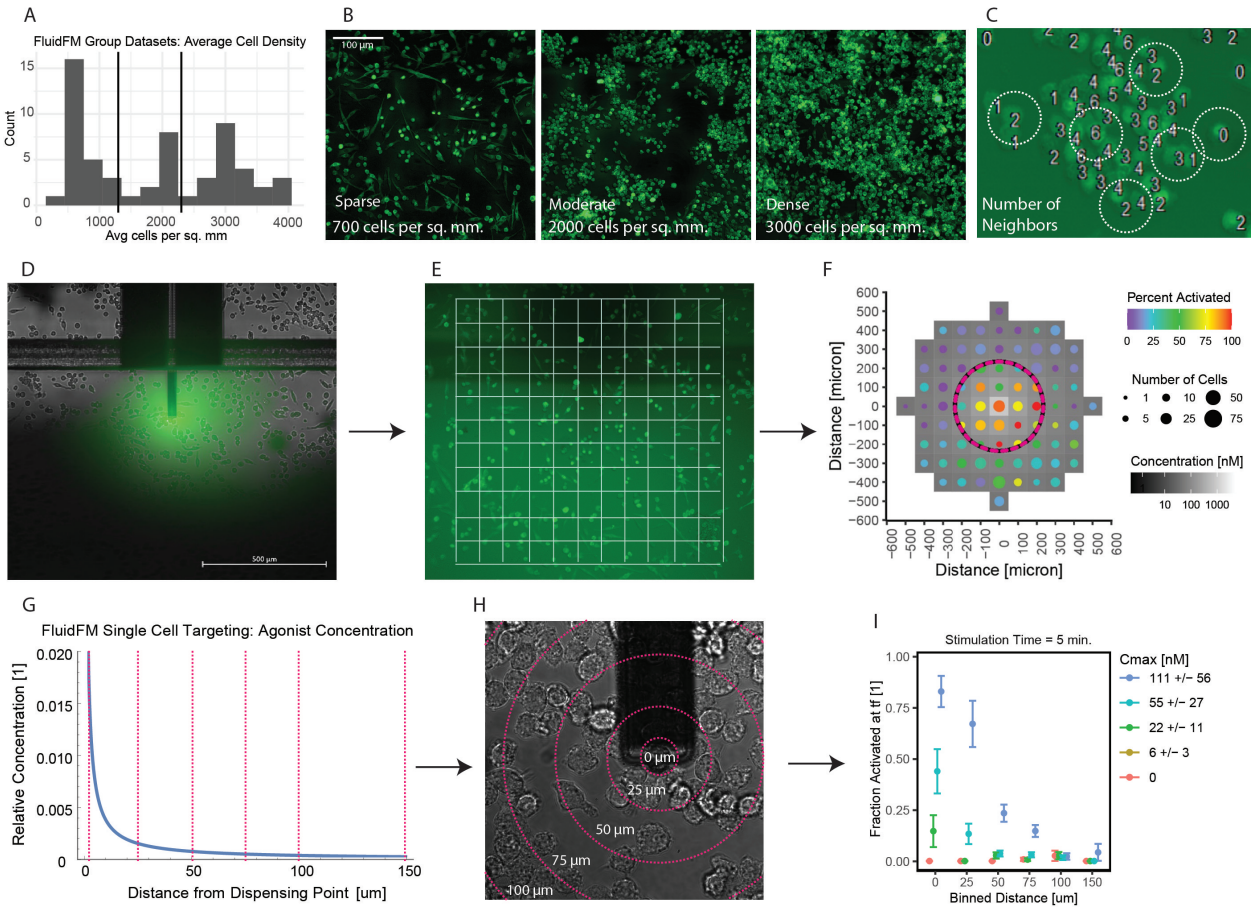

Figure 2.5: (A) histogram of culture densities for FluidFM datasets. Vertical lines divide sparse, moderate, and dense categories at 1300 and 2300 cells per sq. mm. (B) representative images per density in (A), GFP fluorescence of NF$\varkappa$B reporter macrophages, 10x magnification. (C) Number of neighbors counting method. Cells are labeled with their number of neighbors. Circles show 18 µm radius where neighbors were counted. (D-F) Analysis method for FluidFM group stimulation. (D) Overlay of AF488 dispensing image on FluidFM group stimulation image (not same experiment!). (E) overlay of grid onto GFP cell image for grouping cells into bins by location. (F) Final dataset, showing binned cell responses and agonist concentration at that location. (G-I) Analysis method for FluidFM single cell stimulation data. (G) FluidFM single cell stimulation concentration gradient, with vertical lines showing distance bins. (H) Same distance bins overlaid on single-cell stimulation image (bright-field, 100x magnification). (I) Example of final dataset, showing binned cell responses at each distance, grouped by stimulation condition.

and response, as well as other factors like culture density. An overview of these methods is shown in figure 2.5. More details about the analysis can be found in appendix D.4.

CHAPTER 3

DETERMINATION OF THE SINGLE MACROPHAGE ACTIVATION THRESHOLD FOR R848

Although the NF-$\varkappa$B activation of macrophages in culture and in isolation has been studied, the situation of targeted activation of one or a few cells in culture remained elusive. Our initial goal was to determine the concentration of ligand needed to activate a single macrophage in culture using TLR7/8 as a model agonist - a threshold of activation. But first we needed to show that the FluidFM could localize the agonist signal sufficiently to target a single macrophage in culture, as indicated by our theoretical diffusion model. Then, we could modulate the agonist concentration and stimulation time to get our dose curve and find the threshold.

3.1 Single-cell stimulation with Fluidic Force Microscopy

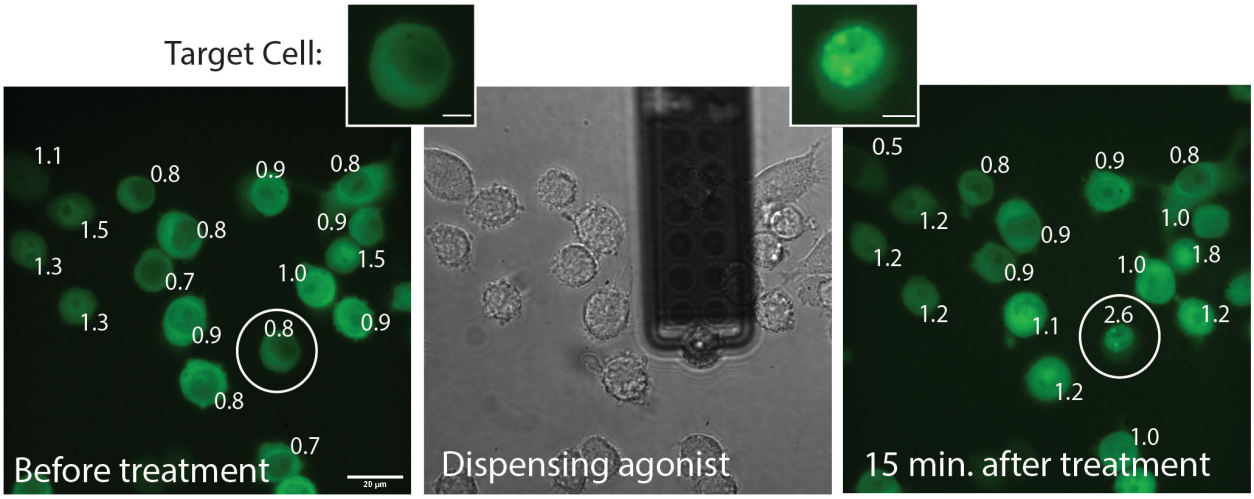

Figure 3.1: Example of FluidFM experiment targeting a single cell. Left to right: GFP fluorescence before dispensing, brightfield image during dispensing, GFP fluorescence 15 min. after dispensing. Target cell circled, numbers are Nuclear/Cytoplasmic GFP ratio. Scale bar 20 µm. Inset: target cell before, after stimulation, scale bar 5 µm.

Proof of concept experiment targeting a single macrophage in culture (figure 3.1). We

used the FluidFM in single-cell targeting mode (figure 2.4) to target a single macrophage in culture. You can see the target cell has higher NF-$\varkappa$B translocation to the nucleus than its neighbors. Due to rapid diffusion of the small-molecule agonist, we could not completely prevent off-target activation of neighboring cells.

We repeated this experiment with concentrations of R848 from 6 to 500 nM at the target cell position, in order to determine the single-cell activation threshold (figure 3.3). But before we could interpret these results, we needed to know how they compared to the more conventional experiment of mixing the agonist into the culture media and stimulating the entire culture uniformly. This turned out to be more difficult that expected, because we needed to remove the agonist after a short stimulation with minimal disturbance of the macrophages.

3.2 Macrophage whole culture stimulation at short timescales

We designed a short-timescale-stimulation version of a conventional dose curve to measure NF-$\varkappa$B activity. In contrast to a conventional dose curve, the short-timescale stimulation necessitated removing the agonist from the media before the end of the experiment. Preliminary results had indicated that disturbance of the cell media environment from an hour before treatment on-wards caused a decrease in the NF-$\varkappa$B response (Figure 3.2B,C). Thus, we needed a way to remove the agonist with minimal disturbance of the cells. We tested various methods of adding and removing the agonist. We selected the method that had the highest NF-$\varkappa$B response at the shortest stimulation times: serial dilution with warm media (Figure 3.2C).

Group Activation Assay Method Development

The general protocol for group activation in chambered slides is to first change the cell media to fresh media with 10% HIFBS, let incubate 1 hr., then add the agonist either by diluting 1:10 in the equilibrated media, or replacing the well contents with warmed, treated

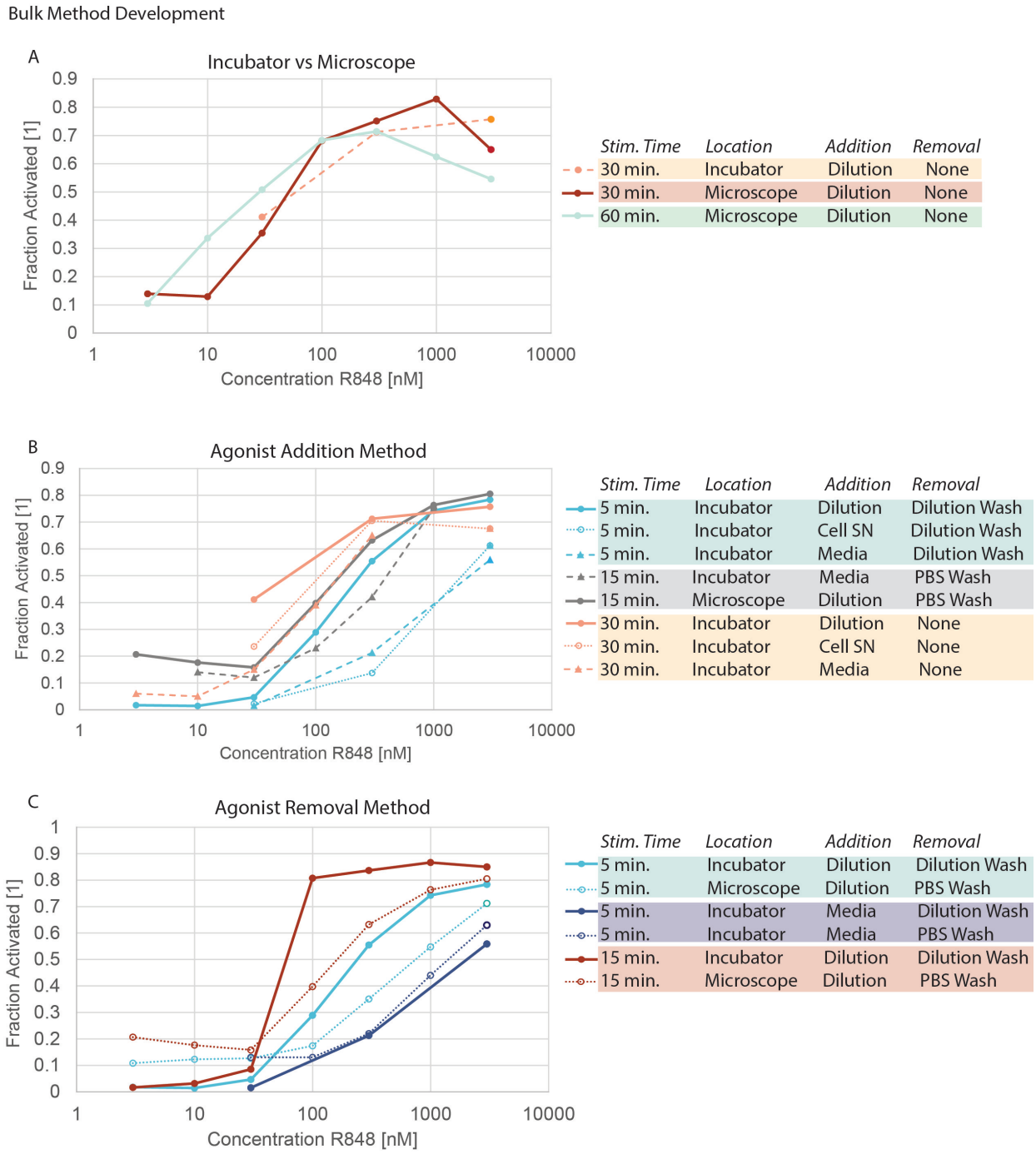

Figure 3.2: Method development for whole culture stimulation of macrophages. Dose curves of concentration R848 vs fraction activated in well, colored by experiment group. Varied assay parameters of (A) incubation location, (B) agonist addition method, and (C) agonist removal method. Details below. Fraction activated calculated from calibration data (Figure 2.1A)

media or cell supernatant. The cells incubate for the given stimulation time, then if the stimulation time was less than 30 min, the agonist is removed by either washing the wells with warm PBS and replacing with warm, untreated media, or by serial dilution (dilute well contents 1:6 with warm, untreated media, repeat 3 times). The cells are fixed at 30 minutes (or 60 minutes for the ts = 60 dataset), and then imaged for GFP fluorescence using the 10x objective. The data is then quantified and the fraction of cells activated calculated according to the calibration data cutoff of 1.48 Nuc/Cyt NFκB ratio (Figure 2.1A).

This experiment could be done either using CO_2-Independent Medium with 2% L-glutamine and 10% HIFBS and the cells incubated on the live cell microscope at 37C and atmospheric CO_2 (solid lines Figure S4F) or using DMEM with 10% HIFBS and the cells incubated in the cell incubator at 37C and 5% CO_2 (dotted line Figure 3.2A). The two methods gave similar results. The experiments could be done more quickly and in parallel using the biological safety cabinets and cell incubator, so that method was chosen.

Next, three methods of agonist addition were tested: dilution of 10x agonist dilutions in fresh media into the equilibrated cell media (solid lines Figure 3.2B), replacing well contents with prepared agonist dilutions in conditioned cell supernatant from untreated, equilibrated cells (dotted lines Figure 3.2B), and replacing well contents with prepared agonist dilutions in fresh media (dashed lines Figure 3.2B). All agonist dilutions were warmed in the incubator before addition to the cells. The results show that for all stimulation times (indicated by line color), the dilution method (solid lines) gave higher activation than either replacement with treated media (dashed lines) or replacement with treated cell supernatant (dotted lines). The difference was most apparent for the shortest stimulation time (5 minutes, blue, Figure 3.2B). Therefore, dilution was chosen as the method for adding agonist.

Lastly, for conditions where the stimulation time was less than 30 minutes (the experiment endpoint), the agonist needed to be removed from the cells and allow them to incubate further in untreated media. Two agonist removal methods were tested: PBS wash (removing well

contents, washing twice with warm PBS, then replacing with warm, untreated media; dotted lines Figure 3.2C) and dilution wash (dilute well contents 1:6 – remove 250 of 300 uL well contents, add 250 uL fresh media, repeat 3x; solid lines Figure 3.2C). For both the 5 and 15 minute stimulation times, when agonist had been added by dilution, removing the agonist by dilution also yielded higher activation than removing the agonist by PBS wash. In the case where the agonist had been added by replacing well contents with treated media – "media" method – there was no difference between agonist removal methods. The dilution method of removing agonist was chosen for future experiments.

Conclusions: Activation is highest when the agonist is added by dilution into equilibrated media and removed by serial dilutions with fresh media. Methods which disturb the local media environment by removing well contents entirely to either add or remove agonist, yield lower activation than the dilution methods which are less disruptive. This effect is most apparent at short stimulation times.

3.3 Single cells activate with a lower concentration stimulus than a culture of the same cells

With a system for single cell activation at the ready, we tested both the concentration and temporal limits of single cell sensitivity with the FluidFM. Single cell targeting with FluidFM reliably activated single cells in culture. We tested concentrations from 6 to 500 nM for 3, 5, and 15 min stimulation and analyzed the response of the target and surrounding cells (Figure 3.3A). The response is highest for the target cell and decreases with increasing distance from the target. The target cell is highly activated, cells immediately adjacent have modest activation, and other cells further away show little change above background (3.3A). We determined concentration of the agonist at the target cell position using the diffusion model, (Figure 2.3E) resulting in a target cell dose curve (Figure 3.3C).

These results demonstrate that stimulation with R848 at a concentration of 100 nM for

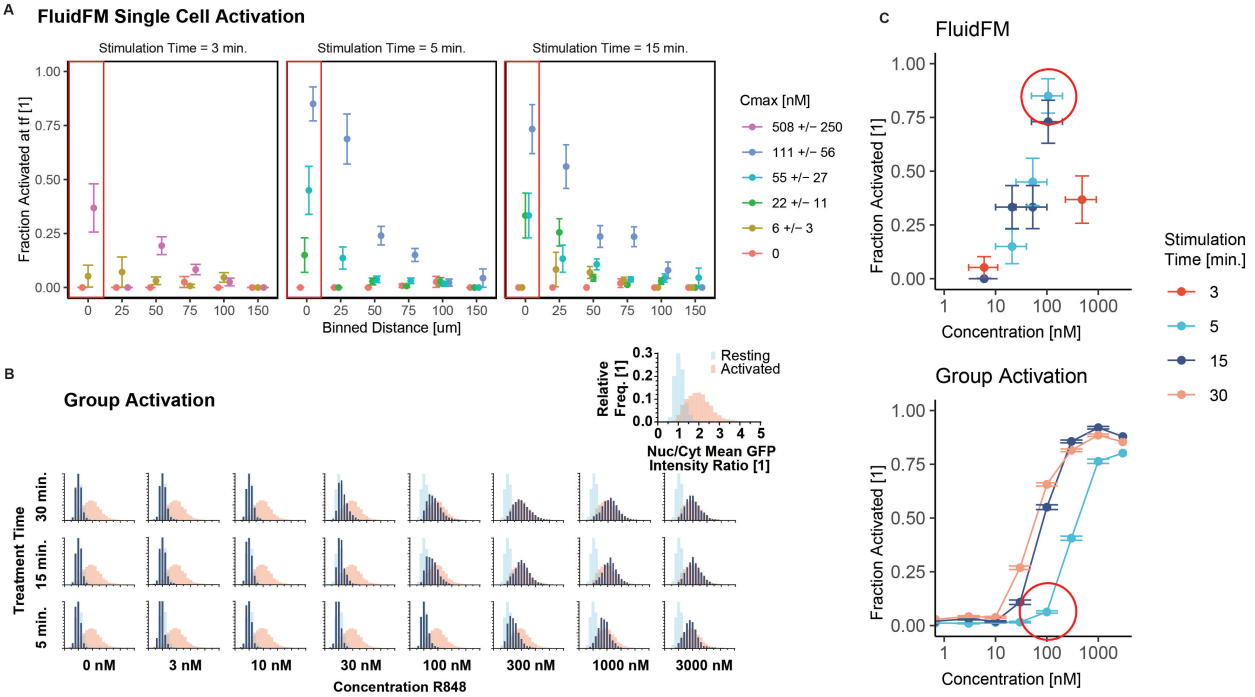

Figure 3.3: (A) Fraction activated vs distance from dispensing point, colors are concentration at target cell position (C_{max}), stimulation times (left to right) are 3, 5, and 15 minutes. Each group has 15-21 independent replicates. (B) Group stimulation in chambered slides. Calibration data (Figure 2.1B) of resting (blue) and activated (red) populations in each panel. Data in navy, all scales same as inset. Histograms arranged by R848 concentration and treatment time. (C) Fraction activated vs concentration, stimulation time from (A) and (B). Top: target cells in single cell stimulation (boxed in A). Horizontal error bar uncertainty in concentration at target cell position (Figure 2.3G). Bottom: group stimulation. Vertical error bars are uncertainty in fraction activated, calculated by the bootstrap method (Appendix D.4.1 item 4). Red circled data points 100 nM 5 min. stimulation significantly different.

5 min is sufficient to activate the majority of macrophages individually. (Note: C_{max} varies between 50 and 200 nM, depending on the distance between the cell surface and the probe. As cell height is variable, this concentration cannot be more precisely known (Figure 2.3G). We use the best estimate of 100 nM for this condition). An activating concentration of 100 nM is consistent with previous reports of NF-$\varkappa$B activation by R848 stimulation, however the 5-minute timing is considerably shorter than most stimulation times for TLR agonists. This initial finding indicated that single macrophages respond to localized and transitory chemical signals.

For the group stimulation experiments we plated the RAW264.7 NF-$\varkappa$B reporter macrophages in 8-well chambered coverslips and stimulated with R848 for between 5 and 30 minutes (figure 3.3B,C). The NF-$\varkappa$B response of the population increases from a resting state to an activated state with increasing concentration and/or stimulation time. Stimulation at or above 100 nM for 15+ minutes is sufficient to cause activation, but for 5-minute stimulation, the concentration threshold is tenfold higher.

The group activation results provide context for the single cell targeting FluidFM results. The minimum concentration for activation with any stimulation time (100 nM) is nearly the same in both experiments. However, in the case of short stimulation time (5 minutes), the group activation threshold is higher than the single cell threshold. Using a permutation analysis (Appendix D.4.2, item 8a), random samples were drawn with replacement from the combined data and the fraction activated calculated. When compared with the experimental result for the single cell activation, none of the 5000 sampled datasets had as high of a fraction activated, meaning $p < 0.0002$. Group stimulation compared to single cell targeting decreased the percent activated by 79% $\pm$ 8% (85% to 6%). From these results we concluded that the activation threshold for R848 is lower for single cells than a group of culture of cells.

CHAPTER 4

MACROPHAGE GROUP ACTIVATION FRACTION DEPENDS ON CULTURE DENSITY AND STIMULATION TIME

Our results thus far indicated two activation regimes – single cell response and group response. We next wanted to probe the transition between these two regimes. If stimulation targeted at a single cell produced a stronger result that a uniform stimulus in the media, what about a stimulus targeted over a large area, but still much smaller than the size of the dish? We used the FluidFM in group targeting mode (Figure 2.4) to stimulate groups of cells number from tens to hundreds.

4.1 Macrophage group activation fraction decreases with increased culture density

For these results, We focused on two C_{max} conditions in the FluidFM Group Targeting experiments: one where the concentration of R848 was just below 100 nM in the center of the dish, and one where the concentration was just below 1 µM at the center of the dish (Figure 4.1A, 4.4B), using a stimulation time of 5 minutes. We also took data at other concentrations, though it was not included in the main analysis (see Figure 4.6).

A C_{max} of 90 nM resulted in a smaller area of responding cells, in the region of 30 – 90 nM agonist concentration. A C_{max} of 900 nM resulted in a larger area of responding cells, in the region of 100 – 900 nM agonist concentration (Figure 4.1A-B, 4.6). Interestingly, increasing C_{max} appeared to increase the activation threshold, restricting activation to a smaller area than expected if the threshold remained at a constant concentration. This result suggested that there was more occurring with cellular activation than just the concentration alone; perhaps the surrounding cells influenced the responses of individual cells.

If cell to cell communication were impacting activation, we would expect to see a de-

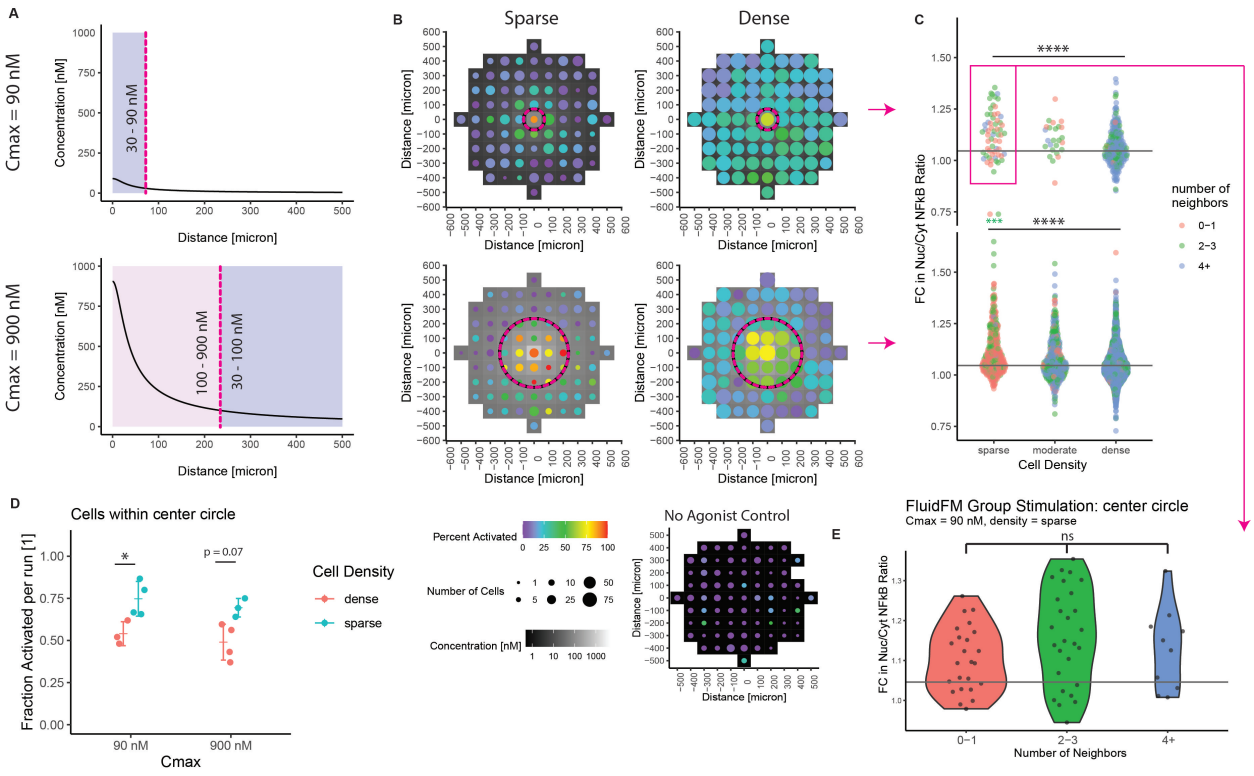

Figure 4.1: Small group targeting with FluidFM. (A) Concentration gradient from dispensing point for C_{max} = 90 nM,900 nM. Vertical dashed line marks where concentration drops below 30 nM (top) or 100 nM (bottom). Lavender panel 30 – 100 nM, pink panel 100 – 900 nM. (B) Group targeting with FluidFM, each plot one representative experiment (Figure 4.6). Top row C_{max} = 90 nM, bottom C_{max} = 900 nM, left column sparse plating, right dense plating, all 5 min. stimulation time. Data binned in 100 µm x 100 µm squares, tile background is agonist concentration, point color is percent activated and point size is the number of cells per bin. Circular dashed line corresponds to dashed line in (A). Negative control (bottom right) (c) Cells within center circle in (B). Fold-change in Nuc/Cyt NF-ϰB ratio vs average cell density and number of neighbors (Figure 2.5A-C). Horizontal line is activation threshold (Figure 2.1H). Significance determined by 3-group permutation ANOVA in R and pairwise comparisons with Wilcoxon test in R. (D) Fraction activated in center per independent experiment. Grouped by stimulation condition (C_{max}) and cell density. Significance from permutation ANOVA in R Appendix D.4.2, item 8b). (E) Boxed data in (D), grouped by number of nearest neighbors. Horizontal line is activation cutoff (Figure 2.1H). No significant difference between groups ($p = 0.29$) (3-group permutation ANOVA in R). Stars: * $p \leq 0.05$ ** $p \leq 0.01$ *** $p \leq 0.001$ **** $p \leq 0.0001$ 'ns' $p > 0.05$.

pendence on cell culture density. To determine if cell density was playing a role, we sub-categorized our data by cell density (Figure 3B). Individual C_{max} experiments were sorted into "sparse", "moderate", and "dense" cell density (Figure 2.5A,B). The "sparse" condition has cell density on par with that observed in tissue resident macrophages (Li et al. [2019], Uderhardt et al. [2019], Jenkins and Allen [2021]) and also the densities used in the single cell targeting experiments (Figure 3.3).

While we categorized the culture images by average density, RAW264.7 macrophages tend to grow in clusters, rather than an even confluency. Therefore, even in experiments with a low overall cell density, there will be a mixture of isolated cells and clusters. We wanted to examine if the dependence on cell density correlated more with the average culture density or the hyper-local number of neighbors surrounding each cell. We determined the number of close neighbors for each cell by counting the number of other cells within 2 cell lengths (Figure 2.5C). Looking just at cell density, we compared the response of cells in a sparse culture to a dense culture (Figure 4.1C). The differences between the populations are highly significant for both C_{max} values, as determined by 3-group permutation ANOVA ($p < 0.0002$ for both) (Appendix D.4.2, item 8b) and pairwise Wilcoxon test for sparse vs dense ($p = 2\text{x}10^{-18}$ and $p = 9\text{x}10^{-14}$ for C_{max} = 90 nM and 900 nM, respectively). The effect sizes for the median fold-change in Nuc/Cyt NF-$\varkappa$B for these pairwise comparisons were -6% ± 1% and -2.2% ± 0.4% for C_{max} = 90 nM and 900 nM, respectively. In both cases the cells were less activated at higher cell density. The number of neighbors (point color, Figure 4.1C) appeared to correlate with cell density, but not activation. We further examined the case of C_{max} = 90 nM, sparse density, and looked at number of neighbors. We found no significant difference between any of the groups with a 3-group permutation ANOVA, excepting the case of C_{max} = 900 nM, spot density = sparse, comparing 0-1 neighbors with 2-3 neighbors (Figures 4.1, 4.2). From this we concluded that differences in overall culture density were more important than the number of neighbors when cells were further apart. This implies

that the signal regulating this process is likely distributed over longer distances.

To confirm the observation of decreasing activation with increasing cell density, we also calculated the fraction activated in the entire center region per experiment (Figures 4.1D, 4.2A). Contrasting replicates with low cell density to those with high cell density, the difference between the two groups is significant for the C_{max} = 90 nM experiments, and p = 0.07 for the C_{max} = 900 nM experiments (Figure 4.1D). The decrease in percent activated was -21% ± 6% and -20% ± 5%, respectively.

By both measures of group activation, the NF-κB response is lower at higher cell density, suggesting a potential role for cell-to-cell communication in tuning macrophage sensitivity. The relative importance of whole culture density versus the hyper-local number of neighbors suggests a longer length and time scale for this communication.

Is this density dependence present in whole-culture stimulation as well? We compared 100 nM 5 minute stimulation with R848 for cells plated at high and low density in chambered slides, incubated in CO_2 independent medium and imaged over time on the live cell microscope (Figure 4.3). Low density cells were grown to 800 cells/mm^2, and high density cells were grown to 3600 cells/mm^2. Cells were treated with 100 nM R848 and washed by dilution method with fresh, warm media (Figure 4.3). Wilcoxon test comparison of the two culture densities showed highly significant difference (p = 2.2x10^{-16}). The decrease in percent activation associated with increased cell density was 13.2% ± 1.7%, error determined by permutation method in R (Appendix D.4.2, item 8b).

4.2 Macrophage group activation fraction depends on stimulation time

A remaining question was if this decreased sensitivity was a permanent or transitory effect. Thus far we had focused on the shortest stimulation times possible with the FluidFM. To investigate the longevity of the phenomenon, we stimulated the groups of cells for longer

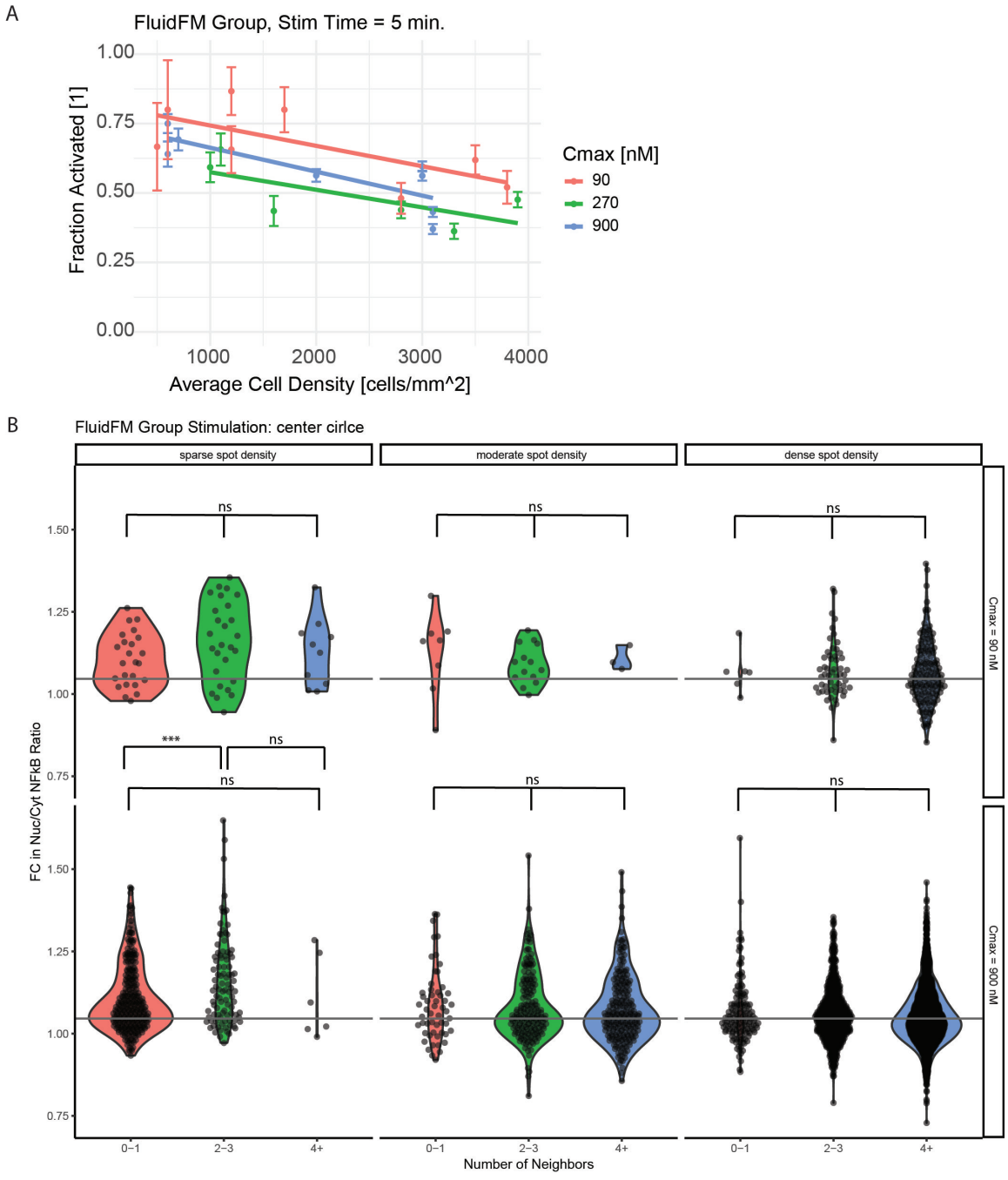

Figure 4.2: Number of Neighbors vs culture density comparison for FluidFM Group Stimulation results (see chpater 4). (A) Fraction activated in center circle from FluidFM Group data, plotted against average cell density in that spot. Color indicates C_{max} for that experiment. (B) Number of cell neighbors vs culture density, single cell Fold-change in Nuc/Cyt NF$\varkappa$B ratio. Pairwise significance from Wilcoxon test in R, after 3-group permutation ANOVA (Appendix D.4.2, item 8b).

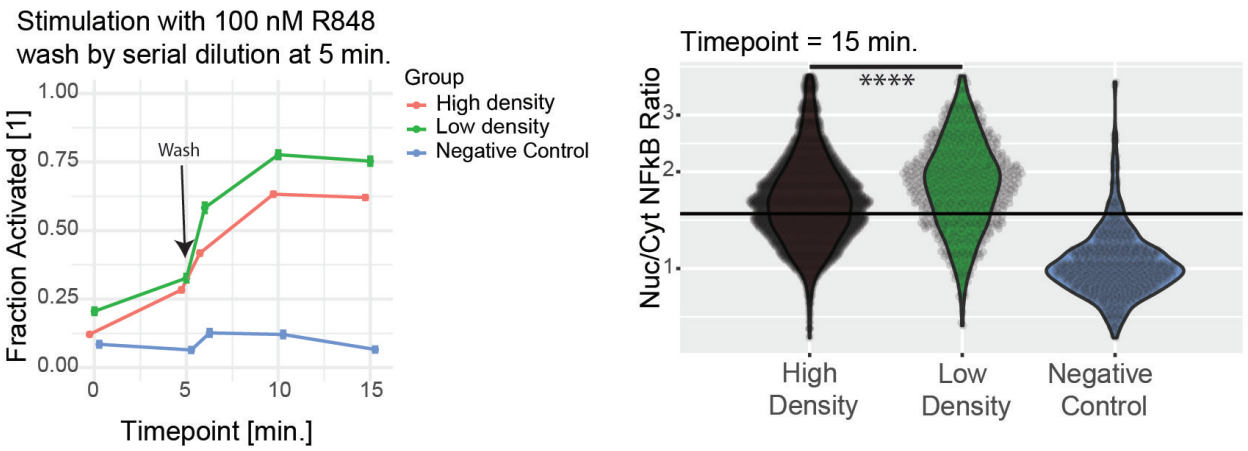

Figure 4.3: Comparison of bulk activation of macrophages plated at high and low density in chambered slides. Left: fraction activated over time for high and low density wells stimulated with 100 nM R848 for 5 minutes, negative control unstimulated. Fraction activated calculated from calibration data (Figure 2.1A). Right: individual cells Nuc/Cyt NFκB ratio at 15 minutes post-stimulation. Significance from Wilcoxon test in R, $p = 2.2 \times 10^{-16}$.

periods of time – analogous to previous culture experiments. Large group stimulation at 15 minutes or longer had an activation threshold around 100 nM or lower, similar to the single cell threshold for 5 minutes (Figure 3.3, 4.4A). Further group targeting FluidFM experiments were done with a 15-minute stimulation time to see if this effect extended to smaller groups of cells as well. In densely plated cells the longer stimulation times showed higher activation (Figure 4.4C-D). This difference was less pronounced in the sparse cells (Figure 4.4D). Increasing the stimulation time from 5 to 15 minutes caused the percent activated in densely plated cells to increase by 25% ± 6% and 22% ± 1% for C_{max} = 90 nM and C_{max} = 900 nM, respectively (Figure 4.4D). These results suggest that the density-dependent suppression of activation is most impactful for transitory stimuli (a few minutes), and if the stimulus persists, the majority of cells respond, resulting in a consistent sensitivity to signal. This combination of results explains (1) how this result would easily have been missed with previous experimental methods and (2) that the mechanism for this process must operate at timescales of 15 mins and over distances of multiple cell lengths.

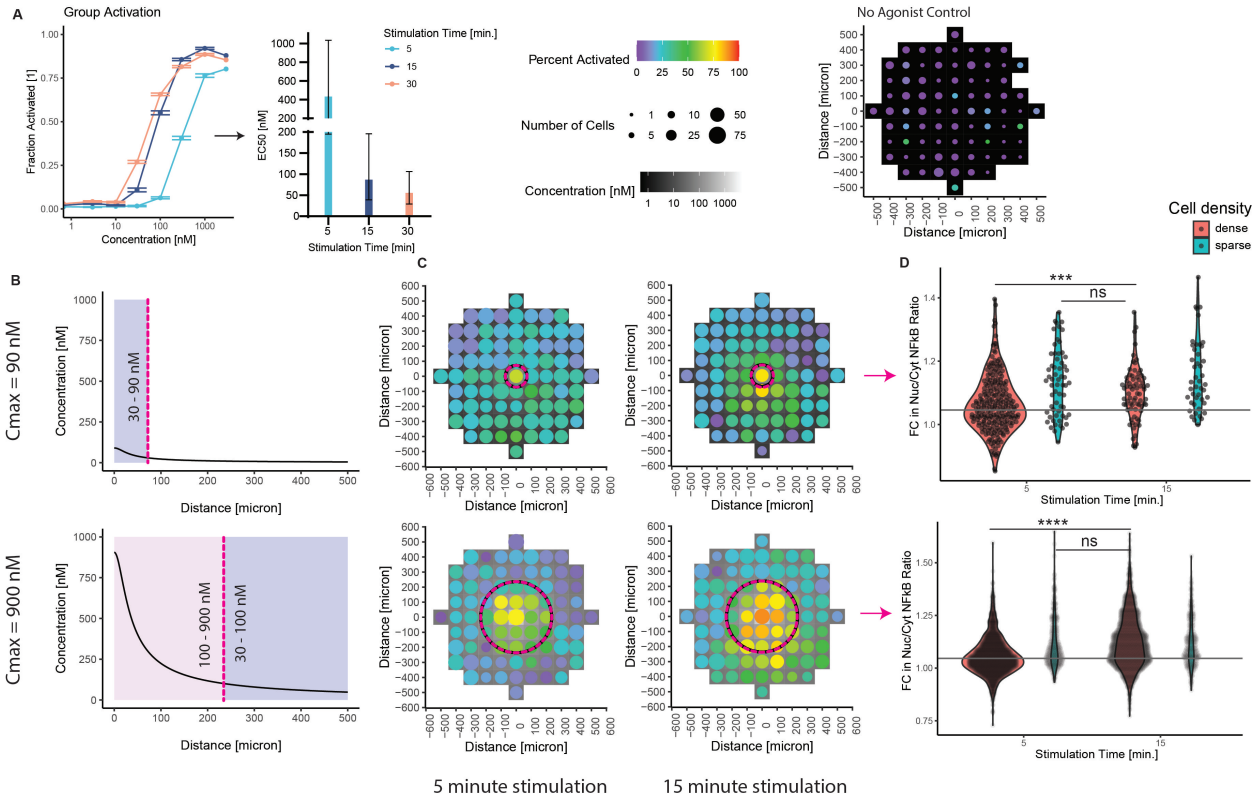

Figure 4.4: (A) Data from Figure 3.3C, EC50 values from dose-response fit (GraphPad Prism). Vertical error is 95% CI. (B-D) Small group targeting with FluidFM. (B) Concentration gradient from dispensing point for C_{max} = 90 nM,900 nM. Vertical dashed line marks where concentration drops below 30 nM (top) or 100 nM (bottom). Lavender panel 30 – 100 nM, pink panel 100 – 900 nM. (C) Group targeting with FluidFM, densely plated cells, each plot one representative experiment (Figure 4.6). Top row C_{max} = 90 nM, bottom C_{max} = 900 nM, left and right columns 5 and 15 min stimulation time. Data binned in 100 µm x 100 µm squares, tile background is agonist concentration, point color is percent activated and point size is the number of cells per bin. Circular dashed line corresponds to dashed line in (B). Negative control (top right) (D) Fold-change in nuclear/cytoplasmic NF-ϰB ratio of individual cells in center regions shown in (C), all replicates aggregated, grouped by C_{max}, stimulation time, and cell density. Horizontal line is activation cutoff (Figure 2.1H). Significance from Wilcoxon test in R. Stars indicate: * $p \leq 0.05$ ** $p \leq 0.01$ *** $p \leq 0.001$ **** $p \leq 0.0001$ 'ns' $p > 0.05$

Cmax [nM]	Concentration threshold [nM]	Threshold location [um]	1st derivative at threshold [nM/um]	2nd derivative at threshold [nM/um^2]
90	~30	71	-0.36	0.008
270	~50	137	-0.34	0.005
900	~100	236	-0.41	0.003
4500	~1000	113	-8	0.128

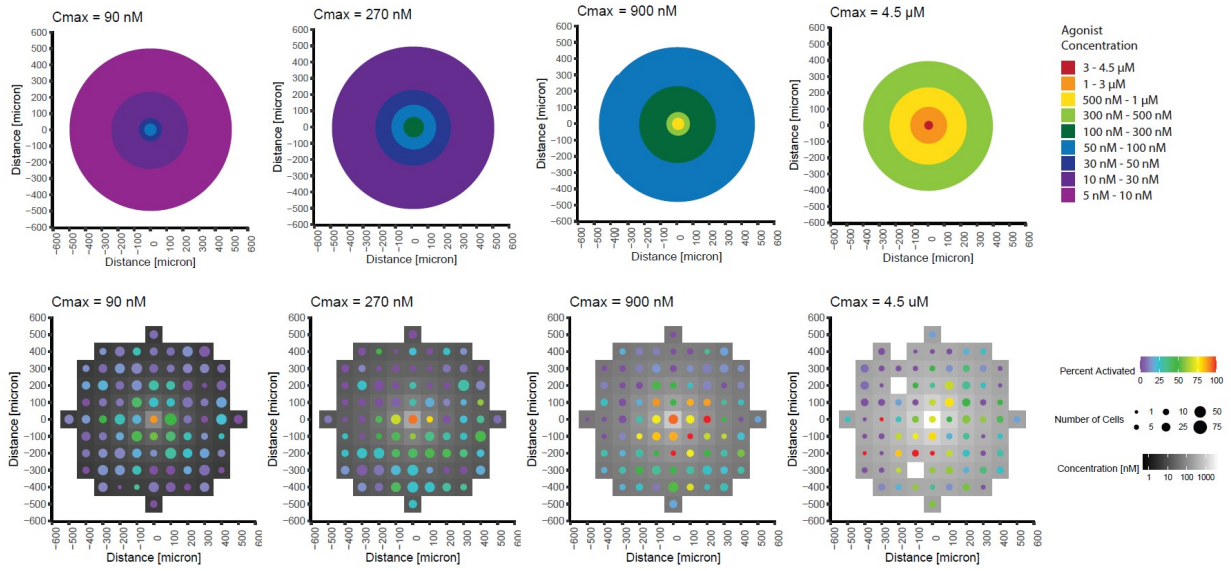

Figure 4.5: Top: table of values for concentration and gradient at the threshold location (boundary between activated and unactivated cells) for FluidFM group datasets. Middle: concentration gradient for each C_{max} condition. Bottom: example dataset from each condition.

4.3 Macrophage group activation spatial extent depends on concentration gradient

One final observation I made from these data is that when I stimulated groups of macrophages in culture, there was a radius beyond which the culture remained quiescent. I had expected this radius to occur at about the same concentration of R848, the place where we reached the single-cell or group activation threshold (somewhere between 30 and 100 nM). However, I found that as I increased C_0, and thus C_{max}, the minimum activating concentration at the edge of this zone increased also. Through a rough estimate of this boundary, I discovered that for a range of C_{max}, this cutoff location occurred at similar values of the concentration gradient (Figure 4.5).

These results require further investigation and a more careful measurement of the boundary from each experiment. But they provide one possible explanation for how groups of macrophages adapt to stimuli over several orders of magnitude to limit the number of responding macrophages and avoid an excessive response.

Note: all FluidFM Group Stimulation datasets are shown in Figure 4.6. Representative plots drawn from this data are shown in Figures 4.1, 4.4, and 4.5.

4.4 Conclusions and future directions

In summary, we observed the temporal and spatial characteristics of PRR signals influence the macrophage response. The FluidFM allowed the unique ability to limit the temporal and spatial extent of the PRR signal to target single macrophages, small groups, and larger collections of cells. We report that macrophages, in a controlled environment, deviate in their sensitivity to transitory (5 minute) PRR signals. Individual macrophages stimulated with PRR signals became more sensitive in windows under 5 mins when they do not experience the same signal concentration as the surrounding culture. This difference in individual

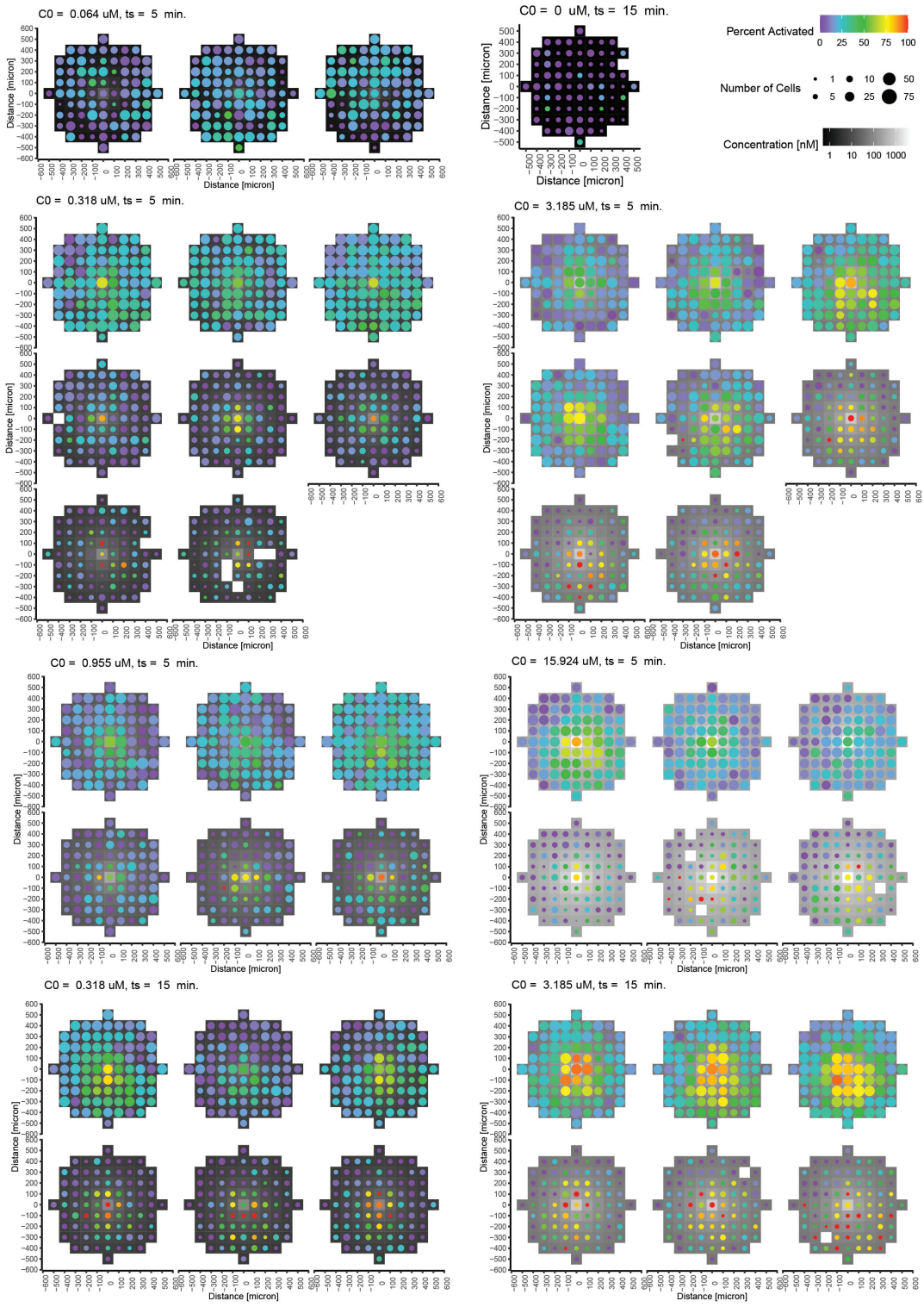

Figure 4.6: All FluidFM Group stimulation data, described in chapter 4. (continued)

Figure 4.6: Data binned in 100 µm x 100 µm squares, tile background is agonist concentration, point color is percent activated and point size is the number of cells per bin. Plots grouped by Stimulation concentration (C0) and time (ts), ordered by culture density.

cell responses led to a lower concentration threshold for NF-κB activation of single cells stimulated with the TLR agonist R848 compared to whole culture stimulation. These observations suggested that each cell gathers information from its environment alongside the concentration of PRR agonist, and potentially a pathogenic threat to determine its response.

Our second question was how the surrounding cell culture influenced the sensitivity of individual cells. Since the FluidFM exposed neighboring cells to differing concentrations of PRR agonist, we wanted to understand how individual cells might integrate information from the larger unstimulated culture or local stimulated group. Cell-to-cell communication has been observed in related contexts - macrophages and other innate immune cells employ quorum licensing to regulate their state and quorum sensing to terminate inflammation (Muldoon et al. [2020], Postat et al. [2018], Hamidzadeh and Mosser [2016], Bardou et al. [2021], Antonioli et al. [2019]). In these cases, culture density during growth or after activation influence individual cell responses. For our experiments, we postulated that either the overall density of cells or the local number of cells would determine the sensitivity of the individually stimulated cells.

In our experiments we examined "sparse" cell densities (similar to the distribution of tissue resident macrophages) and "dense" cell densities (confluent or crowded). Simultaneously, we examined the "number of neighbors" (surrounding cells within a certain distance) in both conditions, to test whether local or global density was the dominant factor. We observed that the density of cells in culture determined the sensitivity of individuals to stimulation, with more dense cultures inhibiting individual cells from responding to lower concentrations of PRR agonist. The "number of neighbors" did not contribute to the phenomenon, leading us to conclude that the larger culture density was dominant in determining the response. Phrased colloquially, it's not the neighbors on your street, but the overall population of your

city that matters. The inhibition of activation at greater cell densities could have relevance to biological situations where macrophage density is increased.

Upon providing evidence of a single cell to large-scale culture transition, and its relation to culture density, we sought to determine how this short-timescale phenomenon of 5 mins related to the more common experiment of stimulating macrophages for more than 30 mins in a culture dish. We performed a series of FluidFM experiments increasing the time of small group (tens to hundreds of cells) stimulations. We observed that the effect of alteration of sensitivity of groups of cells is reduced after 15 mins of sustained PRR exposure. This result suggests that the mechanism of cellular communication must occur at a similar time scale or precede the appearance of the PRR agonist. This observation puts a temporal and spatial limit on potential mechanisms for the decreased activation of densely cultured cells exposed to transitory PRR signals. The next step of this research is an investigation into potential mechanisms that could explain these changes in activation threshold. If such mechanism(s) were identified, they could be used to tune macrophage sensitivity in contexts such as dose-sparing for vaccines or tamping down excess inflammation.

These results also open up more questions about the dynamics of TLR activation and response, potential group coordination of the response, and the role of the local cell environment. The FluidFM provides a valuable tool for this research because it can provide both persistent and transitory stimuli, as well as spatially varying gradients, with a preservation of any secreted factors present before stimulation. In this way it approximates the situation of quiescent cells sparsely distributed encountering localized and/or transitory signals of infection. The cell culture environment can be varied to explore its effect on macrophage sensitivity to these signals. Our experimental approach can be used to study a variety of cell types, environments, stimuli, and responses to explore further questions of single immune cell responses.

CHAPTER 5

POTENTIAL MECHANISMS FOR MACROPHAGE QUORUM COMMUNICATION

5.1 Introduction

Quorum sensing is when a population of cells changes from one state to another upon reaching a certain size, or quorum. First observed in bacteria, recently similar behavior has been observed in immune cell populations, including macrophages (Antonioli et al. [2019]). The mechanism for this behavior is most often a secreted factor that directly or indirectly impacts the immune response of the cell. As the number of immune cells increases, the amount of this secreted factor increases also, changing the response of the population. This signaling can occur before, during, or after inflammation. In the case of signaling prior to immune stimulation, this phenomenon has been termed quorum licensing, and though the signaling factor has not yet been identified, Muldoon et al. [2020] have determined that it leads to a change in resting NF$\varkappa$B levels in macrophages depending the density at which they were grown.

There are more examples of quorum sensing leading to resolution of inflammation, such as nitric oxide production and purinergic signaling. Both of these signals are interesting because they are intially pro-inflammatory, and then later anti-inflammatory. NO at low levels stimulates immune response, and at high levels suppresses immune response through a metabolic mechanism. Purinergic signaling utilizes the extracellular degredation of ATP to ADP, AMP, Adenosine, and then Inosine and re-uptake of each of these molecules, which have different effects on the immune response of the cell, ranging from stimulatory at the start (ATP, ADP), to inhibitory at the end (adenosine). In this way purinergic signaling puts a time limit on the immune response, changing from excitory to inhibitor as the extracellular signal is broken down by cell surface enzymes.

In my previous experiments, I had observed a density-dependence during stimulation. I was unsure if it resulted from a signal at resting state that communicated population density, or something concurrent with TLR activation that quickly modulated the response. The former seemed more likely, especially given the time needed for a secreted signal to diffuse to a large enough area, and the dominance of whole culture density over local clustering. Therefore, I focused on secreted factors that would be present in resting cultures.

There remained the possibility of a contact mechanism of communication as well. Cells can communicate chemical and mechanical signals through cell-cell junctions in a confluent culture (Charras and Yap [2018], Eugenin et al. [2003]). In my preliminary experiments I had observed clusters of cells responding more similarly when one of the cluster was stimulated, than isolated cells and their neighbors. But the behavior was not consistent enough for me to conclude it was responsible for the observed density-dependent effects. Also, as my macrophage cultures were plated below confluency on glass, it seemed unlikely that a mechanical signal could propagate beyond isolated clusters. Even at high density, cluster size remained small. One possibility for distance communication was nanotube connections. I had observed some filamentous connections between macrophages that were nearby but not in contact, which I determined to be tunneling nanotubes. TNTs can communicate signals between macrophages over great distances (Dupont et al. [2018], Lock et al. [2016]). However, I did not observe many of TNTs in my macrophage cultures, which made me doubt there were enough of them to create a widespread network through the culture. Thus, I judged a secreted factor to be more likely the method of communication behind my observation of density-dependent group activation.

5.2 Supernatant swap

The first step in determining the communication mechanism underlying my observed density-dependence of macrophage sensitivity was to distinguish between a mechanical and a secreted

signal. If the signal was in the supernatant, then swapping supernatant from sparse or dense cultures should impact their responses. I hypothesized that a sensitizing factor in spare supernatant could increase the response in dense cells, or an inhibitory factor in dense supernatant could decrease the response in sparse cells. As controls, I also tested switching the media between cultures of the same density, as well as swapping out for fresh media, or leaving the same media on the culture.

Supernatant Swap Experiment Protocol

1. Culture Macrophages in 18-well slides
   (a) Culture G9 NFκB Reporter Macrophages for at least 2 passages in T75 flasks
   (b) Plate macrophages at 470 and 2350 cells/mm^2 in DMEM media with 10%FBS in two 18-well slides (Ibidi 81816), one slide per density.
   (c) Incubate overnight at 37°C and 5%CO_2
2. Prepare reagents
   - CO_2 Independent Medium with 10% HIFBS and 2% L-Glutamine, 15 mL
   - 2 µM R848, 300 µL, in prepared media
   - Hoechst33342 nuclear stain 10 µg/mL in PBS
3. Change media
   (a) Warm prepared media to 37 °C
   (b) Add 40 uL hoechst dilution to 4 mL warm media and vortex to mix
   (c) Remove media from 18-well slides by pipette and immediately replace with 90 µL of the warm media+hoechst mixture
4. Incubate slides at 37 °C and atmospheric CO_2 for 3 hours
5. Supernatant Swap
   (a) Remove 80 µL from the center 12 wells of each slide and replace with 80 µL treatment media as follows (work in triplicate):
   (b) Column 2: No Swap group: do not remove media

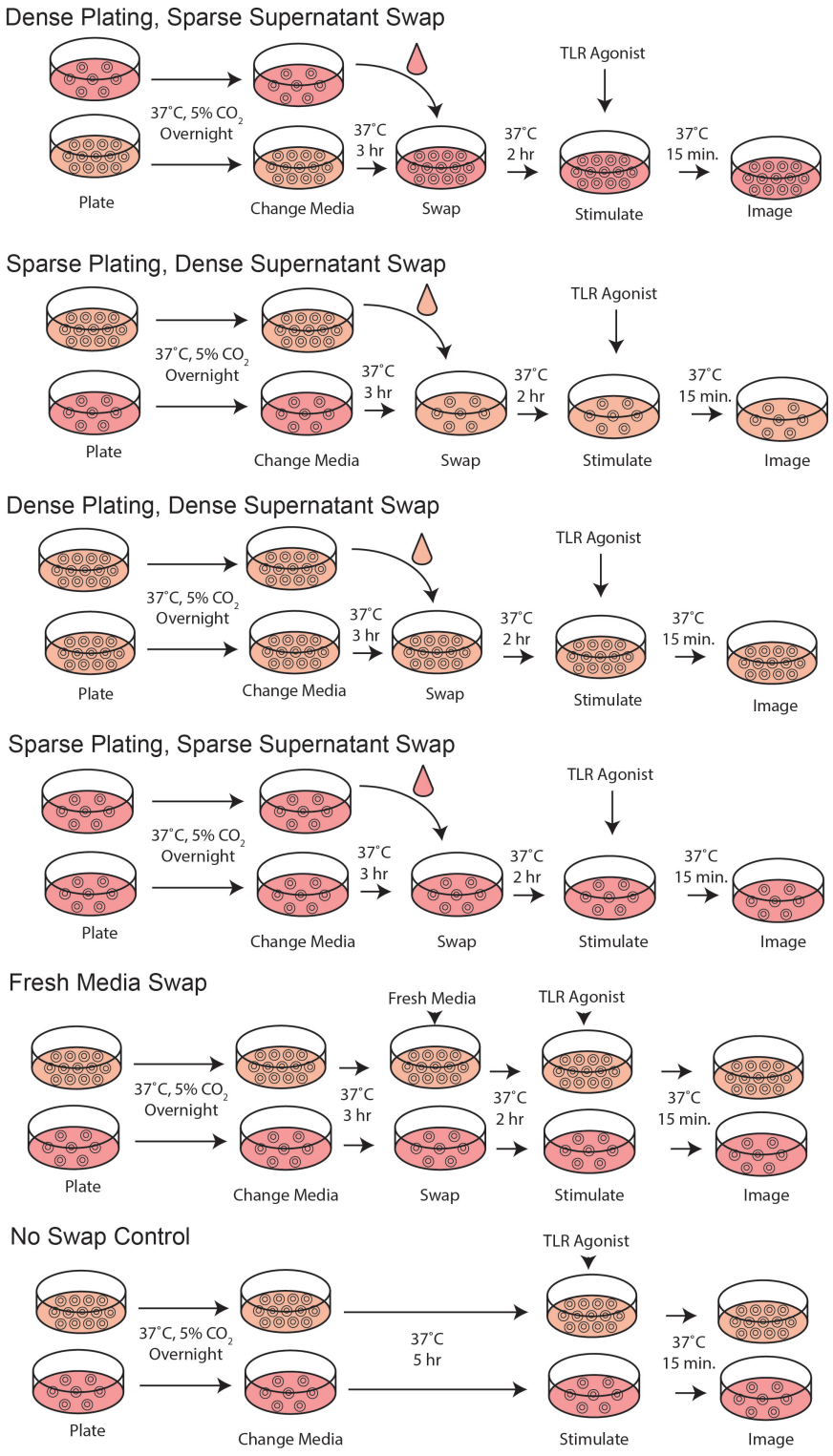

Figure 5.1: Diagram showing the different groups in a supernatant swap experiment (see table 5.2). Cells in dish show contrasting density, media color shows change with addition of new fresh or conditioned media. Incubation times and conditions shown atop arrows.

(c) Column 3: Same SN group: replace with conditioned media from the first column of the same slide

(d) Column 4: Swap SN group: replace with conditioned media from the last column of the other slide

(e) Column 5: Fresh Media group: replace with fresh, warm media

sacrificial	no swap	same SN	swap SN	fresh media	sacrificial
sacrificial	no swap	same SN	swap SN	fresh media	sacrificial
sacrificial	no swap	same SN	swap SN	fresh media	sacrificial

Table 5.1: 18-well slide layout showing swap groups

6. Incubate slides and prepared R848 dilution at 37 °C and atmospheric CO_2 for 2 hours.
7. Stimulate and Image
   (a) Working in parallel, treat all wells in each group as follows:
   (b) Image each well in GFP and DAPI channels at 10x magnification
   (c) Dilute 10 µL of the 2 µM R848 into each well
   (d) Incubate 15 minutes at 37 °C
   (e) Image each well in GFP and DAPI channels at 10x magnification
   (f) Note: for the No Swap control group, image twice, 15 minutes apart, before adding the R848 for an untreated control.
8. Quantify Fraction Activated
   (a) Process the fluorescence images with CellProfiler as described (reference) to generate per-cell nuclear/cytoplasmic GFP fluorescence ratio.
   (b) Using R, calculate the fraction activated per well (reference)
   (c) Average the replicates and plot, comparing the 5 groups and 2 densities, and calculate statistical significance with a t-test (reference).

The results (Figure 5.2) indicated that cells treated with conditioned media, at either density, had a decreased response compared with cells that had fresh media. To follow up on these results, I screened several potential mechanisms using a variation of this experiment, as

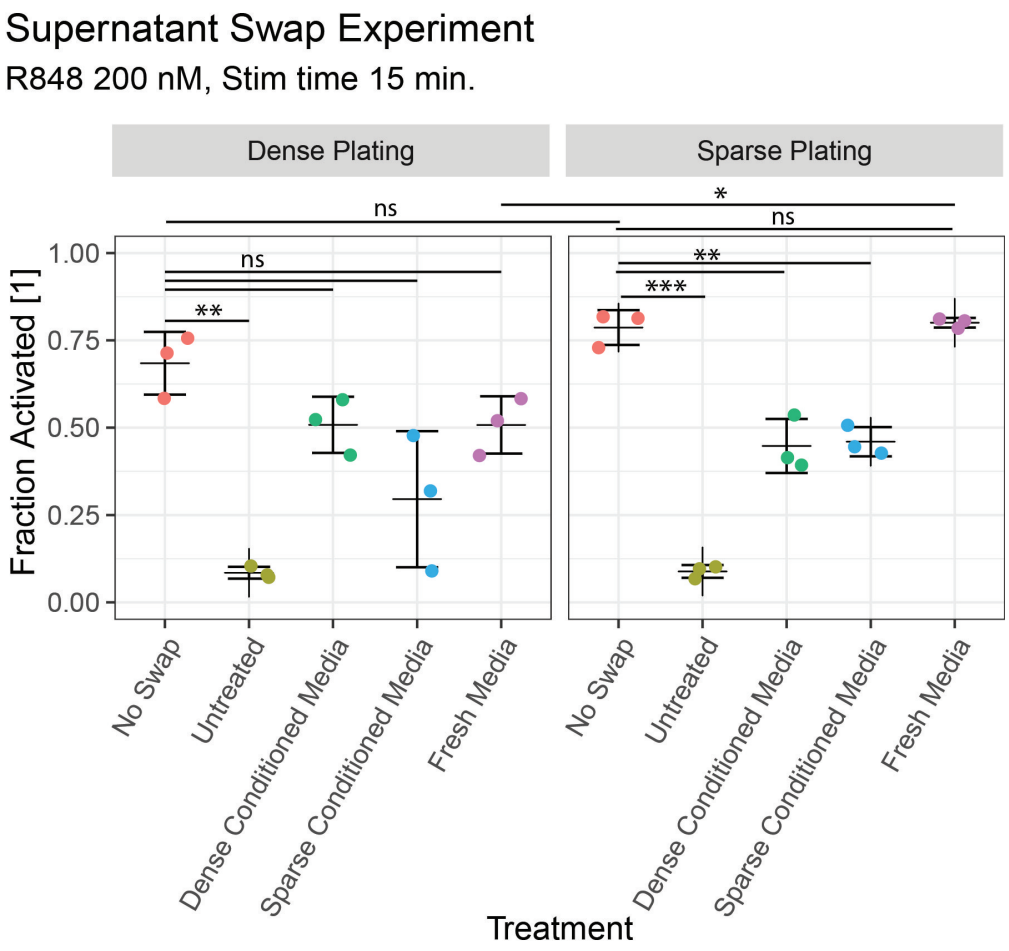

Figure 5.2: Supernatant swap results showing fraction activated per group. Mean and SD from 3 replicates. Groups described in Table 5.2 and Figure 5.1. Stars indicate: * $p \leq 0.05$ ** $p \leq 0.01$ *** $p \leq 0.001$ **** $p \leq 0.0001$ 'ns' $p > 0.05$

Plating	Treatment	R848	Purpose
Both	None	None	Untreated Control
Both	None	200 nM 15 min	Positive Control for Activation
Both	Fresh Media	200 nM 15 min	Recovery time control
Sparse	Sparse Conditioned Media	200 nM 15 min	Swap control for Sparse
Dense	Dense Conditioned Media	200 nM 15 min	Swap control for Dense
Dense	Sparse Conditioned Media	200 nM 15 min	Test for sensitizing factor in sparse media
Sparse	Dense Conditioned Media	200 nM 15 min	Test for inhibitory factor in dense media

Table 5.2: Experiment groups for SN swap experiment with plating (sparse or dense culture), treatment (type of supernatant swap), R848 treatment, and purpose of the experiment group. Groups also described in figure 5.1

well as characterized resting supernatant from cultures at both densities. I have also begin isolation of extracellular vesicles from the supernatant in order to analyze those as well.

5.3 Inhibitor screen

I compiled a list of potential mechanisms to screen from literature sources, especially other quorum communication mechanisms. Below is a list of mechanisms that I tested. These fall into four categories: protein secretion, nitric oxide secretion, extracellular ATP (and, related calcium mobilization Ren et al. [2014]), and extracellular Adenosine. Listed below are the inhibitors I used to test these candidate mechanisms.

Potential mechanisms Tested:

- Protein secretion through the Golgi
  - Brefeldin A (GolgiPlug, BD Biosciences)
  - Monensin (GolgiStop, BD Biosciences)
- Nitric Oxide
  - NSAIDs: Aspririn and Acetominophen
  - L-NIL: iNOS inhibitor

  - NS-398: COX2 inhibitor
- Extracellular ATP
  - EGTA (calcium mobilization leading to ATP release)
  - Apyrase (not shown - endotoxin contamination)
- Adenosine
  - Istradefylline: A2AR antagonist

There remains a major category of mechanisms I haven't tested yet: Chemokines such as (KC, MCP-1, MIP-1b, RANTES), cAMP, Macrophage colony-stimulating factor (CSF-1). This list of chemokines comes from results in Muldoon et al. [2020], where they looking at the secreted factors present in resting macrophage culture that were density-dependent.

For the inhibitors tested so far, I based the protocol for the inhibitor screen off of the supernatant swap protocol above. If the inhibitors caused a decrease in the secreted factor, then that would change the conditioned media and thus its impact on the cultures treated with it. I also looked at the direct effect of the inhibitors on cultures without the media swap. I added the inhibitors at the media change step, prior to the swap. This way any previously present secreted factors would be removed, and the inhibitor would impact any subsequent secretion.

The results thus far are shown in figure 5.3. The main problem with these experiments has been inconsistency in the Untreated controls (i.e. the groups that did not experience a supernatant swap or inhibitor treatment, but were stimulated with R848). There has been varying levels of response in these controls, as well as varying difference between the two density groups. This has made it more difficult to distinguish any impact of the inhibitor. In continuing these experiments, I will also have to be careful in disentangling the impact of the inhibitors on the cells directly, from the impact they would have on secreted factors that would then impact the immune response.

The most promising result thus far is that several of the inhibitors targeted at NO

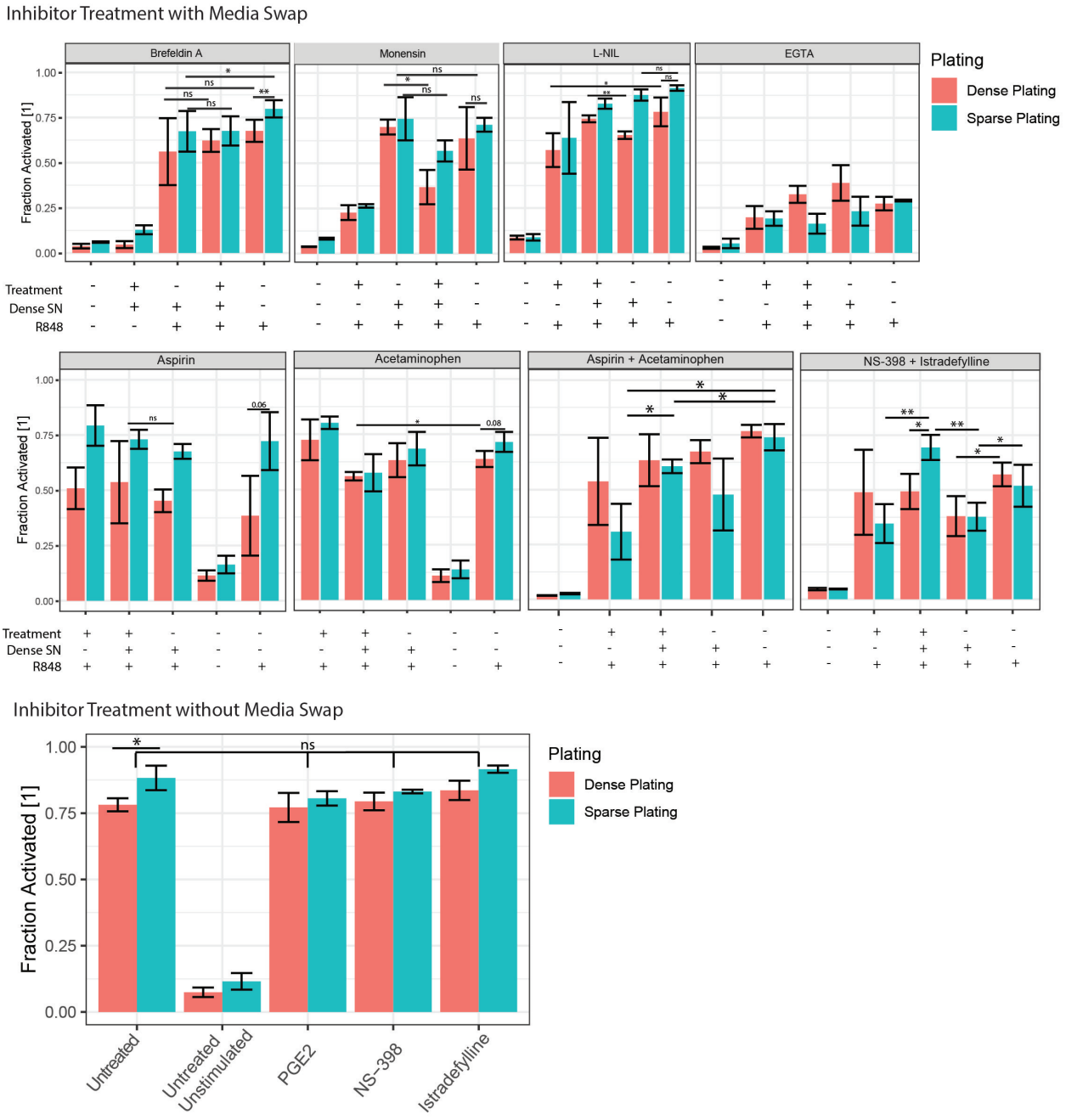

Figure 5.3: Barplots showing fraction activated for macrophages plated at high and low density (bar color). Plus and minus rows below show whether the cells were treated with the inhibitor (Treatment), swapped with dense-conditioned supernatant (Dense SN), and stimulated with R848 (R848). Label above each plot indicates which inhibitor was used. Bottom plot is labelled differently as there was no swap in that experiment - instead, groups are labelled individually by inhibitor name. Stars indicate: * $p \leq 0.05$ ** $p \leq 0.01$ *** $p \leq 0.001$ **** $p \leq 0.0001$ 'ns' $p > 0.05$

production had some effect. While not consistent enough to draw any firm conclusions, this remains an area for future investigation. Previous research into NO-based communication has determined that significant levels are produced only after immune stimulation, so it is difficult to detect or investigate the effect of lower levels that may be present in resting cells. I have been unable to detect NO in resting cells, or in cells after brief R848 stimulation with a Griess Reagent assay, indicating that if NO is the mechanism, the concentrations are below the limit of detection for this assay (about 1 µM).

5.4 Proteomics

I also sent samples of resting supernatant from cultures at high and low density (numbers) to the proteomics core for analysis. Credit to Samuel Wang and Allen Huff for processing the samples and doing initial data analysis. My table of significant results is based off of Allen's analysis.

Supernatant Preparation:

1. Plate macrophages in 6-well plate, 2 mL media per well, 3 wells at 470 cells/mm2, 3 wells at 3000 cells/mm2
2. Incubate overnight at 37C and 5% CO_2
3. Wash cells 3x with warm PBS
4. Incubate in PBS for 4 hr at 37C and 5% CO_2
5. Remove supernatant to 15 mL tubes and spin down at 4000 xg for 10 minutes
6. Transfer supernatant to 1.5 mL tubes and concentrate with speed vac at 30C for 2 hr on high speed, or until about 10x concentrated.
7. Recombine same wells into one tube. Add protease inhibitor and EDTA.
8. Take 75 µL for a BCA to test concentration, bring rest to proteomics core. Freeze at -20 if not testing immediately.

Preliminary Results:

-LOG[P.value]	Dense-Sparse Expression	Description	Accession	Gene.name
2.542365	3.72182	Plastin-2 [OS=Mus musculus]	Q61233	Lcp1
1.76969	3.704694	Galectin-3 [OS=Mus musculus]	P16110	Lgals3
3.326908	2.815759	Heat shock protein HSP 90-beta [OS=Mus musculus]	P11499	Hsp90ab1
2.906075	2.77922	Heat shock protein HSP 90-alpha [OS=Mus musculus]	P07901	Hsp90aa1
2.114881	2.664305	High mobility group protein B2 [OS=Mus musculus]	P30681	Hmgb2
1.886839	2.455326	Superoxide dismutase [Cu-Zn] [OS=Mus musculus]	P08228	Sod1
1.545439	2.403485	Moesin [OS=Mus musculus]	P26041	Msn
1.57532	2.307928	High mobility group protein B1 [OS=Mus musculus]	P63158	Hmgb1
1.938924	2.257456	Macrophage colony-stimulating factor 1 receptor [OS=Mus musculus]	P09581	Csf1r
1.396118	2.201566	Annexin A3 [OS=Mus musculus]	O35639	Anxa3
1.465648	2.189104	Hypoxanthine-guanine phosphoribosyltransferase [OS=Mus musculus]	P00493	Hprt1
1.409842	2.079244	H-2 class I histocompatibility antigen, D-B alpha chain [OS=Mus musculus]	P01899	H2-D1
2.168484	2.043596	Ferritin heavy chain [OS=Mus musculus]	P09528	Fth1
1.989869	1.869885	CD44 antigen [OS=Mus musculus]	P15379	Cd44
1.3981	1.408212	Adenosine kinase [OS=Mus musculus]	P55264	Adk
1.569847	1.21621	Cathepsin S [OS=Mus musculus]	O70370	Ctss
1.574666	-1.03537	Leukocyte immunoglobulin-like receptor subfamily B member 4A [OS=Mus musculus]	Q64281	Lilrb4
1.344498	-1.11315	Pantetheinase [OS=Mus musculus]	Q9Z0K8	Vnn1
2.225504	-1.68566	Insulin-like growth factor II [OS=Mus musculus]	P09535	Igf2
1.323603	-2.02619	Plasminogen [OS=Mus musculus]	P20918	Plg

Figure 5.4: Proteomics screen: top results with keyword "Immune". Column 1, negative log of p-value test for significant difference between replicates. Higher number indicates greater similarity between replicates. Column 2, differential expression between dense and sparse supernatants, normalized to median expression for each group. Larger positive number indicates higher expression in dense culture compared to sparse, larger negative number indicates higher expression in sparse culture compared to dense. Column 3: description of protein from UniProt. Column 4: Accession number for protein in UniProt database. Column 5: Gene name from UniProt database. Results filtered for keyword "Immune" in GOBP (biological process) description, and ordered by differential expression.

The results from the proteomics screen are included in figure 5.4, filtered by significance and the keyword "immune", and ordered by the magnitude of difference between expression in dense culture and expression in sparse culture. Significance was determined by an ANOVA comparing variance between replicates to variance between densities with a p-value cutoff of 0.05. More research needs to be done into each of these results. One that jumps out to me, however, is the Macrophage Colony Stimulating Factor Receptor (CSF1R). CSF-1 is on the list of candidate mechanisms that have yet to be tested in the inhibitor screen.

5.5 Conclusions and future directions

My results from the inhibitor screens thus far have been largely inconsistent. I think this is due to the reliance on the supernatant swap protocol for experiments, which is not consistent enough. I have thus turned more to proteomics-based methods for further ideas. My next step is to follow up on the results from the proteomics of resting culture supernatant. I have also begun isolation of extracellular vesicles from the supernatant in order to compare their abundance and contents. I hope these experiments will yield a more complete picture of factors in the supernatant that might differ between densities, in the case that the phenomenon I observed is not based on only one mechanism.

Another future direction of inquiry is the differences in growth/state between cultures at different densities, and how this might impact their immune functions, possibly through a metabolic mechanism? This possibility needs further reading before planning experiments. Lastly, I plan to continue a version of the inhibitor screen without supernatant swapping, to look further at the NO and Adenosine hypotheses, as well as certain chemokines including CSF-1.

CHAPTER 6

INVESTIGATING PHYSICAL PARAMETERS OF SINGLE HOST-PATHOGEN INTERACTIONS WITH FLUIDFM

6.1 Introduction

One of the main function of macrophages in the immune system is to patrol for invading pathogens and destroy them, and send alarm signals to other immune cells. Macrophages have been observed to literally chase down live pathogens in order to phagocytose them. Macrophages also have surface receptors that detect PAMPS commonly found on the pathogen surface, such as LPS, LTA, and flagellin, proteins found in the bacteria cell wall, membrane, and flagella. These observations would imply that macrophages have a way of sensing when pathogens are nearby, either by contact with their surface proteins, or sensing "shed" proteins that increase in concentration close to the bacterium. Once such a protein is detected, the macrophage should activate, and then take actions to deal with the threat.

Previous research has examined treatment of a macrophage culture with bacteria in solution, as well as isolation of small numbers of macrophages and bacteria in droplets (Jiang et al. [2022]) using microfluidics. This research has established a number of parameters for macrophage-pathogen interactions, including the range of contacts between macrophages and bacteria in free interactions, the bacteria speed when it hits the macrophage surface, macrophage speed in free motion, and the number of bacteria needed to provoke a macrophage response in confinement. Some of this research focuses on pathogen infection as a readout, while others look at macrophage phagocytosis, and others at measures of macrophage activation. We wanted to look at an earlier readout, NFκB activation, which might indicate TLR stimulation by the pathogen. It has been found that NFκB activation should precede other macrophage responses such as phagocytosis and NO production. Looking at NFκB activation alone, however, would allow us to detect earlier signs of pathogen

detection, as well as lower-level activation that may not necessarily lead to downstream responses.

We wanted to examine the case of a single macrophage-bacterium interaction in a controller manner, where we could control the movement of the bacteria with the FluidFM probe, and thus test other physical parameters of interaction between the bacteria and the macrophage. We wanted to determine the minimum threshold for activation of the macrophage, as well as which parameters were most important in that activation. We expected that touching a single, live pathogen to the macrophage surface would garner a strong response, but surprisingly even direct, prolonged contact was often ignored by the macrophage. We are still investigating to determine which parameter we need to change in order to elicit a strong, consistent response.

6.2 Methods

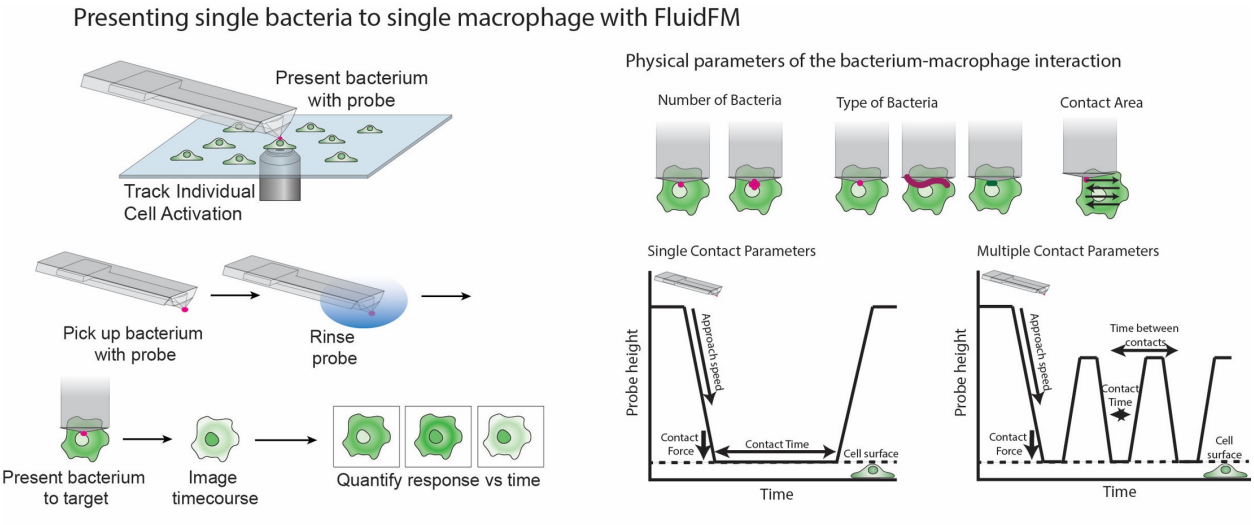

Figure 6.1: Method overview for single macrophage bacterium interaction experiments. Left: single bacterium presentation with FluidFM protocol. Right: physical parameters of the bacterium-macrophage interaction to be studied.

First, I must give credit to Sara Hoggatt, who has been working on this project with me

this past year. She took most of the following data, and helped with developing the protocol. Also thanks are due to Zander Galluppi for help with bacteria culture, and Brad Studnitzer for providing fluorescent micro-particles.

The protocol for single-bacterium presentation with the FluidFM is similar enough to the agonist dispensing protocol that I won't repeat it in full. However, a few parts need to be described:

Preparing fluorescent bacteria: b.Subtilis were grown in 2 mL LB Broth at 37 °C and 235 RPM in a shaking incubator for 1-2 days until increased in density. We then stained them with MemBrite Fix 640/660 from Biotium (30097-T) following manufacturer directions. Stocks were stored in 50% glycerol/LB Broth at -80 °C until ready for use.

To use, an aliquot was thawed and mixed into 1 mL broth in a 50 mm microscope dish (the same as used for macorphage culture for FluidFM experiments) and placed in the live-cell incubation chamber of the microscope to equilibrate at 37 °C until ready to use.

Picking up bacteria and rinsing the probe: To pick up a bacterium, we attached an empty Nanopipette probe (apeture 500 nm) to the FluidFM and placed the bacteria dish underneath it on the stage. We approached the probe to the surface, raised it 1 micron, and positioned it over a single bacterium, using fluorescence microscopy to visualize the bacteria. We then applied -30 mbar underpressure and moved the probe and dish until a bacterium became stuck on the probe opening. We retracted the probe in the dish to make sure it was well-adhered. If not, the underpressure could be increased to -100 or -300 mbar.

To remove any contamination from the bacteria culture, we rinsed the probe 4 times in endotoxin-free water, checking after each rinse that the bacterium was still attached to the tip by looking for the fluorescent signal. After 4 rinses the probe was lowered into the macrophage dish.

Negative controls: For negative controls we used polystyrene microparticles, stained with CY3 or CY5 dye, 1 µm in size (comparable to the b.Subtilis), with a non-immunogenic

coating (Moser et al. [2017]). We also did a washing control by putting the probe in the bacteria dish without picking up any, then rinsing it off and putting it in the macrophage dish to make sure it wouldn't activate the cells.

Multiple contact stimulation with a bacterium: To do the multiple contact experiments, we used the NanoSurf software "force distance spectroscopy" function. This method approaches the cell to a certain setpoint, pauses, then withdraws and repeats a set number of times. The user can specify the approach speed and distance, force setpoint, pause time, withdrawal speed and distance, time between repeats, and number of repeats. In this way we can automate multiple contact stimulation (Figure 6.1).

Area scanning stimulation with bacterium: To do the area scanning stimulation, we used the AFM imaging mode of the FludFM. We set parameters to scan back and forth across the cell surface at a set speed. We defined a square that covered the majority of the cell area, then set a speed and spacing between scanned rows that would cover the surface in a few minutes, but not moving so fast as to damage the cell or prevent contact with the bacterium. We used force feedback mode to ensure the probe followed the contours of the cell surface, rather than remaining at a set height.

Though we were able to successfully scan a b.Subtilis bacterium over the cell surface several times, we never saw a response, so we paused those experiments and did not finish collecting a full dataset. This method, however, could be used again in future if needed.

Other parameters we have explored include:

- Type of bacterium (b.Subtilis, s.Gresius, s.Epidermidis)
- Contact area
- Contact time
- Number of contacts
- Approach speed
- Antigen orientation/binding availability (LTA-coated beads vs b.Subtilis)

- Number of bacteria (in progress)
- Bacteria viability/damage (in progress)

Several of these parameters are included in figure 6.1.

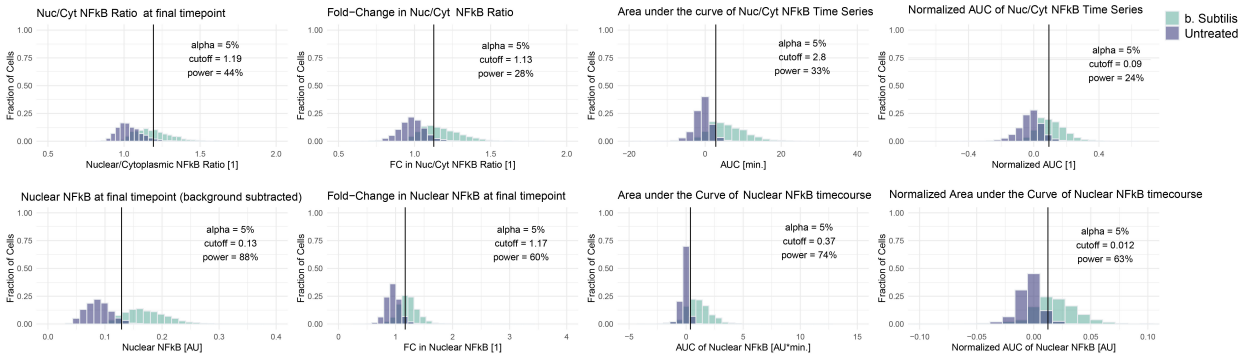

Figure 6.2: Comparison of quantification metrics for activation of macrophages stimulated with b.Subtilis in solution (green bars) compared with untreated control (purple bars). Metric given in title and x-axis title. Each plot labeled with the cutoff value (cutoff), percent negative population above cutoff (alpha, set at 5%), and percent positive population above the cutoff (power). Vertical line shows cutoff location. Significance between groups from Wilcoxon test p = 10^{-16} for all plots.

Quantifying the macrophage response: We quantified this data using the same CellProfiler method as for the single-cell agonist dispensing experiments (see appendix D.2, with pixel sizes matched to 40x magnification. Since we have extensive time series data for these cells, however, we wanted to use a metric that incorporated this information into a more comprehensive (and hopefully sensitive) response than simply the final timepoint measurement. We took calibration data from bulk bacteria stimulation of macrophages, and quantified the response with several metrics. Fluorescence images of NFκB reporter cells quantified with CellProfiler as described in Appendix D.2. In the end, the most sensitive method that incorporated time series information was the nuclear intensity area under the curve over time (Nuclear Intensity AUC) (Figure 6.2).

Details of metrics shown in Figure 6.2:

- Nuc/Cyt NFκB Ratio at final timepoint: For final timepoint images, divide the mean GFP intensity in the nucleus by the cytoplasm value for each cell (after background

subtraction).

- Nuclear NFκB at final timepoint (background subtracted): Final timepoint images, mean GFP intensity in the nucleus (after background subtraction).
- Fold-Change in Nuc/Cyt NFκB Ratio: Fold-change between initial and final timepoint values of the Nuc/Cyt mean GFP intensity ratio.
- Fold-Change in Nuclear NFκB at final timepoint: Fold-change between inital and final timepoint values of nuclear GFP intensity (after background subtraction).
- Area under the curve of Nuc/Cyt NFκB Time Series: Plot Nuc/Cyt mean GFP intensity ratio over time, find the area under the curve, minus the starting value. Data taken in 5 minute intervals from before stimulation to 30-40 minutes after stimulation.
- Area under the curve of Nuclear NFκB timecourse. Plot the nuclear mean GFP intensity (background subtracted) over time, take the area under the curve (same as above item).
- Normalized AUC of Nuc/Cyt NFκB Time Series: normalize the "Area under the curve of Nuc/Cyt NFκB Time Series" by total imaging time.
- Normalized Area under the curve of Nuclear NFκB timecourse: normalize the " Area under the curve of Nuclear NFκB timecourse" by total imaging time.

6.3 Preliminary Results

Types of bacteria or particle:

- Blank bead: polystyrene micro-particle, 1 µm size, coated with TEOS-mercaptosilane as described in Moser et al. [2017], loaded with Cy3 or Cy5 fluorescent dye.
- LTA-coated bead: same as above, with Lipoteichoic acid (LTA) attached to the surface with a PEG linker as described in Moser et al. [2017].
- B.Subtilis: bacilis Subtilis bacterium, stained with WGA 640 R or MemBrite 640/660 membrane stain.

- S. Epidermidis: staph Epidermidis bacterium, stained with MemBrite 640/660 membrane stain.

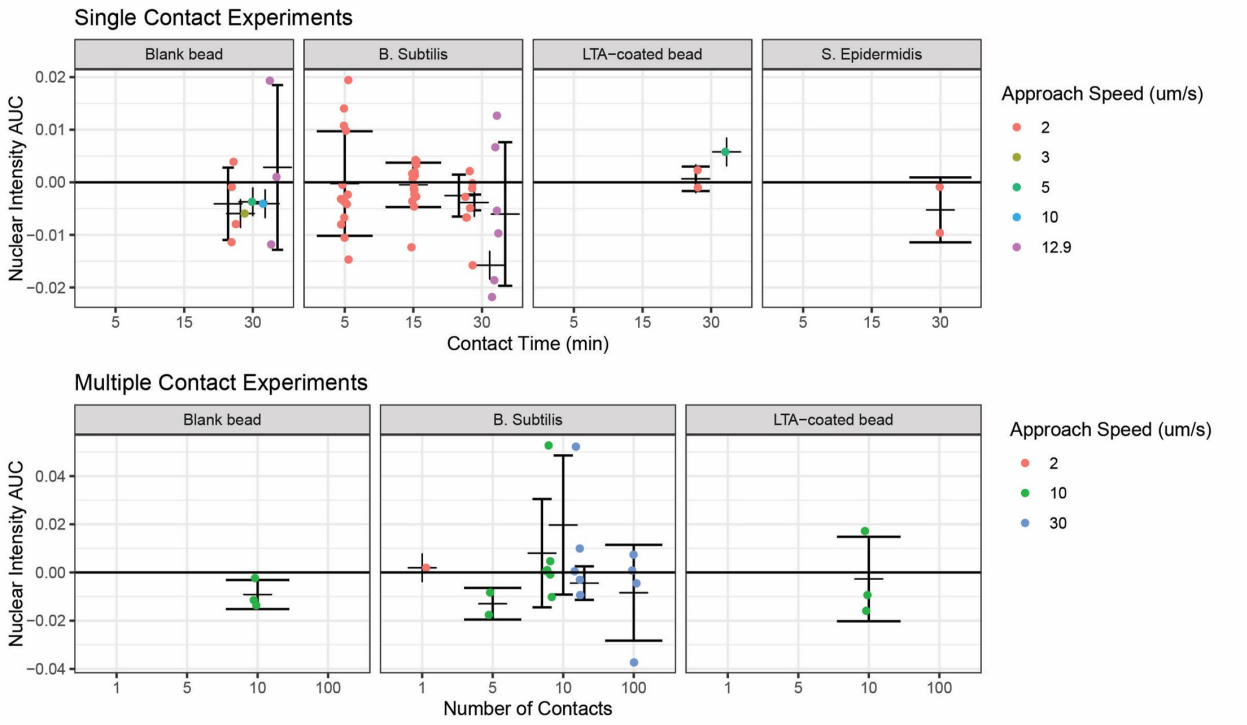

Figure 6.3: Preliminary results from single macrophage bacterium interaction experiments. Points colored by approach speed of the probe to the target cell, vertical axis is nuclear intensity area under the curve. Facets are type of bacteria or particle (see list below). Top row of plots, horizontal axis is contact time between probe and macrophage. Bottom row of plots, horizontal axis is number of contacts between probe and macrophage.

The results so far (figure 6.3) have yielded no significant difference between the negative controls and b.Subtilis stimulation. There have been some indications that increased approach speed and number of contacts might slightly increase the response, but nothing above baseline with multiple repetitions.

We considered that maybe it was an issue with agonist availability, since the LTA coating the bacteria is bound by its lipid tails, which also need to be accessible to bind TLR2. However, using LTA-coated microparticles where the lipid tails face outwards did not yield a higher response, and we put aside that avenue of investigation for now.

6.4 Conclusions and future directions

These results surprised us; although we have seen isolated incidents of single macrophages becoming activated by single bacterium stimulation, nothing has been consistent or strong as one would expect from an immune cell whose job it is to detect pathogens being given sustained and/or repeated contact with a whole pathogen. This result raises several questions. Are the TLR receptors not binding? Or maybe there needs to be more TLR binding, such as multiple bacteria would cause? Is the LTA on the bacteria surface being removed by TLR binding, and thus increased time/contacts does not yield further TLR stimulation? Is TLR binding not the main method of pathogen-detection? Does the bacterium need to be free and detached from the probe for optimal detection? If so, what is different about that situation that would enable a stronger response?

Our most recent hypothesis comes from Kagan [2023], who posits that damaged or otherwise malfunctioning bacteria elicit immune responses while intact, healthy bacteria do not. To this end, our most recent efforts have focused on damaging the bacteria prior to presentation to the macrophages. Sara developed a protocol to use short ethanol exposure for this; we are also looking into antibiotics that would damage the bacteria in different ways. Also still needed is a way to measure the damage done to the bacterium, in order to understand how damaging it would impact its contact with the cell. So far our results with this method have yielded a high rate of macrophage death, so we may shift to look at pyroptosis and inflammasome activation as an alternative readout to NF$\varkappa$B activation.

Following the hypothesis of multiple bacteria needed for a response, we are working on methods to isolate a small number of bacteria on the tip of the FluidFM probe. We have attempted to form bio-films that might be broken up into multi-bacteria chunks, though so far we have not achieved a cohesive join between the bacteria. We are considering other methods to adhere the bacteria together in drops as well, such as by embedding them in an alginate gel, for example using the method described by Zhang et al. [2021].

CHAPTER 7

DISCUSSION

7.1 Results and Conclusions

My research as a whole focused on developing the Fluidic Force Microscopy method for use in single immune cell studies. I determined how to use this methodology to stimulate immune cells, including culture conditions compatible with the instrument and cell responses, and key stimulation parameters for a targeted response. I also derived and fit an analytical model for diffusion from a constantly-dispensing point source that I used to estimate the concentration of a small molecule stimulus dispensed from the probe. This model was key in connecting single-cell responses to FluidFM stimulation with the agonist concentration and gradient at each cell location. With the protocol I developed I was able to concentrate TLR stimulation down to the single-cell level in culture, producing a highly-localized response within a wider, undisturbed environment.

As a first case, I applied this method to studying single macrophages in culture under TLR stimulation, and discovered a surprisingly low temporal threshold for single-cell activation, especially compared to whole culture stimulation. I also observed a density-dependence of the group response at brief stimulation times, leading me to investigate possible cell to cell communication mechanisms for this phenomenon. My initial results from this mechanism search indicated that conditioned media inhibited the whole culture response to stimulation, when compared with fresh media, and treatment with protein-export inhibitors targeting the Golgi did not impact this phenomenon.

My conclusions from this project were first, that Fluidic Force Microscopy was a viable tool for future studies of single immune cell stimulation and group coordination in response. Secondly, the activation threshold of single macrophages stimulated with R848 is estimated to be 5 minutes at 100 nM dose, which is shorter than previously observed TLR stimula-

tion, and also lower than the activation threshold for whole culture stimulation with R848. Thirdly, when the macrophages are stimulated as a group (anywhere from tens to hundreds to hundreds of thousands of cells), sparse cultures have a higher NFκB response than dense cultures. Fourth, this difference in response is most pronounced for short timescale stimulation (5 minutes), and reduces with longer stimulation time (15 minutes), as the group activation threshold decreases to the level of the single-cell activation threshold. Lastly, while I was not able to conclusively identify a single mechanism, my results thus far have put limits on potential mechanisms including: it is likely a secreted factor, it should be present in resting culture or produced quickly after TLR stimulation (within 5 to 15 minutes), it is not secreted via the Golgi Apparatus, it should be related to culture density, it should diffuse throughout the culture beyond just the cell's nearest neighbors, and it should have some effect on the NFκB response to TLR stimulation. In the future I hope to be able to identify this mechanism.

The latter part of my thesis research included a second project on single pathogen-macrophage interactions using the FluidFM. Thus far Sara and I have developed a method to present single pathogens to single immune cells with control over the physical parameters of the interaction such as distance, contact force, duration, area, number, and frequency. We can also pre-treat the pathogens or macrophages before interaction to change their state. Lastly, we can monitor any impact on surrounding cells from the target cell response. So far our results indicate that macrophages are surprisingly insensitive to single-bacteria stimulation. We have ruled out several physical parameters of the interaction as key to a strong response, including contact time, area, speed, and number of contacts. We will continue to explore other parameters such as number of bacteria and bacteria health/integrity. From our preliminary data we have concluded that contact with a single bacteria (and however much TLR stimulation that provides) is insufficient to activate most target macrophages.

7.2 Next Steps and Future Directions

I have several ongoing projects to follow up on my results in this thesis. For the mechanism search, I am continuing to look at potential mechanisms, especially those relating to nitric oxide production, as it has yielded the best results so far, and has been previously shown to function as a quorum sensing signal. When I identify a potential mechanism, I will test several inhibitors as well as activators, in whole culture studies and in FluidFM group stimulation studies, to confirm that it is the mechanism for my observations. I am also continuing to characterize the resting supernatant at different densities. More analysis can be done with the proteomics data, and other factors can be identified in the media. I will continue with extracellular vesicle isolation and analysis. I also want to look for non-protein factors. Lastly, RNA sequencing of the cells themselves might yield insights into culture density impacts on cell state.

For the pathogen presentation project, we are currently working on damaging single bacteria with ethanol or antibiotics. We want to characterize the degree of damage and its impact on cell state. We are following up on some preliminary data that might indicate pyroptosis and inflammasome activation when presented with these damaged bacteria. It may be that NFκB activation is not the best readout for this experiment. We also need to develop better methods for presenting large bacteria that are not easy to immobilize on the probe tip. And we are investigating ways to create bacteria clumps of different sizes, either through bio-film growth, or encapsulation in polymer droplets.

Further in the future, the techniques and results in this thesis could lead in many different directions. First, my methods for dispensing TLR agonist with the FluidFM could be combined with more complex cell culture environments. Cultures of multiple cell types could be used to model resident macrophages in their host tissue, and examine different macrophage densities when present with other cells. Patterned co-culture techniques could expand this to further tune cell type placement and communication (Whitesides et al. [2001]). More recent

techniques can create highly complex cultures (Park et al. [2017]). In co-culture settings, the FluidFM stimulation could be targeted at the non-macrophage cells, to examine how they might cooperate with the macrophages in immune surveillance. The culture could also be plated on a substrate that mimics the extracellular matrix such as collagen or matrigel to look at cell motion and communication when on a softer surface. Treatments could also be incorporated into the cell media to pre-treat the macrophages before stimulation.

My research also focused on the short-term, direct response to stimulation with the FluidFM. However, when stimulated for longer times, more complex NF$\varkappa$B dynamics could be studied, as well as downstream responses like cytokine production. (Yde et al. [2011]) predict that cytokines emitting from a single activated cell would create propagating waves in tissue; the FluidFM technique would be a powerful method for testing this model.

The single-pathogen presentation research could be expanded into these contexts as well, once parameters for reliably activating the target macrophage are identified. Our research so far has focused on gram-positive bacteria, but other pathogens could be studied with this method.

Beyond using the FluidFM, it would be valuable to investigate local stimulation and response of the immune response on the single cell level in an *in vivo* system. For example, zebrafish have been identified as a model system for immunology as they have both an innate and adaptive immune system, can be genetically modified to monitor different cell types, and studied live with fluorescence microscopy (Bailone et al. [2020]). I would be interested in studying the behavior of immune cells near the site of a small stimulation, such as might happen with an infection or vaccine injection. In doing my research I was unable to find answers about the length and timescales of adjuvant or agonist distribution in a tissue during an infection or vaccination. I wanted this information to compare the conditions I had created with the FluidFM. These questions might be better answered in a living system, and could be used to guide *in vitro* experiments with the FluidFM or other techniques. And

examination of individual macrophage responses *in vivo* could confirm or expand my *in vitro* observations.

In summary, my thesis research opened up a lot of experimental possibilities and unanswered questions, which I hope will provide fruitful ground for others to explore in the future.

APPENDIX A

MATERIALS AND RESOURCES

Raw datasets and original code available online at DOI:10.17632/mfyddz6n8k.1

Reagents:

- Resiquimod (R848), Invivogen (tlrl-r848)
- CO_2 Independent Medium, Fisher (18045088)
- Hoechst33342 trihydrochloride, tryhydrate, Fisher (H3570)
- DMEM (Dulbecco's Modified Eagle Medium), Life Technologies (11995-073)
- FBS (Fetal Bovine Serum), Thermo Fisher Scientific (NC0363634)
- HIFBS (Heat-inactivated FBS), Thermo Fisher - Pierce (16140071)
- HEPES sodium salt, Thermo Scientific (A16516.22)
- NovoRinse, Aglient (872B603)
- NovoClean, Aglient (872B602)
- AlexaFluor488, Thermo-Fisher (33077A)
- MemBrite Fix 640/660, Biotium (30097-T)
- WGA-640R, Biotium (29026-1)
- LB Broth, Lennox (BP1427-500)
- GolgiStop, BD Biosciences (554724)
- GolgiPlug, BD Biosciences (555029)
- Aspirin, Sigma-Aldrich (A2093-100G)
- Acetaminophen, Sigma-Aldrich (A7085-100G)
- L-NIL, Cayman (80310)
- NS-398, Millipore Sigma (349254-5MG)
- Istradefylline, Sigma-Aldrich (SML0422-5MG)
- EGTA, Millipore (324626)
- Apyrase, Sigma-Aldrich (A6535-100UN)

- EDTA, Sigma-Aldrich (EDS)
- Protease/Phosphatase Inhibitor, Cell Signaling Technology (5872S)
- QUANTI-Blue (Alkaline phosphatase detection medium), InvivoGen (rep-qbs)
- Griess Reagent, Sigma (G4410-10G)

Cell Lines:

- Murine: RAW264.7 Macrophages, GFP NF-$\varkappa$B reporter, gift from Iain Fraser lab Sung et al. [2014]
- Murine: RAW Blue NF$\varkappa$B SEAP reporter macrophages, InvivoGen (raw-sp)
- b.Subtilis bacteria, Microbiologics (0540K), ATCC 19659
- s.Epidermidis bacteria, ATCC (14990)

Software:

- FIJI, https://fiji.sc, Schindelin et al. [2019]
- CellProfiler. https://cellprofiler.org, McQuin et al. [2018]
- R Studio, http://www.rstudio.com, Team [2020]
- GraphPad Prism, http://graphpad.com
- Mathematica, https://www.wolfram.com/mathematica/, Research [2022]

Instruments:

- FlexAFM, NanoSurf
- Zeiss Axio Observer 7 Inverted Optical Microscope
- Hammatsu Flash sCMOS Camera

Other Materials:

- Microscopy dishes 50 mm x 7 mm, clear wall, glass bottom, TedPella (14027-200)
- 8-well Chambered Coverglass, Ibidi (80826)
- 18-well Chambered Coverglass, Ibidi (81816)
- FluidFM micropipette 2 N/m stiffness, 2 µm aperture, Cytosurge
- FluidFM nanopipette 2 N/m stiffness, 300 µm apeture, Cytosurge

- FluidFM pneumatic connector, Cytosurge

APPENDIX B

DETAILED FLUIDFM PROTOCOL

B.1 Culture NFκB Reporter Macrophages

1. Thaw NFκB reporter macrophages and plate in T75 in DMEM media with 20% FBS
2. Grow 2 days at 37C and 5% CO_2
3. Passage 1 million cells to T75 with DMEM + 10
4. Grow 2-4 days at 37C and 5% CO_2 until ready to passage again
5. Plate cells for FluidFM experiment:
   (a) 500,000 cells in 2 mL media in 50 mm microscope dish for overnight incubation
   (b) 200,000 cells in 2 mL media in 50 mm microscope dish for 2 nights incubation
   (c) Make sure cells are well distributed in dish by shaking gently
6. Incubate cells at 37C and 5% CO_2 for 1 or 2 nights depending on plating density. Final culture density should be around 500 cells/mm^2, relatively sparse with few clumps.

CRITICAL: macrophages should be used between passages 2 and 8 for most consistent results. Replace with new batch about once a month. Do not start experiment if visible blebbing, cell debris in dish, or elevated resting NFκB activation.

B.2 Set up FluidFM and prepare cell culture

1. Warm up microscope and open software
   (a) Open microscope software, Nanosurf C3000 FluidFM software, and Cytosurge software
   (b) Warm up microscope incubation box to 37°C
2. Prepare cells
   (a) Prepare CO_2 independent medium with HIFBS as described above. Warm to 37C.

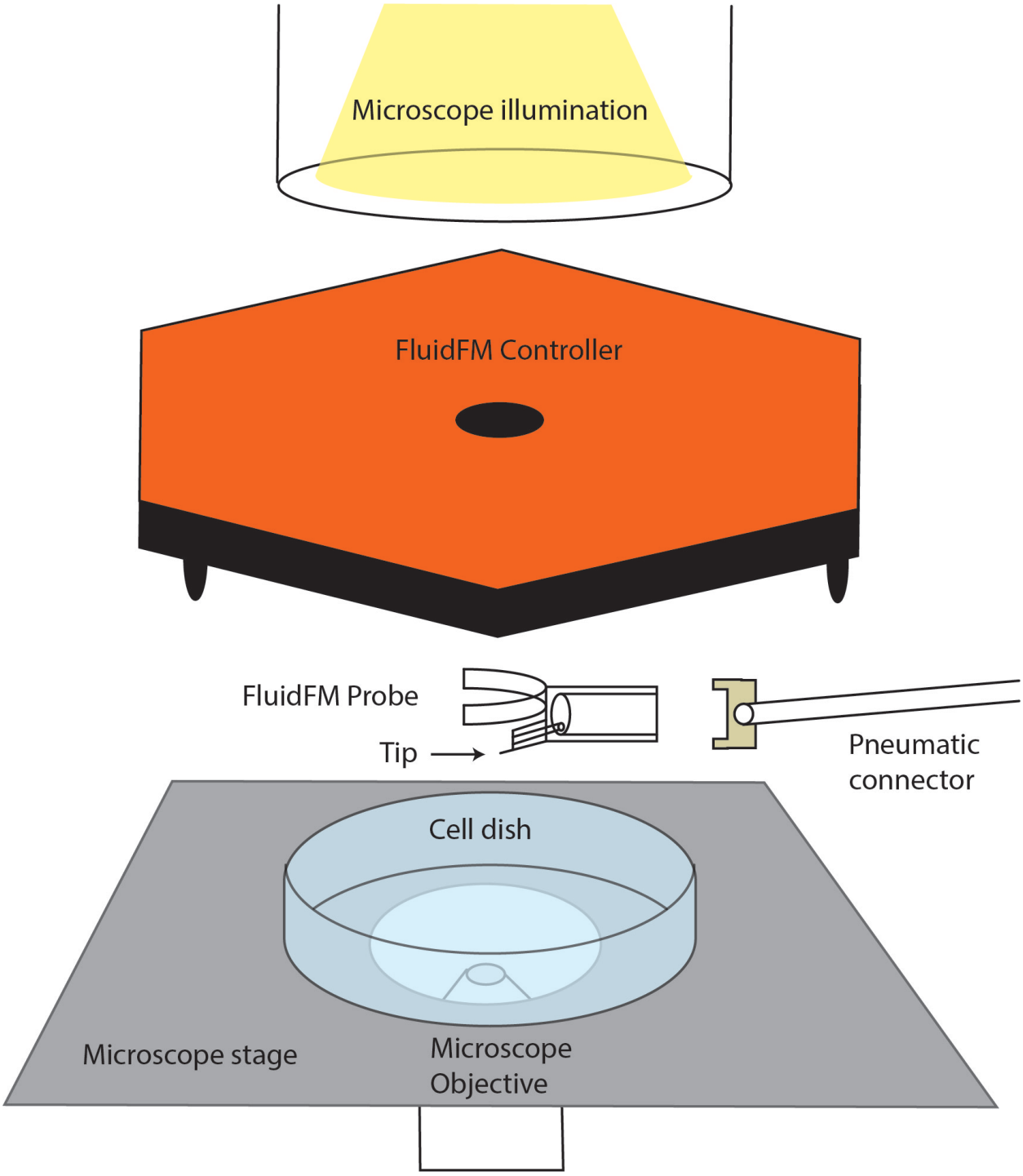

Figure B.1: Diagram of FluidFM Setup. Bottom to top: place cell dish on microscope stage centered over the objective. Fill probe and connect pneumatic connector to back, and clip to underside of controller. Place controller on stage so tip is lowered into dish. Lower microscope illumination head over controller.

(b) Dilute Hoechst 33342 nuclear stain to 10 µg/mL in PBS

(c) Remove growth media from 50 mm culture dishes plated as described above

(d) Replace with 2 mL CO_2 independent medium with HIFBS

(e) Add Hoechst solution 1:100 (final concentration 100 ng/mL) to cell dish

(f) Incubate at 37°C for at least 1 hr. (can put in microscope incubation chamber). Protect from light. CRITICAL: you must allow the cells to equilibrate to their new media at 37°C before stimulating them. If they are not at the correct pH or temperature, they will not be healthy or responsive and the hoechst stain efficiency will decrease.

(g) While the cells are incubating, continue preparing the FluidFM

3. Prepare agonist solution

(a) Dilute agonist in sterile, filtered, endotoxin-free water to desired concentration.

(b) Optional: To reduce chance of clogging, sterile filter solution with a 0.22 µm membrane.

4. Set up FluidFM for dispensing

(a) Clip micropipette probe (2 µm opening, 2 N/m stiffness) onto canticlip holder

(b) Fill probe reservoir with 10 µL of agonist solution

(c) Attach pneumatic tubing to back of probe

5. Set up FluidFM for dispensing

(a) Position controller on stage and connect power cable, pneumatic nozzle, and laser cable

(b) Lift up probe and clip on to controller, attach pneumatic tubing to nozzle. Place coverslip on stage to protect objective. Place controller gently back down, check to make sure probe does not crash into slide.

(c) Align FluidFM laser following instructions in Cytosurge software. If encountering issues, check https://www.cytosurge.com/support or the Troubleshooting section

(d) Fill probe by applying 1000 mbar overpressure until you see a drop forming at the tip. Turn off pressure

(e) Place 500 µL drop of water on coverslip beneath probe

   i. Turn off the laser (in the Nanosurf software, go to "advanced settings -> SPM settings -> laser off". CRITICAL: if you don't turn off the laser, you could damage your eyes when looking at the underside of the probe.

   ii. Gently tilt back the controller with one hand

   iii. With your other hand, pipette a drop of water into the center of the coverslip. CRITICAL: be very careful not to get the pipette tip or your hands anywhere near the probe!

   iv. Gently place the controller back down, making sure the water drop makes good contact with the canticlip holder

(f) Align FluidFM laser in water

   i. Turn the laser back on

   ii. Align the laser same as before. You should have to make just a small adjustment.

(g) Rinse probe to remove any agonist from the outer surface

   i. Remove the previous coverslip and water drop using a folded tissue to absorb the water and stick to the coverslip. CRITICAL: fold the tissue neatly, don't crumple it, and be very careful not to allow any edge of it to go near the probe.

   ii. Place a new coverslip on the stage

   iii. Pipette two drops of endotoxin-free water approximately 250 µL each on either end of the coverslip. Position one in the center underneath the probe.

   iv. Lower the controller so the probe is submerged in the first drop. Let sit 5 min.

v. Lift up the controller and move the coverslip so the second drop is centered

vi. Lower the probe into the second drop. Let sit 5 minutes. Pause point: you can leave the probe soaking for longer if needed.

(h) Position cell dish underneath controller

i. Remove the coverslip as described above

ii. Place the cell dish on the stage underneath the controller with the lid removed.

iii. Replace the controller on the stage to submerge the probe in the media

B.3 Stimulate and Image target area in culture, clean probe

1. Locate area in dish to target: use the microscope software to identify an area of the dish with healthy, unactivated cells and an even density, not too sparse nor overgrown.
2. Approach and position probe
   (a) Use FluidFM controller at 200 mV setpoint to approach probe to an empty spot in your target area.
   (b) Position probe over target cell or spot using the knobs on the side of the stage
3. Image cells before stimulation
   (a) Use the Hoechst, GFP, and Brightfield or DIC channels
   (b) *reduce UV intensity and exposure time as much as possible to prevent irritating the macrophages
   (c) GFP fluorescence will be dim, but be careful not to photobleach! Instead, take a set of 10 images (no delay) at each timepoint and average them together to improve image quality.
4. Dispense agonist to stimulate target cell(s)
   (a) Apply overpressure to dispense agonist for the desired stimulation time. I used 4 mbar overpressure for close-distance single-cell targeting, and 400 mbar pressure for group targeting. I used stimulation times of 5 and 15 minutes.

(b) At end of stimulation time, change pressure setpoint back to zero and retract probe 100 um.

(c) Leave controller in place until imaging is completed - attempting to move it may jostle the cell dish.

5. Image cells to monitor response

(a) Image cells in 5 or 15 minute intervals, as needed, to monitor NF$\varkappa$B response. Save a set of Hoechst, GFP, and Brightfield/DIC images at each timepoint.

(b) The reporter macrophages should reach maximum response by 30-40 minutes, but they can respond in as little as 10-15 minutes.

6. Clean probe for next use

(a) When imaging is completed, remove cell dish from underneath controller, place aside in a safe place, and replace lid.

(b) Put a coverslip on the microscope stage and put a drop of NovoRinse solution in the center. Alternative: another ethanol-based cleaning solution would work here.

(c) Replace controller on stage so probe is submerged. Soak 10 minutes.

(d) Swap out the NovoRinse slide for a clean slide and place two drops of water on it, as described in step 5g above.

(e) Soak the probe in each drop of water for 5 minutes. CRITICAL: multiple rinses are required to remove all of the NovoRinse from the probe, which will irritate the macrophages if not completely rinsed off. Pause Point: you can leave the probe soaking in water for longer if needed.

(f) Remove the water slide, and replace the cell dish back underneath the controller as described in 5h.

(g) Repeat steps 6-11 to take a second dataset. On last dataset, skip step 11 and proceed to cleanup (below) instead.

B.4 Clean Up

1. Clean probe
   (a) Soak the probe in a drop of NovoClean solution for 10 minutes (as described in step 5g). Alternative: use a dilute bleach solution. Be careful, though, as too much exposure will corrode the metal contact at the base of the canticlip holder.
   (b) Rinse briefly with water.
2. Empty and store probe
   (a) Remove probe from FluidFM controller and replace on pedestal
   (b) Remove tubing and empty reservoir with pipette.
   (c) Rinse out reservoir with 10 uL sterile water
   (d) Replace tubing. Detach nozzle from FluidFM controller and reattach to tubing to reconnect probe to pneumatic system
   (e) Locate the syringe port in the pneumatic line. Attach an empty 30 mL syringe to the port. Turn the valve to connect syringe to the probe.
   (f) Apply negative pressure with the syringe to vacuum residual solution from the probe channel into the reservoir. Alternative: you can apply positive syringe pressure to empty the probe as well. It will take longer and has a risk of clogging, but it has lower risk of introducing bubbles into the channel.
   (g) Release the syringe pressure. Disconnect tubing from nozzle and probe and store for reuse.
   (h) Empty and rinse probe reservoir again.
   (i) Remove probe from canticlip holder and place back in box. Add 1 mL sterile water to box to soak probe.
   (j) Tape box closed and store at room temperature. As the water evaporates, it will draw residual solution out of the probe.
3. Store FluidFM and shut down instruments/computers

(a) The FluidFM controller can be left on the microscope stage, or stored in its box, depending on use of the microscope.

   i. Be careful detaching the laser cable, pneumatic tubing, and power cable! Bending the cables near their attachment points can lead to bent pins, frayed wires, or split tubing.

   ii. It is recommended that only trusted instrument users move the FluidFM to and from the microscope stage.

(b) Turn off the instruments and software in the reverse order you turned them on.

B.5 Negative Controls

Run the above protocol with dispensing endotoxin-free water. If there is still NFκB activation of target cell(s), adjust protocol (increase rinsing time or number of rinses, etc) to improve sterility and prevent contamination from cleaning solutions or extra agonist.

APPENDIX C

FLUIDFM TROUBLESHOOTING

Probe clogged after single use

There are several things you can do to prolong probe life and prevent clogging or damage. Cleaning promptly after each use, emptying before storage, storing in water, rinsing off all cleaning solutions thoroughly, etc. When these measures are not sufficient, you can also clean the probe with oxygen plasma.

Probe still clogged or visibly dirty after cleaning

Try cleaning with oxygen plasma. Load probes into a plasma etch instrument (remove from box, place in pyrex dish. Make sure tip will not crash into anything!). Apply Oxygen plasma at 20 cc/min, 200W power, 3-5 minutes duration. Store dry or in water until next use.

Cannot align laser in air

Check that the laser is centered on the probe tip. Sometimes a strong reflection can be mistaken for the laser if it is far off-center. Next, try moving the detector screws so that the detector indicator is far off-center - this can help in picking up a weak signal. Try also moving the laser further up the probe length, and it sometimes gives a stronger signal than at the very tip. If adjusting the laser and detector position doesn't help, the next step is to clean the probe of any gunk that may be scattering the laser light. Soaking in an ethanol or bleach-based solution, followed by water, may help in many cases. For a stronger cleaning, use oxygen plasma as described above. You may also want to clean the canticlip holder window. A 70% EtOH solution applied with lens paper to both the inner and outer surface, followed by an anti-fogging spray applied to the inner surface, usually works well. If none of this helps, switch to a new probe.

Cannot align laser in liquid

The first potential issue is bad liquid contact leading to pockets of air between the

canticlip window and the probe. Especially if the probe is dry before lowering into liquid, this is likely to occur. The probe might be blurry even when in focus, or you might see a shadow cast by an air bubble. The first solution is to tilt the controller vertically and allow any water to run down to the space between the probe and the window, to dislodge any air bubbles. If this doesn't work, hold the controller upside down and VERY CAREFULLY pipette 40 µL of water onto the window to wet it before replacing the controller on the stage. You can tell if you've made good contact because the image should become clear, and the laser alignment should shift just slightly from where it was aligned in air. The image of the laser should be clear; if it is blurry as if seen through wavy glass, that might indicate condensation on the inside of the canticlip holder window. In this case, you will need to clean and reapply anti-fogging spray to the inside of the window. (Without this anti-condensation coating, the combination of heat and water create a humid environment underneath the controller that creates condensation on the glass.) If none of the above helps, the issue may be probe cleanliness. There is often a small drop in signal between air alignment and liquid alignment, so even if the probe was aligned in air it may lose signal in the water. Again, the probe may be cleaned by soaking in an ethanol or bleach-based solution, followed by water. For a stronger cleaning, use oxygen plasma as described above.

Cannot find laser and/or probe

If the laser or the probe are far off-center when you attempt to focus the microscope, the range of motion allowed by the stage control screws or laser control screws will not allow you to find them. First, check that the controller is firmly seated in the divots in the stage beneath each leg. Second, check that the probe is clipped onto the holder and the holder to the controller as far down as possible, centered, and level. Third, try using a lower-magnification objective to locate the probe and center it, before switching to a higher magnification objective that has a smaller field of view. Try moving the stage downwards to find the edge of the plastic where the tip is attached, then move along the edge until you

see the tip come into view. If you cannot find the laser, try first looking for its reflection to give some direction. Check that the laser cable is fully plugged in and the "laser off" box is unchecked in the NanoSurf software. Also try moving the stage and laser to their limits to search the space. Check that the probe is centered, because focusing on an off-center probe can lead to the laser being out of view. Try taking the probe off the controller and replacing it, and repositioning everything. Try moving the probe to home position, where the laser should be in view. Do a systematic sweep of the space using the laser control screws.

Probe will not fill or dispense

There are two possible explanations for this; either there is a clog preventing the probe from filling, or there is a pressure leak somewhere in the pneumatic system. To clear a clog, see cleaning methods suggested above. To test for a leak, apply manual pressure with a 10 mL syringe of air applied to the port in the pressure line. If you are able to push the plunger all the way down, there is a leak. The most common place for a leak to occur is in the pneumatic connector, right behind the attachment to the probe. The delicate tubing often splits there, because it requires some force to attach the connector to the probe and it is difficult to avoid pressing on the tubing. If the tubing is split, replace with a new pneumatic connector. Leaking tubing can be fixed with a small amount of epoxy.

Approach failed or stops early

The approach will fail due to loss of laser signal, or stop early if the force feedback is triggered by a stray vibration. Try increasing the force set-point. Check that the laser is on and still aligned. Sometimes a last that was badly aligned in water will lose signal in media and need to be re-aligned or cleaned to get a stronger signal. Sometimes you will get the "approach failed" error when you contact the surface, because the deflection of the probe moved the laser beyond the limits of the detector. That's okay, because you can still find the surface. To avoid issues with the automatic approach, get the best laser alignment possible before placing the probe into the cell dish. A clean probe and window will generally yield

the best results.

Negative control activating

If your negative controls are causing activation of the macrophages, review your probe cleaning protocols. Any stray ethanol or bleach solution on the probe will irritate the cells. You could increase the number or duration of water rinses. Also make sure the water drop makes complete contact with the probe and holder. Keep your rinsing water as sterile as possible. If still experiencing issues, try dispensing at a greater height or lower pressure, so the dispensed water does not displace the media but rather diffuses into it.

Clean pneumatic tubing

Sometimes when using negative pump pressure, media from the cell dish can get into the pneumatic system. To clean the pneumatic tubing, detach the lengths of tubing from the pump and trap and hang them vertically. Prepare a syringe with a large-bore needle inserted into a spare rubber connector that you would use to attach the tubing to the nozzle. Attach the rubber connector to the nozzle, and screw in one of the pieces of tubing. Fill the syringe with water and push through the tubing. Repeat with second tubing. Then push through air until no more liquid comes out the bottom. Hang to air dry overnight, then reconnect.

Nuclear stain poor quality

If the nuclear stain is old, or the media is not maintaining pH correctly, there may be poor uptake or fluorescence of the nuclear stain. This is especially a problem when the FluidFM probe is positioned over the target cell, because it casts a reflection in the Hoechst channel images that will interfere with segmentation later. To improve nuclear stain quality, use fresh stain and media. You can also clean up a dim image by averaging multiple frames together, adjusting the image thresholds, or increasing exposure time. A background subtraction process will also help. For images where the probe reflection is an issue, use ImageJ to select and delete those sections of the image as best you can. You can also fix uneven illumination in ImageJ by using a flatfield correction, or selecting sections to adjust brightness and contrast

separate from the rest of the image. It is essential for data quality to be able to draw accurate boundaries around each nucleus, so the quality of the nuclear image is important.

TrackObjects in CellProfiler giving bad results

To correlate responses of individual cells across timepoints, you need to be able to track individual cells between consecutive images. CellProfiler has a module for this, but it isn't always perfect. There could be a few reasons for object tracking errors: individual cells may move more than the rest, or die or divide, or their nuclear stain may fail to be detected in all frames. The field of view may shift and cause some cells at the edges to be cut off, or all to be mis-aligned. A lot of this can be addressed with better nuclear staining, and being careful not to disturb the cell dish during imaging. Clumps of cells may be incorrectly segmented frame to frame. The choice of tracking algorithm and parameters may not be optimized for this data, and need some tweaking. One persistent issue is that cells may move unexpectedly and change shape/position dramatically. For these, you may need to correct errors in cell numbering by hand, afterwards.

APPENDIX D

ORIGINAL CODE AND PIPELINES

Original code described below; actual files can be found on Mendeley Data at `DOI:10.17632/mfyddz6n8k.1`.

D.1 Diffusion model in ImageJ and Mathematica

D.1.1 Process Fluorophore dispensing in ImageJ

Intensity and Size vs Time Macro

Quantify dispensed cloud intensity and size over time. Determine time to equilibrium concentration gradient, and time to decay after end of dispensing.

1. Set the scale in px per micron
2. Initialize an empty array to hold the results, include columns for:
    - image name
    - image time-point
    - peak location x and y
    - cloud size in x and y (measure standard deviation of intensity)
    - maxima location
    - maxima mean, median, mode, min, and max intensity
3. Open all images for one run in ImageJ. Make an array to loop over using getImageID().
4. Get the title of the "before dispensing" image of the probe. Remove it from the list of images to loop over (it's not part of the time series).
5. Define global variables:
    - Dispensing time
    - Maxima location for first image without cantilever (best way to identify peak

location without the probe shadow/reflection interfering). Use these coordinates for all images without cantilever.

- Maxima locaiton for images with cantilever: move the y coordinate down 6 microns (convert to px), x coordinate is the same.

6. loop over image array from step 3.
   (a) Get metadata from image filename, convert frame index to time in seconds
   (b) use imageCalculator() to subtract before dispensing cantilever image from dispensing images with cantilever in frame.
   (c) save maxima location according to global variables defined above
   (d) run moment calculator and store results in array from step 2.
   (e) to measure peak brightness, draw an oval centered on the maxima location with a radius equal to 0.14 of standard deviation in x and y (based on a Gaussian dropping to 99% value). measure intensity inside the oval and save to results.
   (f) draw the oval on the image for QC and save.
   (g) save the results to a text file. close all windows.

Intensity vs Distance Macro

1. Set global scale px to micron based on objective
2. Open image of last timepoint before end of dispensing, when cloud is at equilibrium
3. Find maxima location
4. Define a function to make a line, get intensity values along the line with plot profile, record both intensity and distance in the results window, and draw the line on the image.
5. Use the function to measure five lines from maxima to edges of image, avoid cantilever.
6. Save image with lines on it and results window
7. In Excel, average replicates to get an average and SD for concentration vs distance

from the dispensing point for each set of dispensing conditions (AF488 concentration, probe height, and applied pressure). Save as CSV file.

AF488 Reference Slides

1. Open the the cellphone picture of the slides in ImageJ
2. Set the scale for the image using the coverslip dimensions
3. Using the freehand drawing tool, measure the area of each fluorophore drop.
4. Open the fluorescence image for each drop and measure the modal intensity/
5. Record the area and modal intensity for each drop, along with its AF488 concentration.
6. Calculate the drop thickness by dividing the known volume of 1 µL by the measured area.
7. Plot thickness*concentration for each slide against modal intensity
8. Do a linear fit and record the slope. This is the conversion factor of brightness*depth to intensity you need for the diffusion model.

D.1.2 Chi-sq fit of model to data in Mathematica

1. Import intensity vs distance information you got from AF488 dispensing and reference slides
2. Define a function for concentration vs distance, following the theoretical model, then define a function for intensity vs distance, using the conversion factor you got from the calibration slides.
3. Use the SEGWE calculator `https://nmr.chemistry.manchester.ac.uk/?q=node/432` to estimate the diffusion coefficients for AF488 in room temperature water, and your agonist in warm water.
4. Use a chi-square fit to fit the theoretical expression to the dispensing data
   (a) The parameters zmax and A were fit by minimizing chi-squared for the difference

between the dispensing data between 0 and 100 µm distance from the dispensing point and the predicted value for those same points. (In the single cell targeting experiments most cells are within 100 µm of the dispensing point. Including larger distances weighted the distribution too heavily towards the tail, rather than the center where accuracy is most important in order to compute the concentration at the target cell location).

(b) Define a function to compute the chi-sq distance between two lists

(c) Make a list of zmax values to loop over: 400 to 1000 µm, step size 100 µm

(d) Make a list of A values to loop over: 0.4 to 0.7, step size 0.05

(e) Generate predicted I(ρ) curve for each pair of A and zmax values for $\rho = 0$ to 100 µm. Note: cut off data at $r = 235\mu m$ (index 1450) because data is unreliable past this point.

(f) Compute chi-square distance between AF488 dispensing data and the predicted curves

(g) Find pair of parameters that have the smallest chi-square value

(h) Best values for 4 mbar dispensing at 4 µm height: $A = 0.55, zmax = 900\mu m$

(i) Best values for 400 mbar dispensing at 20 µm height: $A = 1.1, zmax = 700\mu m$

5. Once you have the fit parameter, use the model to plot concentration vs distance from the dispensing point at the dish surface for your agonist (make sure to change the diffusion coefficient).

6. Note: we want to change from the spherical coordinate rho to the polar coordinate r so that we can later match concentration values to cell location coordinates in the plane of the dish. For the single-cell targeting at short height the distinction is negligible, but for dispensing at greater heights it is important.

7. Determine the "dilution factor"

(a) Use the concentration model to determine the ratio of concentration at the center

of the dish vs concentration loaded into the probe, called the "dilution factor"

(b) Use the dilution factor to calculate what concentration of agonist to use in order to stimulate the cells at a desired concentration.

D.2 CellProfiler pipeline summary

Pipeline for 100x images:

1. Load GFP and HOECHST images
2. Extract metadata from file names (dataset, channel, timepoint)
3. In NamesAndTypes match up the pairs of channel images and put them in order for processing
4. Group the datasets to be processed separately (so the cell tracking only applies within each dataset)
5. Run "rescale intensity" to brighten the nuclear images (to improve segmentation): set values of 0.6 and above to 1.0
6. Smooth the nuclei with a 30 px median filter
7. Run Identify Primary Objects on the smoothed nuclei. Object diameters 80-250 px, use global thresholding, Otsu method, two classes, correction factor 0.9. (determined empirically to get best results)
8. Run Track Objects. Tracking method LAP, search radius 3 SD, search radius limit 100-2000 px, no second phase. Save "tracked cells" image
9. Expand nuclei objects by 100 px and save as "cell regions" objects
10. Expand the nuclei objects by 10 px and save as "outer ring" to capture the bit of the cytoplasm closest to the nucleus
11. Shrink the nuclei by 16 px to capture a nuclear ROI and correct for oversized nuclei from the brightening in (5) and save as "shrunken nuclei"
12. Run Identify Tertiary Objects and subtract the nuclei objects from the outer ring ob-

jects and save as "cytoplasm" (captures the ring of cytoplasm right outside the nucleus. This approach was chosen because in widefield images the difference in thickness between cytoplasm and nucleus parts of the cell cause the nucleus to seem brighter and the cytoplasm dimmer and this throws off the results. As in Ding et.al. 1998 J. Bio. Chem., sampling the portion of cytoplasm nearest to the nucleus, where the thicknesses are more similar, is a better measure of nuclear vs cytoplasmic GFP fluorescence.)

13. Create a masked image where the "cell regions" objects are masked
14. Measure the intensity of the masked image to get a measure of background intensity
15. Use Image Math to subtract the mean intensity of the masked image from the GFP image, save as "NFκB background subtracted"
16. Measure the GFP intensity in the shrunken nuclei objects
17. Measure the GFP intensity in the cytoplasm objects
18. Use Calculate Math to divide the mean intensity of the shrunken nucleus by the mean intensity of the cytoplasm for each object
19. Make an Overlay Outlines image showing the nucleus, cytoplasm, and cell regions
20. Use Display Data on Image to add the cell numbers from "track objects" and the nuc/cyt ratio from "calculate math" to write these values by each cell on the outlines overlay image
21. Save the annotated images
22. Export the data to spreadsheet

Pipeline for 10x images:

1. Load GFP and HOECHST images
2. Extract metadata from file names (dataset, channel, timepoint)
3. In NamesAndTypes match up the pairs of channel images and put them in order for processing
4. Run Rescale Intensity to brighten the images: set values of 0.6 and above to 1.0

5. Smooth the nuclei with a 3 px median filter
6. Run Enhance or Suppress Features to enhance the smoothed nuclei using "enhance speckles" with feature size of 20 px
7. Run Identify Primary Objects on the smoothed nuclei. Object diameters 8-25 px, use global thresholding, Otsu method, two classes, correction factor 0.9. (determined empirically to get best results)
8. Expand nuclei objects by 10 px and save as "cell regions" objects
9. Expand the nuclei objects by 1 px and save as "outer ring" to capture the bit of the cytoplasm closest to the nucleus
10. Shrink the nuclei by 1 px to capture a nuclear ROI and correct for oversized nuclei from the brightening in (4) and save as "shrunken nuclei"
11. Run Identify Tertiary Objects and subtract the nuclei objects from the outer ring objects and save as "cytoplasm" (captures the ring of cytoplasm right outside the nucleus)
12. Create a masked image where the "cell regions" objects are masked
13. Measure the intensity of the masked image to get a measure of background intensity
14. Use Image Math to subtract the mean intensity of the masked image from the GFP image, save as "NFκB background subtracted"
15. Measure the GFP intensity in the shrunken nuclei objects
16. Measure the GFP intensity in the cytoplasm objects
17. Use Calculate Math to divide the mean intensity of the shrunken nucleus by the mean intensity of the cytoplasm for each object
18. Make an Overlay Outlines image showing the nucleus, cytoplasm, and cell regions
19. Use Display Data on Image to add the nuc/cyt ratio from "calculate math" to write these values by each cell on the outlines overlay image
20. Save the annotated images

21. Export the data to spreadsheet

D.3 Calibration data in R

Find quantitative cutoff for categorizing cells as activated using calibration data.

1. Set up R and import the tidyverse library
2. Read in the csv file with the quantified calibration data (output from CellProfiler).
3. Drop all rows with missing data
4. Find the cutoff value for the top 5% of resting cells
   (a) Count the number of resting cells, multiply by 0.05
   (b) Use "slice max" and "order" to extract the top 5% of the resting cell data
   (c) Get the lowest value from that list, round.
5. Find the power of this cutoff: the percentage of Activated cells above the cutoff.

D.4 Analysis in R

D.4.1 FluidFM Single Cell Targeting Analysis

1. Set up R and import the following libraries: tidyverse, patchwork, ggbeeswarm, and ggforce
2. Import data: single cell data and metadata (from CellProfiler), concentration gradient informaiton (from Mathematica)
3. Data wrangling
   (a) Make a unique run identifier column for the data and metadata
   (b) Use the dilution factor to convert C_0 to C_{max}
   (c) Extract the target cell position for each run and time-point from the cell data (cell data has locations, metadata has target cell number), add to metadata, then join back to cell data.

(d) Compute the distance from the target cell for each cell, in microns

(e) Pivot Wider: transform the data table to one row per cell per run, with the Nuc/Cyt Ratio at each time-point in a separate column

(f) Make "Nuc/Cyt Before" and "Nuc/Cyt Final" columns with values from first and last time-points, then take their ratio to get the Fold-Change in Nuc/Cyt Ratio.

4. Define a bootstrap function for calculating uncertainty in fraction activated (for error bars)

```
#input list of activation data (binary, cutoff already applied)
bootstrap <- function(data) {
#initialize an array to hold the fraction activated values
a <- as.numeric(rep(NA,5000))
n <- length(data) #size of each sample
#sample with replacement and get 5000 fraction activated values
for(i in 1:5000){
    s <- sample(data, size = n, replace = T) #sample the data
    a[i] <- sum(s,na.rm = T)/sum(!is.na(s)) #compute fraction activated
}
sd(a) #compute the variance in the fraction activated values
}
```

5. Bin cells by distance from target to compute fraction activated

(a) Create “binned distance” column and binary “activated” columns using the cutoffs determined from calibration data

(b) Group by Run, binned distance and summarize data. Compute fraction activated based on the two activation metrics: Nuc/Cyt NFκB ratio at final timepoint, and the fold-change “rNC”, and the uncertainty for both using the bootstrap function

6. Make Target cells dose-response curve
    (a) Filter target cells from data by distance = 0
    (b) add binary "activated" columns
    (c) Summarize replicates and calculated fraction activated with uncertainty
    (d) Compute uncertainty in C_{max} form the diffusion model

D.4.2 FluidFM Group Targeting Analysis

1. Set up R and import the following libraries: tidyverse, patchwork, ggbeeswarm, and ggforce
2. Import data: cell data and metadata (from CellProfiler), concentration gradient information (from Mathematica)
3. Data wrangling
    (a) Calculate distance from dispensing point in microns
    (b) Join metadata to data, convert C_0 to Molar units
    (c) Bin cell data by distance from dispensing point, add column for binary activation
    (d) Use pivot wider to match up cells across time-points
    (e) Compute fold-change in Nuc/Cyt ratio between initial and final timepoints
    (f) Group by treatment conditions and run, compute fraction activated
4. Count number of nearest neighbors
    (a) Define a function to count the number of other cells within 18 microns of the target cell
    (b) Loop over cells, grouped by run, and add the number of neighbors to the cell data frame.
5. Compare number of neighbors to culture density
    (a) Filter cells in the center activation zone so as not to weight the data with the outlying unstimulated cells. Distance cutoff depends on C_{max}, determined to be

30 and 100 um from center for 90 nM and 900 nM, respectively.

(b) Determine culture density for each run, based on field of view size and number of cells per image.

(c) Bin number of neighbors, group by treatment condion, density, and number of neighbors bin and summarize fraction activated. use Bootstrap for SE.

6. Bin data in xy grid to calculate fraction activated, join concentration information

(a) Join concentration information to cell data

(b) Create an xy grid of bins, join relative concentration information

(c) Sort cells into bins by locaiton

(d) Group by Run and xy bin, summarise to get fraction activated

(e) Join concentration information for each bin.

7. Plot xy binned data with concentration, number of cells per bin, and fraction activated

8. Functions for statistical significance and effect size:

(a) Permutation analysis for comparing small group to large group. Input combined activation data for two groups you want to compare (binary), size of smaller group for sampling, and experimental fraction activated of small group.

```
perm <- function(data, n, exp_a) {
    a <- as.numeric(rep(NA,5000))
    for(i in 1:5000){
        s <- sample(data, size = n, replace = T)
        a[i] <- sum(s,na.rm = T)/sum(!is.na(s))
    }
    pval = sum(a >= exp_a)/5000
    return(pval)
}
```

(b) Permutation ANOVA to detect significant difference among multiple groups

```
permutation_anova <- function(dat){
    colnames(dat) <- c("g", "d")
    F_exp <- summary(aov(d~g, data=dat))[[1]][1,4]
    groups <- unique(dat$g)
    F_vals <- vector(mode = "numeric")
    for (i in 1:5000) {
        sampled_data <- data.frame(g = dat$g, d = as.numeric(NA))
        n = nrow(sampled_data)
        sampled_data$d <- sample(dat$d, size=n, replace=T)
        F_vals[i] <- summary(aov(d~g, data=sampled_data))[[1]][1,4]
    }
    p_val <- sum(F_vals >= F_exp)/5000
    return(list(p_val, F_exp, F_vals))
}
```

(c) Permutation to determine Effect Size with Uncertainty

```
effect_size3 <- function(dat, g1, g2) {
   #rename columns of dataframe to d and g
   colnames(dat) <- c("g", "d")
   a <- as.numeric(rep(NA,5000))
   group1 <- filter(dat, g==g1)
   group2 <- filter(dat, g==g2)
   n1 <- nrow(group1)
   n2 <- nrow(group2)
   a1 <- sum(group1$d,na.rm = T)/sum(!is.na(group1$d))
```

```
    a2 <- sum(group2$d,na.rm = T)/sum(!is.na(group2$d))
    d_exp <- a2 - a1
    for (i in 1:5000) {
       sample1 <- unlist(sample(group1$d, size=n1, replace=T))
       sample2 <- unlist(sample(group2$d, size=n2, replace=T))
       s1 <- sum(sample1,na.rm = T)/sum(!is.na(sample1))
       s2 <- sum(sample2,na.rm = T)/sum(!is.na(sample2))
       a[i] <- s2 - s1
    }
    SE <- sd(a, na.rm = T)
    return(list(d_exp, SE, a1, a2))
}
```

(d) Use the above funcitons and the R Wilcoxon Test to determine statistical significance and effect size: filter data you want to compare, run the permutation ANOVA for all groups, use the Wilcoxon test (non-parametric pairwise comparisons) to determine pairwise significance, and run the effect size code.

D.4.3 FluidFM Whole Culture Stimulation Analysis

1. Set up R and import the following libraries: tidyverse, patchwork, ggbeeswarm, and ggforce
2. Import data: cell data (from CellProfiler) with metadata
3. Define the bootstrap function for calculating uncertainty in fraction activated as above in section D.4.1, item 4
4. Group data by stimulation concentration and time, summarize to compute fraction activated with uncertainty. (use the activation cutoff from calibration data)

REFERENCES

Antony Adamson, Christopher Boddington, Polly Downton, William Rowe, James Bagnall, Connie Lam, Apolinar Maya-Mendoza, Lorraine Schmidt, Claire V. Harper, David G. Spiller, David A. Rand, Dean A. Jackson, Michael R. H. White, and Pawel Paszek. Signal transduction controls heterogeneous NF-κB dynamics and target gene expression through cytokine-specific refractory states. *Nature Communications*, 7(1):12057, July 2016. ISSN 2041-1723. doi:10.1038/ncomms12057. URL https://www.nature.com/articles/ncomms12057. Number: 1 Publisher: Nature Publishing Group.

Adewunmi Adelaja, Brooks Taylor, Katherine M. Sheu, Yi Liu, Stefanie Luecke, and Alexander Hoffmann. Six distinct NFκB signaling codons convey discrete information to distinguish stimuli and enable appropriate macrophage responses. *Immunity*, 54 (5):916–930.e7, May 2021. ISSN 1074-7613. doi:10.1016/j.immuni.2021.04.011. URL https://www.sciencedirect.com/science/article/pii/S1074761321001734.

Mathias J. Aebersold, Harald Dermutz, László Demkó, José F. Saenz Cogollo, Shiang-Chi Lin, Conrad Burchert, Moritz Schneider, Doris Ling, Csaba Forró, Hana Han, Tomaso Zambelli, and János Vörös. Local Chemical Stimulation of Neurons with the Fluidic Force Microscope (FluidFM). *ChemPhysChem*, 19(10):1234–1244, May 2018. ISSN 1439-4235. doi:10.1002/cphc.201700780. URL https://chemistry-europe-onlinelibrary-wiley-com.proxy.uchicago.edu/doi/full/10.1002/cphc.201700780. Publisher: John Wiley & Sons, Ltd.

Mini Aga, Jyoti J. Watters, Zachary A. Pfeiffer, Gregory J. Wiepz, Julie A. Sommer, and Paul J. Bertics. Evidence for nucleotide receptor modulation of cross talk between MAP kinase and NF-κB signaling pathways in murine RAW 264.7 macrophages. *American Journal of Physiology-Cell Physiology*, 286(4):C923–C930, April 2004. ISSN 0363-6143. doi:10.1152/ajpcell.00417.2003. URL https://journals.physiology.org/doi/full/10.1152/ajpcell.00417.2003. Publisher: American Physiological Society.

Jeonghyun Ahn and Glen N. Barber. STING signaling and host defense against microbial infection. *Experimental & Molecular Medicine*, 51(12):1–10, December 2019. ISSN 2092-6413. doi:10.1038/s12276-019-0333-0. URL http://www.nature.com/articles/s12276-019-0333-0. Number: 12 Publisher: Nature Publishing Group.

Alar Ainla, Gavin Jeffries, and Aldo Jesorka. Hydrodynamic Flow Confinement Technology in Microfluidic Perfusion Devices. *Micromachines*, 3(2):442–461, June 2012. doi:10.3390/mi3020442. URL https://www.mdpi.com/2072-666X/3/2/442. Number: 2 Publisher: Molecular Diversity Preservation International.

Cem Albayrak, Christian A. Jordi, Christoph Zechner, Jing Lin, Colette A. Bichsel, Mustafa Khammash, and Savaş Tay. Digital Quantification of Proteins and mRNA in Single Mammalian Cells. *Molecular Cell*, 61(6):914–924, March 2016. ISSN 1097-2765. doi:10.1016/j.molcel.2016.02.030. URL https://www.sciencedirect.com/science/article/pii/S109727651600174X.

Grégoire Altan-Bonnet, Thierry Mora, and Aleksandra M. Walczak. Quantitative immunology for physicists. *Physics Reports*, 849:1–83, March 2020. ISSN 0370-1573. doi:10.1016/j.physrep.2020.01.001. URL http://www.sciencedirect.com/science/article/pii/S0370157320300090.

Paul Anderson. Post-transcriptional regulons coordinate the initiation and resolution of inflammation. *Nature Reviews Immunology*, 10(1):24–35, January 2010. ISSN 1474-1741. doi:10.1038/nri2685. URL http://www.nature.com/articles/nri2685. Number: 1 Publisher: Nature Publishing Group.

Luca Antonioli, Corrado Blandizzi, Pál Pacher, Martin Guilliams, and György Haskó. Rethinking communication in the immune system: The quorum sensing concept. *Trends in Immunology*, 2019. doi:10.1016/j.it.2018.12.002.

Vanessa F. Arnaud-Sampaio, Izadora L. A. Rabelo, Carolina A. Bento, Talita Glaser, Jean Bezerra, Robson Coutinho-Silva, Henning Ulrich, and Claudiana Lameu. Using Cytometry for Investigation of Purinergic Signaling in Tumor-Associated Macrophages. *Cytometry Part A*, 97(11):1109–1126, 2020. ISSN 1552-4930. doi:10.1002/cyto.a.24035. URL http://onlinelibrary.wiley.com/doi/abs/10.1002/cyto.a.24035. _eprint: https://onlinelibrary.wiley.com/doi/pdf/10.1002/cyto.a.24035.

Louise Ashall, Caroline A. Horton, David E. Nelson, Pawel Paszek, Claire V. Harper, Kate Sillitoe, Sheila Ryan, David G. Spiller, John F. Unitt, David S. Broomhead, Douglas B. Kell, David A. Rand, Violaine Sée, and Michael R. H. White. Pulsatile Stimulation Determines Timing and Specificity of NF-κB-Dependent Transcription. *Science*, 324(5924): 242–246, April 2009. ISSN 0036-8075, 1095-9203. doi:10.1126/science.1164860. URL http://science.sciencemag.org/content/324/5924/242. Publisher: American Association for the Advancement of Science Section: Report.

Roi Avraham, Nathan Haseley, Douglas Brown, Cristina Penaranda, Humberto B. Jijon, John J. Trombetta, Rahul Satija, Alex K. Shalek, Ramnik J. Xavier, Aviv Regev, and Deborah T. Hung. Pathogen Cell-to-Cell Variability Drives Heterogeneity in Host Immune Responses. *Cell*, 162(6):1309–1321, September 2015. ISSN 0092-8674. doi:10.1016/j.cell.2015.08.027. URL https://www.sciencedirect.com/science/article/pii/S0092867415010417.

J. Bagnall, C. Boddington, J. Boyd, R. Brignall, W. Rowe, N. A. Jones, L. Schmidt, D. G. Spiller, M. R. H. White, and P. Paszek. Quantitative dynamic imaging of immune cell signalling using lentiviral gene transfer. *Integr. Biol.*, 7(6):713–725, June 2015. ISSN 1757-9708. doi:10.1039/C5IB00067J. URL http://pubs.rsc.org/en/content/articlelanding/2015/ib/c5ib00067j. Publisher: The Royal Society of Chemistry.

James Bagnall, Christopher Boddington, Hazel England, Ruth Brignall, Polly Downton, Zainab Alsoufi, James Boyd, William Rowe, Alexander Bennett, Catherine Walker, Antony Adamson, Nisha M. X. Patel, Ronan O'Cualain, Lorraine Schmidt, David G. Spiller, Dean A. Jackson, Werner Müller, Mark Muldoon, Michael R. H. White, and Pawel

Paszek. Quantitative analysis of competitive cytokine signaling predicts tissue thresholds for the propagation of macrophage activation. *Sci. Signal.*, 11(540), July 2018. ISSN 1945-0877, 1937-9145. doi:10.1126/scisignal.aaf3998. URL https://stke.sciencemag.org/content/11/540/eaaf3998. Publisher: American Association for the Advancement of Science Section: Research Article.

Ricardo Lacava Bailone, Hirla Costa Silva Fukushima, Bianca Helena Ventura Fernandes, Luís Kluwe De Aguiar, Tatiana Corrêa, Helena Janke, Princia Grejo Setti, Roberto De Oliveira Roça, and Ricardo Carneiro Borra. Zebrafish as an alternative animal model in human and animal vaccination research. *Laboratory Animal Research*, 36 (1):13, May 2020. ISSN 2233-7660. doi:10.1186/s42826-020-00042-4. URL https://doi.org/10.1186/s42826-020-00042-4.

Margot Bardou, Jérémy Postat, Clémence Loaec, Fabrice Lemaître, Gustave Ronteix, Zacarias Garcia, and Philippe Bousso. Quorum sensing governs collective dendritic cell activation in vivo. *The EMBO Journal*, n/a(n/a):e107176, June 2021. ISSN 0261-4189. doi:10.15252/embj.2020107176. URL https://www.embopress.org/doi/abs/10.15252/embj.2020107176. Publisher: John Wiley & Sons, Ltd.

Soumen Basak, Marcelo Behar, and Alexander Hoffmann. Lessons from mathematically modeling the NF-κB pathway. *Immunol Rev*, 246(1):221–238, March 2012. ISSN 0105-2896. doi:10.1111/j.1600-065X.2011.01092.x. URL https://www.ncbi.nlm.nih.gov/pmc/articles/PMC3343698/.

Sangeeta N. Bhatia, Martin L. Yarmush, and Mehmet Toner. Controlling cell interactions by micropatterning in co-cultures: Hepatocytes and 3T3 fibroblasts. *Journal of Biomedical Materials Research*, 34(2):189–199, 1997. ISSN 1097-4636. doi:10.1002/(SICI)1097-4636(199702)34:2<189::AID-JBM8>3.0.CO;2-M. _eprint: https://onlinelibrary.wiley.com/doi/pdf/10.1002/%28SICI%291097-4636%28199702%2934%3A2%3C189%3A%3AAID-JBM8%3E3.0.CO%3B2-M.

Elyse Y. Bissonnette, Jean-François Lauzon-Joset, Jason S. Debley, and Steven F. Ziegler. Cross-Talk Between Alveolar Macrophages and Lung Epithelial Cells is Essential to Maintain Lung Homeostasis. *Frontiers in Immunology*, 11, 2020. ISSN 1664-3224. URL https://www.frontiersin.org/articles/10.3389/fimmu.2020.583042.

Camille Blériot, Svetoslav Chakarov, and Florent Ginhoux. Determinants of resident tissue macrophage identity and function. *Immunity*, 52(6):957–970, 2020. ISSN 1074-7613. doi:https://doi.org/10.1016/j.immuni.2020.05.014. URL https://www.sciencedirect.com/science/article/pii/S1074761320302302.

Giuseppina Bonizzi and Michael Karin. The two NF-κB activation pathways and their role in innate and adaptive immunity. *Trends in Immunology*, 25(6):280–288, June 2004. ISSN 1471-4906, 1471-4981. doi:10.1016/j.it.2004.03.008. URL http://www.cell.com/trends/immunology/abstract/S1471-4906(04)00100-0. Publisher: Elsevier.

M. J. L. Bours, E. L. R. Swennen, F. Di Virgilio, B. N. Cronstein, and P. C. Dagnelie. Adenosine 5-triphosphate and adenosine as endogenous signaling molecules in immunity and inflammation. *Pharmacology & Therapeutics*, 112(2):358–404, November 2006. ISSN 0163-7258. doi:10.1016/j.pharmthera.2005.04.013. URL http://www.sciencedirect.com/science/article/pii/S0163725806000660.

David Brough, Rosalind A. Le Feuvre, Rachel D. Wheeler, Natasha Solovyova, Sabine Hilfiker, Nancy J. Rothwell, and Alex Verkhratsky. Ca2+ Stores and Ca2+ Entry Differentially Contribute to the Release of IL-1β and IL-1α from Murine Macrophages. *The Journal of Immunology*, 170(6):3029–3036, March 2003. ISSN 0022-1767, 1550-6606. doi:10.4049/jimmunol.170.6.3029. URL https://www.jimmunol.org/content/170/6/3029. Publisher: American Association of Immunologists Section: CELLULAR IMMUNOLOGY AND IMMUNE REGULATION.

Geoffrey Burnstock. Purinergic signalling. *British Journal of Pharmacology*, 147(S1): S172–S181, 2006. ISSN 1476-5381. doi:10.1038/sj.bjp.0706429. URL https://bpspubs.onlinelibrary.wiley.com/doi/abs/10.1038/sj.bjp.0706429. _eprint: https://bpspubs.onlinelibrary.wiley.com/doi/pdf/10.1038/sj.bjp.0706429.

Dorothea Busse, Maurus de la Rosa, Kirstin Hobiger, Kevin Thurley, Michael Flossdorf, Alexander Scheffold, and Thomas Höfer. Competing feedback loops shape IL-2 signaling between helper and regulatory T lymphocytes in cellular microenvironments. *PNAS*, 107 (7):3058–3063, February 2010. ISSN 0027-8424, 1091-6490. doi:10.1073/pnas.0812851107. URL https://www.pnas.org/content/107/7/3058. Publisher: National Academy of Sciences Section: Biological Sciences.

Konyshev I. V. Byvalov A. A., Kononenko V. L. Interaction of yersinia pseudotuberculosis and yersinia pestis lipopolosaccharides with j774 macrophage membrane by power spectroscopy using optical tweezers. *Biological membranes: Journal of membrane and cell biology*, (2, 2018, 35):115–130, 2018. URL https://www.libnauka.ru/item.php?doi=10.7868/S0233475518020032.

Andrew B. Caldwell, Zhang Cheng, Jesse D. Vargas, Harry A. Birnbaum, and Alexander Hoffmann. Network dynamics determine the autocrine and paracrine signaling functions of TNF. *Genes Dev.*, 28(19):2120–2133, October 2014. ISSN 0890-9369, 1549-5477. doi:10.1101/gad.244749.114. URL http://genesdev.cshlp.org/content/28/19/2120. Company: Cold Spring Harbor Laboratory Press Distributor: Cold Spring Harbor Laboratory Press Institution: Cold Spring Harbor Laboratory Press Label: Cold Spring Harbor Laboratory Press Publisher: Cold Spring Harbor Lab.

Johnathan Canton. Macropinocytosis: New Insights Into Its Underappreciated Role in Innate Immune Cell Surveillance. *Frontiers in Immunology*, 9, 2018. ISSN 1664-3224. URL https://www.frontiersin.org/articles/10.3389/fimmu.2018.02286.

Daria Capece, Daniela Verzella, Irene Flati, Paola Arboretto, Jessica Cornice, and Guido Franzoso. NF-ϰB: blending metabolism, immunity, and inflammation. *Trends*

in Immunology, 43(9):757–775, September 2022. ISSN 1471-4906, 1471-4981. doi:10.1016/j.it.2022.07.004. URL http://www.cell.com/trends/immunology/abstract/S1471-4906(22)00141-7. Publisher: Elsevier.

Caglar Cekic and Joel Linden. Purinergic regulation of the immune system. *Nature Reviews Immunology*, 16(3):177–192, March 2016. ISSN 1474-1741. doi:10.1038/nri.2016.4. URL https://www.nature.com/articles/nri.2016.4. Number: 3 Publisher: Nature Publishing Group.

Guillaume Charras and Alpha S. Yap. Tensile forces and mechanotransduction at cell-cell junctions. *Current Biology*, 2018. doi:10.1016/j.cub.2018.02.003.

Neha Cheemalavagu and Rachel A. Gottschalk. Time will tell: The temporal code of immune threats. *Immunity*, 54(5):845–847, May 2021. ISSN 1074-7613. doi:10.1016/j.immuni.2021.04.018. URL https://www.sciencedirect.com/science/article/pii/S1074761321001801.

Christopher S. Chen, Milan Mrksich, Sui Huang, George M. Whitesides, and Donald E. Ingber. Geometric Control of Cell Life and Death. *Science*, 276(5317):1425–1428, May 1997. ISSN 0036-8075, 1095-9203. doi:10.1126/science.276.5317.1425. URL https://science-sciencemag-org.proxy.uchicago.edu/content/276/5317/1425. Publisher: American Association for the Advancement of Science Section: Report.

Yu Ting Chow, Shuxun Chen, Ran Wang, Chichi Liu, Chi-wing Kong, Ronald A. Li, Shuk Han Cheng, and Dong Sun. Single Cell Transfection through Precise Microinjection with Quantitatively Controlled Injection Volumes. *Scientific Reports*, 6(1):24127, April 2016. ISSN 2045-2322. doi:10.1038/srep24127. URL https://www.nature.com/articles/srep24127. Number: 1 Publisher: Nature Publishing Group.

Yishan Chuang, Brianne K. Knickel, and Joshua N. Leonard. Regulation of the IL-10-driven macrophage phenotype under incoherent stimuli. *Innate Immun*, 22(8):647–657, November 2016. ISSN 1753-4259. doi:10.1177/1753425916668243. URL https://www.ncbi.nlm.nih.gov/pmc/articles/PMC5292318/.

Erik Clarke and Scott Sherrill-Mix. ggbeeswarm: Categorical Scatter (Voilin Point) Plots. 2017.

Ross Corriden and Paul A. Insel. Basal Release of ATP: An Autocrine-Paracrine Mechanism for Cell Regulation. *Sci. Signal.*, 3(104), January 2010. ISSN 1945-0877, 1937-9145. doi:10.1126/scisignal.3104re1. URL https://stke.sciencemag.org/content/3/104/re1. Publisher: American Association for the Advancement of Science Section: Review.

Markus W. Covert, Thomas H. Leung, Jahlionais E. Gaston, and David Baltimore. Achieving Stability of Lipopolysaccharide-Induced NF-κB Activation. *Science*, 309(5742):1854–1857, September 2005. ISSN 0036-8075, 1095-9203. doi:10.1126/science.1112304. URL https://science.sciencemag.org/content/309/5742/1854. Publisher: American Association for the Advancement of Science Section: Report.

Balázs Csóka, Zsolt Selmeczy, Balázs Koscsó, Zoltán H. Németh, Pal Pacher, Peter J. Murray, Diane Kepka-Lenhart, Sidney M. Morris Jr., William C. Gause, S. Joseph Leibovich, and György Haskó. Adenosine promotes alternative macrophage activation via A2A and A2B receptors. *The FASEB Journal*, 26(1):376–386, 2012. ISSN 1530-6860. doi:10.1096/fj.11-190934. URL http://onlinelibrary.wiley.com/doi/abs/10.1096/fj.11-190934. _eprint: https://faseb.onlinelibrary.wiley.com/doi/pdf/10.1096/fj.11-190934.

Cytosurge. Measuring the flow in a FluidFM probe | Cytosurge. URL https://www.cytosurge.com/forum/fluidfm-forum-1/question/measuring-the-flow-in-a-fluidfm-probe-126.

Luke C. Davies, Stephen J. Jenkins, Judith E. Allen, and Philip R. Taylor. Tissue-resident macrophages. *Nature Immunology*, 14(10):986–995, October 2013. ISSN 1529-2916. doi:10.1038/ni.2705. URL https://www.nature.com/articles/ni.2705. Number: 10 Publisher: Nature Publishing Group.

Mialy M. DeFelice, Helen R. Clark, Jacob J. Hughey, Inbal Maayan, Takamasa Kudo, Miriam V. Gutschow, Markus W. Covert, and Sergi Regot. NF-κB signaling dynamics is controlled by a dose-sensing autoregulatory loop. *Science Signaling*, 12(579), April 2019. ISSN 1945-0877, 1937-9145. doi:10.1126/scisignal.aau3568. URL http://stke.sciencemag.org/content/12/579/eaau3568. Publisher: American Association for the Advancement of Science Section: Research Article.

Zi Di, Bram Herpers, Lisa Fredriksson, Kuan Yan, Bob van de Water, Fons J. Verbeek, and John H. N. Meerman. Automated Analysis of NF-$\varkappa$B Nuclear Translocation Kinetics in High-Throughput Screening. *PLOS ONE*, 7(12):e52337, December 2012. ISSN 1932-6203. doi:10.1371/journal.pone.0052337. URL https://journals.plos.org/plosone/article?id=10.1371/journal.pone.0052337. Publisher: Public Library of Science.

Gloria J. F. Ding, Paul A. Fischer, Robert C. Boltz, Jack A. Schmidt, James J. Colaianne, Albert Gough, Richard A. Rubin, and Douglas K. Miller. Characterization and Quantitation of NF-$\varkappa$B Nuclear Translocation Induced by Interleukin-1 and Tumor Necrosis Factor-α DEVELOPMENT AND USE OF A HIGH CAPACITY FLUORESCENCE CYTOMETRIC SYSTEM. *J. Biol. Chem.*, 273(44):28897–28905, October 1998. ISSN 0021-9258, 1083-351X. doi:10.1074/jbc.273.44.28897. URL http://www.jbc.org/content/273/44/28897. Publisher: American Society for Biochemistry and Molecular Biology.

P. Dorig, D. Pssola, A. M. Truong, M. Graf, F. Stauffer, J. Voros, and T. Zambelli. Exchangeable Colloidal AFM Probes for the Quantification of Irreversible and Long-Term Interactions. *Biophysical Journal*, 105, 2013.

Dorrington and Fraser. NF-kB Signaling in Macrophages: Dynamics, Crosstalk, and Signal Integration. *Frontiers in Immunology*, 10:1–12, 2019a.

Michael G. Dorrington and Iain D. C. Fraser. NF-$\varkappa$B Signaling in Macrophages: Dynamics, Crosstalk, and Signal Integration. *Front. Immunol.*, 10, 2019b. ISSN 1664-3224. doi:10.3389/fimmu.2019.00705. URL https://www.frontiersin.org/articles/10.3389/fimmu.2019.00705/full. Publisher: Frontiers.

Christabel Thembela Dube, Yasmin Hui Binn Ong, Kelly Wemyss, Siddharth Krishnan, Tiak Ju Tan, Baptiste Janela, John R. Grainger, Matthew Ronshaugen, Kimberly A. Mace, and Chin Yan Lim. Age-Related Alterations in Macrophage Distribution and Function Are Associated With Delayed Cutaneous Wound Healing. *Frontiers in Immunology*, 13, 2022. ISSN 1664-3224. URL https://www.frontiersin.org/articles/10.3389/fimmu.2022.943159.

Maeva Dupont, Shanti Souriant, Geanncarlo Lugo-Villarino, Isabelle Maridonneau-Parini, and Christel Vérollet. Tunneling nanotubes: Intimate communication between myeloid cells. *Frontiers in Immunology*, 9, 2018. ISSN 1664-3224. doi:10.3389/fimmu.2018.00043. URL https://www.frontiersin.org/articles/10.3389/fimmu.2018.00043.

Malcolm S. Duthie, Hillarie Plessner Windish, Christopher B. Fox, and Steven G. Reed. Use of defined TLR ligands as adjuvants within human vaccines. *Immunol Rev*, 239(1): 178–196, January 2011. ISSN 0105-2896. doi:10.1111/j.1600-065X.2010.00978.x. URL https://www.ncbi.nlm.nih.gov/pmc/articles/PMC5872835/.

Slava Epelman, Kory J. Lavine, and Gwendalyn J. Randolph. Origin and Functions of Tissue Macrophages. *Immunity*, 41(1):21–35, July 2014. ISSN 1074-7613. doi:10.1016/j.immuni.2014.06.013. URL https://www.cell.com/immunity/abstract/S1074-7613(14)00235-0. Publisher: Elsevier.

Eliseo A. Eugenin, Maria C. Branes, Joan W. Berman, and Juan C. Saez. TNF-α Plus IFN-γ Induce Connexin43 Expression and Formation of Gap Junctions Between Human Monocytes/Macrophages That Enhance Physiological Responses 1. *The Journal of Immunology*, 170(3):1320–1328, 02 2003. ISSN 0022-1767. doi:10.4049/jimmunol.170.3.1320.

Robert Evans, Guilherme Dal Poggetto, Mathias Nilsson, and Gareth A. Morris. Improving the Interpretation of Small Molecule Diffusion Coefficients. *Anal. Chem.*, 90(6):3987–3994, March 2018. ISSN 0003-2700. doi:10.1021/acs.analchem.7b05032. URL https://doi.org/10.1021/acs.analchem.7b05032. Publisher: American Chemical Society.

Katherine A. Fitzgerald and Jonathan C. Kagan. Toll-like Receptors and the Control of Immunity. *Cell*, 180(6):1044–1066, March 2020. ISSN 0092-8674. doi:10.1016/j.cell.2020.02.041. URL https://www.sciencedirect.com/science/article/pii/S009286742030218X.

Albert Folch and Mehmet Toner. Cellular Micropatterns on Biocompatible Materials. *Biotechnology Progress*, 14(3):388–392, 1998. ISSN 1520-6033. doi:10.1021/bp980037b. URL http://aiche.onlinelibrary.wiley.com/doi/abs/10.1021/bp980037b. _eprint: https://onlinelibrary.wiley.com/doi/pdf/10.1021/bp980037b.

Spencer A. Freeman, Stefan Uderhardt, Amra Saric, Richard F. Collins, Catherine M. Buckley, Sivakami Mylvaganam, Parastoo Boroumand, Jonathan Plumb, Ronald N. Germain, Dejian Ren, and Sergio Grinstein. Lipid-gated monovalent ion fluxes regulate endocytic traffic and support immune surveillance. *Science*, 367(6475):301–305, January 2020. ISSN 0036-8075, 1095-9203. doi:10.1126/science.aaw9544. URL `http://science.sciencemag.org/content/367/6475/301`. Publisher: American Association for the Advancement of Science Section: Report.

Gaël Galli and Maya Saleh. Immunometabolism of Macrophages in Bacterial Infections. *Front Cell Infect Microbiol*, 10:607650, 2020. ISSN 2235-2988. doi:10.3389/fcimb.2020.607650.

Ronald N. Germain, Martin Meier-Schellersheim, Aleksandra Nita-Lazar, and Iain D. C. Fraser. Systems Biology in Immunology – A Computational Modeling Perspective. *Annu Rev Immunol*, 29:527–585, April 2011. ISSN 0732-0582. doi:10.1146/annurev-immunol-030409-101317. URL `https://www.ncbi.nlm.nih.gov/pmc/articles/PMC3164774/`.

Stephen E. Girardin, Ivo G. Boneca, Jérôme Viala, Mathias Chamaillard, Agnès Labigne, Gilles Thomas, Dana J. Philpott, and Philippe J. Sansonetti. Nod2 Is a General Sensor of Peptidoglycan through Muramyl Dipeptide (MDP) Detection. *J. Biol. Chem.*, 278 (11):8869–8872, March 2003. ISSN 0021-9258, 1083-351X. doi:10.1074/jbc.C200651200. URL `http://www.jbc.org/content/278/11/8869`. Publisher: American Society for Biochemistry and Molecular Biology.

Siamon Gordon and Luisa Martinez-Pomares. Physiological roles of macrophages. *Pflugers Arch*, 469(3):365–374, 2017. ISSN 0031-6768. doi:10.1007/s00424-017-1945-7. URL `https://www.ncbi.nlm.nih.gov/pmc/articles/PMC5362657/`.

Rachel A. Gottschalk, Andrew J. Martins, Bastian R. Angermann, Bhaskar Dutta, Caleb E. Ng, Stefan Uderhardt, John S. Tsang, Iain D. C. Fraser, Martin Meier-Schellersheim, and Ronald N. Germain. Distinct NF-κB and MAPK Activation Thresholds Uncouple Steady-State Microbe Sensing from Anti-pathogen Inflammatory Responses. *cels*, 2(6):378–390, June 2016. ISSN 2405-4712. doi:10.1016/j.cels.2016.04.016. URL `https://www.cell.com/cell-systems/abstract/S2405-4712(16)30150-8`. Publisher: Elsevier.

Raphael R. Grüter, János Vörös, and Tomaso Zambelli. FluidFM as a lithography tool in liquid: spatially controlled deposition of fluorescent nanoparticles. *Nanoscale*, 5(3):1097–1104, January 2013. ISSN 2040-3372. doi:10.1039/C2NR33214K. URL `http://pubs.rsc.org/en/content/articlelanding/2013/nr/c2nr33214k`. Publisher: The Royal Society of Chemistry.

Orane Guillaume-Gentil, Tomaso Zambelli, and Julia A. Vorholt. Isolation of single mammalian cells from adherent cultures by fluidic force microscopy. *Lab Chip*, 14(2): 402–414, December 2013. ISSN 1473-0189. doi:10.1039/C3LC51174J. URL `http://pubs.rsc.org/en/content/articlelanding/2014/lc/c3lc51174j`. Publisher: The Royal Society of Chemistry.

Orane Guillaume-Gentil, Eva Potthoff, Dario Ossola, Clemens M. Franz, Tomaso Zambelli, and Julia A. Vorholt. Force-controlled manipulation of single cells: from AFM to FluidFM. *Trends in Biotechnology*, 32(7):381–388, July 2014. ISSN 0167-7799, 1879-3096. doi:10.1016/j.tibtech.2014.04.008. URL http://www.cell.com/trends/biotechnology/abstract/S0167-7799(14)00085-7. Publisher: Elsevier.

Orane Guillaume-Gentil, Rashel V. Grindberg, Romain Kooger, Livie Dorwling-Carter, Vincent Martinez, Dario Ossola, Martin Pilhofer, Tomaso Zambelli, and Julia A. Vorholt. Tunable Single-Cell Extraction for Molecular Analyses. *Cell*, 166(2):506–516, July 2016. ISSN 0092-8674, 1097-4172. doi:10.1016/j.cell.2016.06.025. URL https://www.cell.com/cell/abstract/S0092-8674(16)30793-0. Publisher: Elsevier.

Orane Guillaume-Gentil, Eva Potthoff, Dario Ossola, Pablo Dörig, Tomaso Zambelli, and Julia A. Vorholt. Force-Controlled Fluidic Injection into Single Cell Nuclei. *Small*, 9(11):1904–1907, 2013. ISSN 1613-6829. doi:10.1002/smll.201202276. URL http://onlinelibrary.wiley.com/doi/abs/10.1002/smll.201202276. _eprint: https://onlinelibrary.wiley.com/doi/pdf/10.1002/smll.201202276.

Miriam V. Gutschow, Jacob J. Hughey, Nicholas A. Ruggero, Bryce T. Bajar, Sean D. Valle, and Markus W. Covert. Single-Cell and Population NF-κB Dynamic Responses Depend on Lipopolysaccharide Preparation. *PLOS ONE*, 8(1):e53222, January 2013. ISSN 1932-6203. doi:10.1371/journal.pone.0053222. URL https://journals.plos.org/plosone/article?id=10.1371/journal.pone.0053222. Publisher: Public Library of Science.

Kajal Hamidzadeh and David M. Mosser. Purinergic Signaling to Terminate TLR Responses in Macrophages. *Front. Immunol.*, 7, 2016. ISSN 1664-3224. doi:10.3389/fimmu.2016.00074. URL https://www.frontiersin.org/articles/10.3389/fimmu.2016.00074/full. Publisher: Frontiers.

Peter J. Hanley, Boris Musset, Vijay Renigunta, Sven H. Limberg, Alexander H. Dalpke, Rainer Sus, Klaus M. Heeg, Regina Preisig-Müller, and Jürgen Daut. Extracellular ATP induces oscillations of intracellular Ca2+ and membrane potential and promotes transcription of IL-6 in macrophages. *PNAS*, 101(25):9479–9484, June 2004. ISSN 0027-8424, 1091-6490. doi:10.1073/pnas.0400733101. URL https://www.pnas.org/content/101/25/9479. Publisher: National Academy of Sciences Section: Biological Sciences.

Jan Hasenauer, Steffen Waldherr, Malgorzata Doszczak, Nicole Radde, Peter Scheurich, and Frank Allgöwer. Identification of models of heterogeneous cell populations from population snapshot data. *BMC Bioinformatics*, 12(1):125, April 2011. ISSN 1471-2105. doi:10.1186/1471-2105-12-125. URL https://doi.org/10.1186/1471-2105-12-125.

György Haskó, Pál Pacher, Edwin A. Deitch, and E. Sylvester Vizi. Shaping of monocyte and macrophage function by adenosine receptors. *Pharmacology & Therapeutics*, 113(2):264–275, February 2007. ISSN 0163-7258. doi:10.1016/j.pharmthera.2006.08.003. URL https://www.sciencedirect.com/science/article/pii/S0163725806001501.

James B. Hayes, Linda M. Sircy, Lauren E. Heusinkveld, Wandi Ding, Rachel N. Leander, Erin E. McClelland, and David E. Nelson. Modulation of Macrophage Inflammatory Nuclear Factor κB (NF-κB) Signaling by Intracellular Cryptococcus neoformans. *J. Biol. Chem.*, 291(30):15614–15627, July 2016. ISSN 0021-9258, 1083-351X. doi:10.1074/jbc.M116.738187. URL http://www.jbc.org.proxy.uchicago.edu/content/291/30/15614. Publisher: American Society for Biochemistry and Molecular Biology.

David A. Hill, Hee-Woong Lim, Yong Hoon Kim, Wesley Y. Ho, Yee Hoon Foong, Victoria L. Nelson, Hoang C. B. Nguyen, Kavya Chegireddy, Jihoon Kim, Andreas Habertheuer, Prashanth Vallabhajosyula, Taku Kambayashi, Kyoung-Jae Won, and Mitchell A. Lazar. Distinct macrophage populations direct inflammatory versus physiological changes in adipose tissue. *PNAS*, 115(22):E5096–E5105, May 2018. ISSN 0027-8424, 1091-6490. doi:10.1073/pnas.1802611115. URL https://www.pnas.org/content/115/22/E5096. Publisher: National Academy of Sciences Section: PNAS Plus.

Alexander Hoffmann, Andre Levchenko, Martin L. Scott, and David Baltimore. The IκB-NF-κB Signaling Module: Temporal Control and Selective Gene Activation. *Science*, 298(5596):1241–1245, November 2002. ISSN 0036-8075, 1095-9203. doi:10.1126/science.1071914. URL http://science.sciencemag.org/content/298/5596/1241. Publisher: American Association for the Advancement of Science Section: Report.

Jun Huang, Mario Brameshuber, Xun Zeng, Jianming Xie, Qi-jing Li, Yueh-hsiu Chien, Salvatore Valitutti, and Mark M. Davis. A single peptide-major histocompatibility complex ligand triggers digital cytokine secretion in CD4+ T cells. *Immunity*, 39(5), November 2013. ISSN 1074-7613. doi:10.1016/j.immuni.2013.08.036. URL https://www.ncbi.nlm.nih.gov/pmc/articles/PMC3846396/.

Hughey, Gutschow, Bajar, and Covert. Single-cell variation leads to population invariance in NF-kB signaling dynamics. *Molecular Biology of the Cell*, 26:583–590, 2015.

Jacob J. Hughey, Miriam V. Gutschow, Bryce T. Bajar, and Markus W. Covert. Single-cell variation leads to population invariance in NF-κB signaling dynamics. *MBoC*, 26(3):583–590, December 2014. ISSN 1059-1524. doi:10.1091/mbc.E14-08-1267. URL https://www.molbiolcell.org/doi/full/10.1091/mbc.E14-08-1267. Publisher: American Society for Cell Biology (mboc).

Brian P. Ingalls and Herbert M. Sauro. Sensitivity analysis of stoichiometric networks: an extension of metabolic control analysis to non-steady state trajectories. *Journal of Theoretical Biology*, 222(1):23–36, May 2003. ISSN 0022-5193. doi:10.1016/S0022-5193(03)00011-0. URL http://www.sciencedirect.com/science/article/pii/S0022519303000110.

Juno Jang, Soo-Jin Moon, Sung-Hwan Hong, and Ik-Hwan Kim. Colorimetric pH measurement of animal cell culture media. *Biotechnol Lett*, 32(11):1599–1607, November 2010. ISSN 1573-6776. doi:10.1007/s10529-010-0341-6. URL https://doi.org/10.1007/s10529-010-0341-6.

Stephen J. Jenkins and Judith E. Allen. The expanding world of tissue-resident macrophages. *European Journal of Immunology*, 51(8):1882–1896, 2021. doi:https://doi.org/10.1002/eji.202048881. URL https://onlinelibrary.wiley.com/doi/abs/10.1002/eji.202048881.

Zhongyun Jiang, Sidi Liu, Xiang Xiao, Guimei Jiang, Qing Qu, Xingxing Miao, Renfei Wu, Rui Shi, Ruochen Guo, and Jian Liu. High-throughput probing macrophage–bacteria interactions at the single cell level with microdroplets. *Lab Chip*, 22:2944–2953, 2022. doi:10.1039/D2LC00516F.

Wolfgang G. Junger. Immune cell regulation by autocrine purinergic signalling. *Nature Reviews Immunology*, 11(3):201–212, March 2011. ISSN 1474-1741. doi:10.1038/nri2938. URL https://www.nature.com/articles/nri2938. Number: 3 Publisher: Nature Publishing Group.

Michael Junkin, Alicia J. Kaestli, Zhang Cheng, Christian Jordi, Cem Albayrak, Alexander Hoffmann, and Savaş Tay. High-Content Quantification of Single-Cell Immune Dynamics. *Cell Reports*, 15(2):411–422, April 2016. ISSN 2211-1247. doi:10.1016/j.celrep.2016.03.033. URL https://www.sciencedirect.com/science/article/pii/S2211124716302893.

Jonathan C. Kagan. Infection infidelities drive innate immunity. *Science*, 379(6630):333–335, 2023. doi:10.1126/science.ade9733. URL https://www.science.org/doi/abs/10.1126/science.ade9733.

Hirokazu Kaji, Gulden Camci-Unal, Robert Langer, and Ali Khademhosseini. Engineering systems for the generation of patterned co-cultures for controlling cell-cell interactions. *Biochim Biophys Acta*, 1810(3):239–250, March 2011. ISSN 0006-3002. doi:10.1016/j.bbagen.2010.07.002. URL https://www.ncbi.nlm.nih.gov/pmc/articles/PMC3026923/.

Mridul K. Kalita, Khachik Sargsyan, Bing Tian, Adriana Paulucci-Holthauzen, Habib N. Najm, Bert J. Debusschere, and Allan R. Brasier. Sources of Cell-to-cell Variability in Canonical Nuclear Factor-κB (NF-κB) Signaling Pathway Inferred from Single Cell Dynamic Images. *J. Biol. Chem.*, 286(43):37741–37757, October 2011. ISSN 0021-9258, 1083-351X. doi:10.1074/jbc.M111.280925. URL http://www.jbc.org/content/286/43/37741. Publisher: American Society for Biochemistry and Molecular Biology.

Ravi S Kane, Shuichi Takayama, Emanuele Ostuni, Donald E Ingber, and George M Whitesides. Patterning proteins and cells using soft lithography. *Biomaterials*, 20(23): 2363–2376, December 1999. ISSN 0142-9612. doi:10.1016/S0142-9612(99)00165-9. URL http://www.sciencedirect.com/science/article/pii/S0142961299001659.

Jihee Lee Kang, Kyungeun Lee, and Vincent Castranova. Nitric oxide up-regulates DNA-binding activity of nuclear factor-κB in macrophages stimulated with silica and inflammatory stimulants. *Mol Cell Biochem*, 215(1):1–9, December 2000. ISSN 1573-4919. doi:10.1023/A:1026581301366. URL https://doi.org/10.1023/A:1026581301366.

Atsuo Kanno, Natsuko Tanimura, Masayuki Ishizaki, Kentaro Ohko, Yuji Motoi, Masahiro Onji, Ryutaro Fukui, Takaichi Shimozato, Kazuhide Yamamoto, Takuma Shibata, Shigetoshi Sano, Akiko Sugahara-Tobinai, Toshiyuki Takai, Umeharu Ohto, Toshiyuki Shimizu, Shin-ichiroh Saitoh, and Kensuke Miyake. Targeting cell surface TLR7 for therapeutic intervention in autoimmune diseases. *Nature Communications*, 6(1):6119, February 2015. ISSN 2041-1723. doi:10.1038/ncomms7119. URL `https://www.nature.com/articles/ncomms7119`. Number: 1 Publisher: Nature Publishing Group.

Shang-Jyh Kao, Hui-Chieh Lei, Chen-Tzu Kuo, Ming-Shyan Chang, Bing-Chang Chen, Yau-Chong Chang, Wen-Ta Chiu, and Chien-Huang Lin. Lipoteichoic acid induces nuclear factor-κB activation and nitric oxide synthase expression via phosphatidylinositol 3-kinase, Akt, and p38 MAPK in RAW 264.7 macrophages. *Immunology*, 115(3): 366–374, 2005. ISSN 1365-2567. doi:10.1111/j.1365-2567.2005.02160.x. URL `http://onlinelibrary.wiley.com/doi/abs/10.1111/j.1365-2567.2005.02160.x`. _eprint: https://onlinelibrary.wiley.com/doi/pdf/10.1111/j.1365-2567.2005.02160.x.

Wolfgang Kastenmüller, Parizad Torabi-Parizi, Naeha Subramanian, Tim Lämmermann, and Ronald N. Germain. A Spatially-Organized Multicellular Innate Immune Response in Lymph Nodes Limits Systemic Pathogen Spread. *Cell*, 150(6):1235–1248, September 2012. ISSN 0092-8674, 1097-4172. doi:10.1016/j.cell.2012.07.021. URL `https://www.cell.com/cell/abstract/S0092-8674(12)00889-6`. Publisher: Elsevier.

Ryan A. Kellogg, Chengzhe Tian, Martin Etzrodt, and Savaş Tay. Cellular Decision Making by Non-Integrative Processing of TLR Inputs. *Cell Reports*, 19(1):125–135, April 2017. ISSN 2211-1247. doi:10.1016/j.celrep.2017.03.027. URL `http://www.sciencedirect.com/science/article/pii/S2211124717303595`.

Mahmoud G. Khalafalla, Lucas T. Woods, Jean M. Camden, Aslam A. Khan, Kirsten H. Limesand, Michael J. Petris, Laurie Erb, and Gary A. Weisman. P2X7 receptor antagonism prevents IL-1β release from salivary epithelial cells and reduces inflammation in a mouse model of autoimmune exocrinopathy. *J Biol Chem*, 292(40):16626–16637, October 2017. ISSN 1083-351X. doi:10.1074/jbc.M117.790741.

H. Kojima, K. Sakurai, K. Kikuchi, S. Kawahara, Y. Kirino, H. Nagoshi, Y. Hirata, T. Akaike, H. Maeda, and T. Nagano. Development of a fluorescent indicator for the bioimaging of nitric oxide. *Biol Pharm Bull*, 20(12):1229–1232, December 1997. ISSN 0918-6158. doi:10.1248/bpb.20.1229.

Chen-Tzu Kuo, Ling-Ling Chiang, Chun-Nin Lee, Ming-Chih Yu, Kuan-Jen Bai, Horng-Mo Lee, Wen-Sen Lee, Joen-Rong Sheu, and Chien-Huang Lin. Induction of Nitric Oxide Synthase in RAW 264.7 Macrophages by Lipoteichoic Acid from *Staphylococcus aureus:* Involvement of Protein Kinase C- and Nuclear Factor-κB-Dependent Mechanisms. *J Biomed Sci*, 10(1):136–145, 2003. ISSN 1423-0127, 1021-7770. doi:10.1159/000068076. URL `http://www.karger.com/doi/10.1159/000068076`.

Keara Lane, David Van Valen, Mialy M. DeFelice, Derek N. Macklin, Takamasa Kudo, Ariel Jaimovich, Ambrose Carr, Tobias Meyer, Dana Peer, Stéphane C. Boutet, and Markus W. Covert. Measuring Signaling and RNA-Seq in the Same Cell Links Gene Expression to Dynamic Patterns of NF-κB Activation. *Cell Systems*, 4(4):458–469.e5, April 2017. ISSN 2405-4712. doi:10.1016/j.cels.2017.03.010. URL http://www.sciencedirect.com/science/article/pii/S2405471217301321.

Robin E. C. Lee, Sarah R. Walker, Kate Savery, David A. Frank, and Suzanne Gaudet. Fold Change of Nuclear NF-κB Determines TNF-Induced Transcription in Single Cells. *Molecular Cell*, 53(6):867–879, March 2014. ISSN 1097-2765. doi:10.1016/j.molcel.2014.01.026. URL https://www.cell.com/molecular-cell/abstract/S1097-2765(14)00087-2. Publisher: Elsevier.

Robin E. C. Lee, Mohammad A. Qasaimeh, Xianfang Xia, David Juncker, and Suzanne Gaudet. NF-κB signalling and cell fate decisions in response to a short pulse of tumour necrosis factor. *Sci Rep*, 6(1):39519, December 2016. ISSN 2045-2322. doi:10.1038/srep39519. URL https://www.nature.com/articles/srep39519. Number: 1 Publisher: Nature Publishing Group.

Timothy K. Lee, Elissa M. Denny, Jayodita C. Sanghvi, Jahlionais E. Gaston, Nathaniel D. Maynard, Jacob J. Hughey, and Markus W. Covert. A Noisy Paracrine Signal Determines the Cellular NF-κB Response to Lipopolysaccharide. *Sci Signal*, 2(93):ra65, October 2009. ISSN 1937-9145. doi:10.1126/scisignal.2000599. URL https://www.ncbi.nlm.nih.gov/pmc/articles/PMC2778577/.

Joe H. Levine, Yihan Lin, and Michael B. Elowitz. Functional Roles of Pulsing in Genetic Circuits. *Science*, 342(6163):1193–1200, December 2013. ISSN 0036-8075, 1095-9203. doi:10.1126/science.1239999. URL https://science-sciencemag-org.proxy.uchicago.edu/content/342/6163/1193. Publisher: American Association for the Advancement of Science Section: Review.

Christophe Leys, Christophe Ley, Olivier Klein, Philippe Bernard, and Laurent Licata. Detecting outliers: Do not use standard deviation around the mean, use absolute deviation around the median. *Journal of Experimental Social Psychology*, 49(4):764–766, July 2013. ISSN 0022-1031. doi:10.1016/j.jesp.2013.03.013. URL http://www.sciencedirect.com/science/article/pii/S0022103113000668.

Ning Li, Jing Sun, Zachary L. Benet, Ze Wang, Souhaila Al-Khodor, Sinu P. John, Bin Lin, Myong-Hee Sung, and Iain D. C. Fraser. Development of a cell system for siRNA screening of pathogen responses in human and mouse macrophages. *Scientific Reports*, 5(1):9559, April 2015. ISSN 2045-2322. doi:10.1038/srep09559. URL https://www.nature.com/articles/srep09559. Number: 1 Publisher: Nature Publishing Group.

Ning Li, Samuel Katz, Bhaskar Dutta, Zachary L. Benet, Jing Sun, and Iain D.C. Fraser. Genome-wide siRNA screen of genes regulating the LPS-induced NF-κB and TNF-α responses in mouse macrophages. *Sci Data*, 4, March 2017. ISSN 2052-4463.

doi:10.1038/sdata.2017.8. URL https://www.ncbi.nlm.nih.gov/pmc/articles/PMC5332015/.

Weizhe Li, Ronald N. Germain, and Michael Y. Gerner. High-dimensional cell-level analysis of tissues with Ce3D multiplex volume imaging. *Nature Protocols*, 14(6):1708–1733, June 2019. ISSN 1750-2799. doi:10.1038/s41596-019-0156-4. URL https://www.nature.com/articles/s41596-019-0156-4. Number: 6 Publisher: Nature Publishing Group.

Foo Y. Liew, Damo Xu, Elizabeth K. Brint, and Luke A. J. O//Neill. Negative regulation of Toll-like receptor-mediated immune responses. *Nature Reviews Immunology*, 5(6):446–458, June 2005. ISSN 1474-1741. doi:10.1038/nri1630. URL http://www.nature.com/articles/nri1630. Number: 6 Publisher: Nature Publishing Group.

Guangwei Liu and Hui Yang. Modulation of macrophage activation and programming in immunity. *Journal of Cellular Physiology*, 228(3):502–512, 2013. ISSN 1097-4652. doi:10.1002/jcp.24157. URL http://onlinelibrary.wiley.com/doi/abs/10.1002/jcp.24157. _eprint: https://onlinelibrary.wiley.com/doi/pdf/10.1002/jcp.24157.

Jeffrey T. Lock, Ian Parker, and Ian F. Smith. Communication of Ca2+ signals via tunneling membrane nanotubes is mediated by transmission of inositol trisphosphate through gap junctions. *Cell Calcium*, 60(4):266–272, October 2016. ISSN 0143-4160. doi:10.1016/j.ceca.2016.06.004. URL http://www.sciencedirect.com/science/article/pii/S0143416016300975.

Yao Lu, Qiong Xue, Markus R. Eisele, Endah S. Sulistijo, Kara Brower, Lin Han, Elad David Amir, Dana Pe'er, Kathryn Miller-Jensen, and Rong Fan. Highly multiplexed profiling of single-cell effector functions reveals deep functional heterogeneity in response to pathogenic ligands. *PNAS*, 112(7):E607–E615, February 2015. ISSN 0027-8424, 1091-6490. doi:10.1073/pnas.1416756112. URL https://www.pnas.org/content/112/7/E607. Publisher: National Academy of Sciences Section: PNAS Plus.

Evan Z. Macosko, Anindita Basu, Rahul Satija, James Nemesh, Karthik Shekhar, Melissa Goldman, Itay Tirosh, Allison R. Bialas, Nolan Kamitaki, Emily M. Martersteck, John J. Trombetta, David A. Weitz, Joshua R. Sanes, Alex K. Shalek, Aviv Regev, and Steven A. McCarroll. Highly Parallel Genome-wide Expression Profiling of Individual Cells Using Nanoliter Droplets. *Cell*, 161(5):1202–1214, May 2015. ISSN 0092-8674, 1097-4172. doi:10.1016/j.cell.2015.05.002. URL https://www.cell.com/cell/abstract/S0092-8674(15)00549-8. Publisher: Elsevier.

Orla Maguire, Christine Collins, Kieran O//Loughlin, Jeffrey Miecznikowski, and Hans Minderman. Quantifying nuclear p65 as a parameter for NF-κB activation: Correlation between ImageStream cytometry, microscopy, and Western blot. *Cytometry Part A*, 79A(6):461–469, 2011. ISSN 1552-4930. doi:10.1002/cyto.a.21068. URL http://onlinelibrary.wiley.com/doi/abs/10.1002/cyto.a.21068. _eprint: https://onlinelibrary.wiley.com/doi/pdf/10.1002/cyto.a.21068.

Shreya Maiti, Wei Dai, Robert C. Alaniz, Juergen Hahn, and Arul Jayaraman. Mathematical Modeling of Pro- and Anti-Inflammatory Signaling in Macrophages. *Processes*, 3(1):1–18, March 2015. doi:10.3390/pr3010001. URL https://www.mdpi.com/2227-9717/3/1/1. Number: 1 Publisher: Multidisciplinary Digital Publishing Institute.

Rock J. Mancini, Lalisa Stutts, Troy Moore, and Aaron P. Esser-Kahn. Controlling the origins of inflammation with a photoactive lipopeptide immunopotentiator. *Angew. Chem. Int. Ed. Engl.*, 54(20):5962–5965, May 2015. ISSN 1521-3773. doi:10.1002/anie.201500416.

J McIntrye, D Rowley, and Gr Jenkin. The Functional Heterogeneity of Macrophages at the Single Cell Level. *Australian Journal of Experimental Biology and Medical Science*, 45(6):675–680, 1967. ISSN 1440-1711. doi:10.1038/icb.1967.67. URL https://onlinelibrary.wiley.com/doi/abs/10.1038/icb.1967.67. _eprint: https://onlinelibrary.wiley.com/doi/pdf/10.1038/icb.1967.67.

Claire McQuin, Allen Goodman, Vasiliy Chernyshev, Lee Kamentsky, Beth A. Cimini, Kyle W. Karhohs, Minh Doan, Liya Ding, Susanne M. Rafelski, Derek Thirstrup, Winfried Wiegraebe, Shantanu Singh, Tim Becker, Juan C. Caicedo, and Anne E. Carpenter. CellProfiler 3.0: Next-generation image processing for biology. *PLOS Biology*, 16(7): e2005970, July 2018. ISSN 1545-7885. doi:10.1371/journal.pbio.2005970. URL https://journals.plos.org/plosbiology/article?id=10.1371/journal.pbio.2005970. Publisher: Public Library of Science.

André Meister, Michael Gabi, Pascal Behr, Philipp Studer, János Vörös, Philippe Niedermann, Joanna Bitterli, Jérôme Polesel-Maris, Martha Liley, Harry Heinzelmann, and Tomaso Zambelli. FluidFM: Combining Atomic Force Microscopy and Nanofluidics in a Universal Liquid Delivery System for Single Cell Applications and Beyond. *Nano Lett.*, 9(6):2501–2507, June 2009. ISSN 1530-6984. doi:10.1021/nl901384x. URL https://doi.org/10.1021/nl901384x. Publisher: American Chemical Society.

Katie Moore, Luke Howard, Cindi Brownmiller, Inah Gu, Sun-Ok Lee, and Andy Mauromoustakos. Inhibitory effects of cranberry polyphenol and volatile extracts on nitric oxide production in LPS activated RAW 264.7 macrophages. *Food & Function*, 10(11):7091–7102, 2019. doi:10.1039/C9FO01500K. URL http://pubs.rsc.org/en/content/articlelanding/2019/fo/c9fo01500k. Publisher: Royal Society of Chemistry.

Brittany A. Moser and Aaron P. Esser-Kahn. A Photoactivatable Innate Immune Receptor for Optogenetic Inflammation. *ACS Chem. Biol.*, 12(2):347–350, February 2017. ISSN 1554-8929. doi:10.1021/acschembio.6b01012. URL https://doi.org/10.1021/acschembio.6b01012. Publisher: American Chemical Society.

Brittany A. Moser, Rachel C. Steinhardt, and Aaron P. Esser-Kahn. Surface Coating of Nanoparticles Reduces Background Inflammatory Activity while Increasing Particle Uptake and Delivery. *ACS Biomater Sci Eng*, 3(2):206–213, February 2017. ISSN 2373-9878. doi:10.1021/acsbiomaterials.6b00473.

Joseph J. Muldoon, Yishan Chuang, Neda Bagheri, and Joshua N. Leonard. Macrophages employ quorum licensing to regulate collective activation. *Nature Communications*, 11 (1):878, February 2020. ISSN 2041-1723. doi:10.1038/s41467-020-14547-y. URL https://www.nature.com/articles/s41467-020-14547-y. Number: 1 Publisher: Nature Publishing Group.

Yousuke Murakami, Hitoshi Kohsaka, Hidero Kitasato, and Tohru Akahoshi. Lipopolysaccharide-Induced Up-Regulation of Triggering Receptor Expressed on Myeloid Cells-1 Expression on Macrophages Is Regulated by Endogenous Prostaglandin E2. *The Journal of Immunology*, 178(2):1144–1150, January 2007. ISSN 0022-1767, 1550-6606. doi:10.4049/jimmunol.178.2.1144. URL https://www.jimmunol.org/content/178/2/1144. Publisher: American Association of Immunologists Section: INFLAMMATION.

Kenneth Murphy, Paul Travers, Mark Walport, and Charles Janeway. *Janeway//s immunobiology*. Garland Science, New York, 8th ed edition, 2012. ISBN 978-0-8153-4243-4. OCLC: ocn733935898.

Peter J. Murray and Stephen T. Smale. Restraint of inflammatory signaling by interdependent strata of negative regulatory pathways. *Nature Immunology*, 13(10):916–924, October 2012. ISSN 1529-2916. doi:10.1038/ni.2391. URL https://www.nature.com/articles/ni.2391. Number: 10 Publisher: Nature Publishing Group.

José F. Muñoz, Toni Delorey, Christopher B. Ford, Bi Yu Li, Dawn A. Thompson, Reeta P. Rao, and Christina A. Cuomo. Coordinated host-pathogen transcriptional dynamics revealed using sorted subpopulations and single macrophages infected with Candida albicans. *Nat Commun*, 10(1):1607, April 2019. ISSN 2041-1723. doi:10.1038/s41467-019-09599-8. URL http://www.nature.com/articles/s41467-019-09599-8. Number: 1 Publisher: Nature Publishing Group.

D. E. Nelson, A. E. C. Ihekwaba, M. Elliott, J. R. Johnson, C. A. Gibney, B. E. Foreman, G. Nelson, V. See, C. A. Horton, D. G. Spiller, S. W. Edwards, H. P. McDowell, J. F. Unitt, E. Sullivan, R. Grimley, N. Benson, D. Broomhead, D. B. Kell, and M. R. H. White. Oscillations in NF-$\varkappa$B Signaling Control the Dynamics of Gene Expression. *Science*, 306 (5696):704–708, October 2004. ISSN 0036-8075, 1095-9203. doi:10.1126/science.1099962. URL https://science-sciencemag-org.proxy.uchicago.edu/content/306/5696/704. Publisher: American Association for the Advancement of Science Section: Report.

Rachel H. Nelson and David E. Nelson. Signal Distortion: How Intracellular Pathogens Alter Host Cell Fate by Modulating NF-$\varkappa$B Dynamics. *Front. Immunol.*, 9, 2018. ISSN 1664-3224. doi:10.3389/fimmu.2018.02962. URL https://www.frontiersin.org/articles/10.3389/fimmu.2018.02962/full. Publisher: Frontiers.

Ashley Page, Minkyung Kang, Alexander Armitstead, David Perry, and Patrick R. Unwin. Quantitative Visualization of Molecular Delivery and Uptake at Living Cells

with Self-Referencing Scanning Ion Conductance Microscopy-Scanning Electrochemical Microscopy. *Anal. Chem.*, 89(5):3021–3028, March 2017. ISSN 0003-2700. doi:10.1021/acs.analchem.6b04629. URL https://doi.org/10.1021/acs.analchem.6b04629. Publisher: American Chemical Society.

T M Palmer and M A Trevethick. Suppression of inflammatory and immune responses by the A2A adenosine receptor: an introduction. *British Journal of Pharmacology*, 153(S1):S27–S34, 2008. ISSN 1476-5381. doi:10.1038/sj.bjp.0707524. URL http://onlinelibrary.wiley.com/doi/abs/10.1038/sj.bjp.0707524. _eprint: https://bpspubs.onlinelibrary.wiley.com/doi/pdf/10.1038/sj.bjp.0707524.

Narayanan Parameswaran and Sonika Patial. Tumor Necrosis Factor-α Signaling in Macrophages. *Crit Rev Eukaryot Gene Expr*, 20(2):87–103, 2010. ISSN 1045-4403. URL https://www.ncbi.nlm.nih.gov/pmc/articles/PMC3066460/.

Ju An Park, Sejeong Yoon, Jimin Kwon, Hesung Now, Young Kwon Kim, Woo-Jong Kim, Joo-Yeon Yoo, and Sungjune Jung. Freeform micropatterning of living cells into cell culture medium using direct inkjet printing. *Scientific Reports*, 7(1):14610, November 2017. ISSN 2045-2322. doi:10.1038/s41598-017-14726-w. URL https://www.nature.com/articles/s41598-017-14726-w. Number: 1 Publisher: Nature Publishing Group.

Pawel Paszek, Sheila Ryan, Louise Ashall, Kate Sillitoe, Claire V. Harper, David G. Spiller, David A. Rand, and Michael R. H. White. Population robustness arising from cellular heterogeneity. *PNAS*, 107(25):11644–11649, June 2010. ISSN 0027-8424, 1091-6490. doi:10.1073/pnas.0913798107. URL https://www.pnas.org/content/107/25/11644. Publisher: National Academy of Sciences Section: Biological Sciences.

Pooja Patheja and Khageswar Sahu. Macrophage conditioned medium induced cellular network formation in MCF-7 cells through enhanced tunneling nanotube formation and tunneling nanotube mediated release of viable cytoplasmic fragments. *Experimental Cell Research*, 355(2):182–193, June 2017. ISSN 0014-4827. doi:10.1016/j.yexcr.2017.04.008. URL http://www.sciencedirect.com/science/article/pii/S0014482717302215.

Thomas Lin Pedersen. patchwork: The Composer of Plots. 2020.

Pablo Pelegrin and Annmarie Surprenant. Pannexin-1 mediates large pore formation and interleukin-1β release by the ATP-gated P2X7 receptor. *The EMBO Journal*, 25(21):5071–5082, November 2006. ISSN 0261-4189. doi:10.1038/sj.emboj.7601378. URL https://www.embopress.org/doi/10.1038/sj.emboj.7601378. Publisher: John Wiley & Sons, Ltd.

Karin Pelka, Damien Bertheloot, Elisa Reimer, Kshiti Phulphagar, Susanne V. Schmidt, Anette Christ, Rainer Stahl, Nicki Watson, Kensuke Miyake, Nir Hacohen, Albert Haas, Melanie M. Brinkmann, Ann Marshak-Rothstein, Felix Meissner, and Eicke Latz. The Chaperone UNC93B1 Regulates Toll-like Receptor Stability Independently of Endosomal TLR Transport. *Immunity*, 48(5):911–922.e7, May 2018. ISSN 1074-7613.

doi:10.1016/j.immuni.2018.04.011. URL https://www.cell.com/immunity/abstract/S1074-7613(18)30180-8. Publisher: Elsevier.

Silvia Penuela, Ruchi Gehi, and Dale W. Laird. The biochemistry and function of pannexin channels. *Biochimica et Biophysica Acta (BBA) - Biomembranes*, 1828(1):15–22, January 2013. ISSN 0005-2736. doi:10.1016/j.bbamem.2012.01.017. URL http://www.sciencedirect.com/science/article/pii/S0005273612000211.

Carlene Petes, Natalya Odoardi, and Katrina Gee. The Toll for Trafficking: Toll-Like Receptor 7 Delivery to the Endosome. *Front. Immunol.*, 8, 2017. ISSN 1664-3224. doi:10.3389/fimmu.2017.01075. URL https://www.frontiersin.org/articles/10.3389/fimmu.2017.01075/full. Publisher: Frontiers.

Dana J. Philpott, Shoji Yamaoka, Alain Israël, and Philippe J. Sansonetti. Invasive Shigella flexneri Activates NF-κB Through a Lipopolysaccharide-Dependent Innate Intracellular Response and Leads to IL-8 Expression in Epithelial Cells. *The Journal of Immunology*, 165(2):903–914, July 2000. ISSN 0022-1767, 1550-6606. doi:10.4049/jimmunol.165.2.903. URL https://www.jimmunol.org/content/165/2/903. Publisher: American Association of Immunologists Section: Host Defense.

Jérémy Postat, Romain Olekhnovitch, Fabrice Lemaître, and Philippe Bousso. A Metabolism-Based Quorum Sensing Mechanism Contributes to Termination of Inflammatory Responses. *Immunity*, 49(4):654–665.e5, October 2018. ISSN 1074-7613. doi:10.1016/j.immuni.2018.07.014. URL https://www.cell.com/immunity/abstract/S1074-7613(18)30334-0. Publisher: Elsevier.

Jeremy E. Purvis and Galit Lahav. Encoding and Decoding Cellular Information through Signaling Dynamics. *Cell*, 152(5):945–956, February 2013. ISSN 0092-8674, 1097-4172. doi:10.1016/j.cell.2013.02.005. URL https://www.cell.com/cell/abstract/S0092-8674(13)00153-0. Publisher: Elsevier.

Steven G. Reed, Mark T. Orr, and Christopher B. Fox. Key roles of adjuvants in modern vaccines. *Nature Medicine*, 19(12):1597–1608, December 2013. ISSN 1546-170X. doi:10.1038/nm.3409. URL https://www.nature.com/articles/nm.3409. Number: 12 Publisher: Nature Publishing Group.

Hua Ren, Yunfei Teng, Binghe Tan, Xiaoyu Zhang, Wei Jiang, Mingyao Liu, Wenzheng Jiang, Bing Du, and Min Qian. Toll-Like Receptor-Triggered Calcium Mobilization Protects Mice against Bacterial Infection through Extracellular ATP Release. *Infection and Immunity*, 82(12):5076–5085, December 2014. ISSN 0019-9567, 1098-5522. doi:10.1128/IAI.02546-14. URL https://iai.asm.org/content/82/12/5076. Publisher: American Society for Microbiology Journals Section: Host Response and Inflammation.

Wolfram Research. Mathematica Version 12, 2022. URL https://www.wolfram.com/mathematica.

Amin Rustom, Rainer Saffrich, Ivanka Markovic, Paul Walther, and Hans-Hermann Gerdes. Nanotubular Highways for Intercellular Organelle Transport. *Science*, 303(5660):1007–1010, February 2004. ISSN 0036-8075, 1095-9203. doi:10.1126/science.1093133. URL http://science.sciencemag.org/content/303/5660/1007. Publisher: American Association for the Advancement of Science Section: Report.

Keun Ah Ryu, Lalisa Stutts, Janine K. Tom, Rock J. Mancini, and Aaron P. Esser-Kahn. Stimulation of Innate Immune Cells by Light-Activated TLR7/8 Agonists. *J. Am. Chem. Soc.*, 136(31):10823–10825, August 2014. ISSN 0002-7863. doi:10.1021/ja412314j. URL https://doi.org/10.1021/ja412314j. Publisher: American Chemical Society.

Keun Ah Ryu, Bethany McGonnigal, Troy Moore, Tawnya Kargupta, Rock J. Mancini, and Aaron P. Esser-Kahn. Light Guided In-vivo Activation of Innate Immune Cells with Photocaged TLR 2/6 Agonist. *Scientific Reports*, 7(1):8074, August 2017. ISSN 2045-2322. doi:10.1038/s41598-017-08520-x. URL https://www.nature.com/articles/s41598-017-08520-x. Number: 1 Publisher: Nature Publishing Group.

Tamás Röszer. Understanding the Biology of Self-Renewing Macrophages. *Cells*, 7(8), August 2018. ISSN 2073-4409. doi:10.3390/cells7080103. URL https://www.ncbi.nlm.nih.gov/pmc/articles/PMC6115929/.

Johannes Schindelin, Ignacio Arganda-Carreras, Erwin Frise, Verena Kaynig, Mark Longair, Tobias Pietzch, Stephan Preibisch, Curtis Rueden, Stephan Saalfeld, Benjamin Schmid, Jean-Yves Tinevez, Daniel James White, Volker Hartenstein, Kevin Eliceiri, Pavel Tomancak, and Albert Cardona. Fiji: an open-source platform for biological-image analysis. *Nature Methods*, 9:676–682, 2019.

Kate Schroder and Jurg Tschopp. The Inflammasomes. *Cell*, 140(6):821–832, March 2010. ISSN 0092-8674. doi:10.1016/j.cell.2010.01.040. URL http://www.sciencedirect.com/science/article/pii/S0092867410000759.

Julia E Sero, Heba Zuhair Sailem, Rico Chandra Ardy, Hannah Almuttaqi, Tongli Zhang, and Chris Bakal. Cell shape and the microenvironment regulate nuclear translocation of NF-κB in breast epithelial and tumor cells. *Mol Syst Biol*, 11(3), March 2015. ISSN 1744-4292. doi:10.15252/msb.20145644. URL https://www.ncbi.nlm.nih.gov/pmc/articles/PMC4380925/.

Chao Shi and Eric G. Pamer. Monocyte recruitment during infection and inflammation. *Nature Reviews Immunology*, 11(11):762–774, November 2011. ISSN 1474-1741. doi:10.1038/nri3070. URL https://www.nature.com/articles/nri3070. Number: 11 Publisher: Nature Publishing Group.

R. Singhvi, A. Kumar, G. P. Lopez, G. N. Stephanopoulos, D. I. Wang, G. M. Whitesides, and D. E. Ingber. Engineering cell shape and function. *Science*, 264(5159):696–698, April 1994. ISSN 0036-8075, 1095-9203. doi:10.1126/science.8171320. URL https://science-sciencemag-org.proxy.uchicago.edu/content/264/5159/696. Publisher: American Association for the Advancement of Science Section: Reports.

Minjun Son, Andrew G. Wang, Hsiung-Lin Tu, Marie Oliver Metzig, Parthiv Patel, Kabir Husain, Jing Lin, Arvind Murugan, Alexander Hoffmann, and Savaş Tay. NF-κB responds to absolute differences in cytokine concentrations. *Science Signaling*, 14(666):eaaz4382, January 2021. doi:10.1126/scisignal.aaz4382. URL https://www.science.org/doi/10.1126/scisignal.aaz4382. Publisher: American Association for the Advancement of Science.

Beáta Sperlágh, György Haskó, Zoltán Németh, and E. Sylvester Vizi. ATP released by LPS increases nitric oxideproduction in raw 264.7 macrophage cell line viaP2Z, P2X7 receptorsfn1fn1Due to circumstancesbeyond the Publishers control, this article appears withoutthe authors corrections. *Neurochemistry International*, 33(3):209–215, September 1998. ISSN 0197-0186. doi:10.1016/S0197-0186(98)00025-4. URL http://www.sciencedirect.com/science/article/pii/S0197018698000254.

Philipp Stiefel, Florian I. Schmidt, Pablo Dörig, Pascal Behr, Tomaso Zambelli, Julia A. Vorholt, and Jason Mercer. Cooperative Vaccinia Infection Demonstrated at the Single-Cell Level Using FluidFM. *Nano Lett.*, 12(8):4219–4227, August 2012. ISSN 1530-6984. doi:10.1021/nl3018109. URL https://doi.org/10.1021/nl3018109. Publisher: American Chemical Society.

Lalisa Stutts and Aaron P. Esser-Kahn. A Light-Controlled TLR4 Agonist and Selectable Activation of Cell Subpopulations. *Chembiochem*, 16(12):1744–1748, August 2015. ISSN 1439-7633. doi:10.1002/cbic.201500164.

Myong-Hee Sung, Ning Li, Qizong Lao, Rachel A. Gottschalk, Gordon L. Hager, and Iain D. C. Fraser. Switching of the Relative Dominance Between Feedback Mechanisms in Lipopolysaccharide-Induced NF-κB Signaling. *Sci. Signal.*, 7(308):ra6–ra6, January 2014. ISSN 1945-0877, 1937-9145. doi:10.1126/scisignal.2004764. URL https://stke-science-mag-org.proxy.uchicago.edu/content/7/308/ra6. Publisher: American Association for the Advancement of Science Section: Research Article.

Csaba Szabó, Gwen S Scott, László Virág, Greg Egnaczyk, Andrew L Salzman, Thomas P Shanley, and György Haskó. Suppression of macrophage inflammatory protein (MIP)-1α production and collagen-induced arthritis by adenosine receptor agonists. *British Journal of Pharmacology*, 125(2):379–387, 1998. ISSN 1476-5381. doi:10.1038/sj.bjp.0702040. URL http://onlinelibrary.wiley.com/doi/abs/10.1038/sj.bjp.0702040. _eprint: https://bpspubs.onlinelibrary.wiley.com/doi/pdf/10.1038/sj.bjp.0702040.

Savaş Tay, Jacob J. Hughey, Timothy K. Lee, Tomasz Lipniacki, Stephen R. Quake, and Markus W. Covert. Single-cell NF-κB dynamics reveal digital activation and analog information processing in cells. *Nature*, 466(7303):267–271, July 2010. ISSN 0028-0836. doi:10.1038/nature09145. URL https://www.ncbi.nlm.nih.gov/pmc/articles/PMC3105528/.

RStudio Team. RStudio: Integrated Development for R. 2020. Place: Boston, MA.

Kevin Thurley, Daniel Gerecht, Elfriede Friedmann, and Thomas Höfer. Three-Dimensional Gradients of Cytokine Signaling between T Cells. *PLOS Computational Biology*, 11(4): e1004206, April 2015. ISSN 1553-7358. doi:10.1371/journal.pcbi.1004206. URL https://journals.plos.org/ploscompbiol/article?id=10.1371/journal.pcbi.1004206. Publisher: Public Library of Science.

Stefan Uderhardt, Andrew J. Martins, John S. Tsang, Tim Lämmermann, and Ronald N. Germain. Resident Macrophages Cloak Tissue Microlesions to Prevent Neutrophil-Driven Inflammatory Damage. *Cell*, 177(3):541–555.e17, April 2019. ISSN 0092-8674, 1097-4172. doi:10.1016/j.cell.2019.02.028. URL https://www.cell.com/cell/abstract/S0092-8674(19)30211-9. Publisher: Elsevier.

Manojlovic V., Djonlagic J., Obradovic B., Nedovic V., and Bugarski B. Immobilization of cells by electrostatic droplet generation: a model system for potential application in medicine. *Int J Nanomedicine*, 2006. doi:10.2147/nano.2006.1.2.163.

Alexis Vandenbon, Shunsuke Teraguchi, Shizuo Akira, Kiyoshi Takeda, and Daron M. Standley. Systems biology approaches to toll-like receptor signaling. *WIREs Systems Biology and Medicine*, 4(5):497–507, 2012. ISSN 1939-005X. doi:10.1002/wsbm.1178. URL https://onlinelibrary.wiley.com/doi/abs/10.1002/wsbm.1178. _eprint: https://onlinelibrary.wiley.com/doi/pdf/10.1002/wsbm.1178.

Francesco Di Virgilio, Davide Ferrari, Marco Idzko, Elisabeth Panther, Johannes Norgauer, Andrea la Sala, and Giampiero Girolomoni. Extracellular ATP, P2 receptors, and inflammation. *Drug Development Research*, 59(1):171–174, 2003. ISSN 1098-2299. doi:10.1002/ddr.10191. URL http://onlinelibrary.wiley.com/doi/abs/10.1002/ddr.10191. _eprint: https://onlinelibrary.wiley.com/doi/pdf/10.1002/ddr.10191.

Sean Wallis. Binomial Confidence Intervals and Contingency Tests: Mathematical Fundamentals and the Evaluation of Alternative Methods. *Journal of Quantitative Linguistics*, 20(3):178–208, August 2013. ISSN 0929-6174, 1744-5035. doi:10.1080/09296174.2013.799918. URL http://www.tandfonline.com/doi/abs/10.1080/09296174.2013.799918.

Qing Wang, Xiaojie Jiao, Chang Liu, Song He, Liancheng Zhao, and Xianshun Zeng. A rhodamine-based fast and selective fluorescent probe for monitoring exogenous and endogenous nitric oxide in live cells. *J. Mater. Chem. B*, 6(24):4096–4103, June 2018. ISSN 2050-7518. doi:10.1039/C8TB00646F. URL http://pubs.rsc.org/en/content/articlelanding/2018/tb/c8tb00646f. Publisher: The Royal Society of Chemistry.

Hemamali J. Warshakoon, Jennifer D. Hood, Matthew R. Kimbrell, Subbalakshmi Malladi, Wen Yan Wu, Nikunj Shukla, Geetanjali Agnihotri, Diptesh Sil, and Sunil A. David. Potential adjuvantic properties of innate immune stimuli. *Human Vaccines*, 5(6):381–394, June 2009. ISSN 1554-8600. doi:10.4161/hv.5.6.8175. URL https://doi.org/10.4161/hv.5.6.8175. Publisher: Taylor & Francis _eprint: https://doi.org/10.4161/hv.5.6.8175.

Kristin Westphalen, Galina A. Gusarova, Mohammad N. Islam, Manikandan Subramanian, Taylor S. Cohen, Alice S. Prince, and Jahar Bhattacharya. Sessile alveolar macrophages communicate with alveolar epithelium to modulate immunity. *Nature*, 506(7489):503–506, February 2014. ISSN 1476-4687. doi:10.1038/nature12902. URL https://www.nature.com/articles/nature12902. Number: 7489 Publisher: Nature Publishing Group.

G. M. Whitesides, E. Ostuni, S. Takayama, X. Jiang, and D. E. Ingber. Soft lithography in biology and biochemistry. *Annu Rev Biomed Eng*, 3:335–373, 2001. ISSN 1523-9829. doi:10.1146/annurev.bioeng.3.1.335.

Hadley et. al. Wickham. Welcome to the tidyverse. *Journal of Open Source Software*, 4: 1686, 2019.

Dylan Wright, Bimalraj Rajalingam, Selvapraba Selvarasah, Mehmet R. Dokmeci, and Ali Khademhosseini. Generation of static and dynamic patterned co-cultures using microfabricated parylene-C stencils. *Lab Chip*, 7(10):1272–1279, September 2007. ISSN 1473-0189. doi:10.1039/B706081E. URL http://pubs.rsc.org/en/content/articlelanding/2007/lc/b706081e. Publisher: The Royal Society of Chemistry.

Qiong Xue, Yao Lu, Markus R. Eisele, Endah S. Sulistijo, Nafeesa Khan, Rong Fan, and Kathryn Miller-Jensen. Analysis of single-cell cytokine secretion reveals a role for paracrine signaling in coordinating macrophage responses to TLR4 stimulation. *Sci. Signal.*, 8(381): ra59–ra59, June 2015. ISSN 1945-0877, 1937-9145. doi:10.1126/scisignal.aaa2155. URL http://stke.sciencemag.org/content/8/381/ra59. Publisher: American Association for the Advancement of Science Section: Research Article.

Pernille Yde, Benedicte Mengel, Mogens H. Jensen, Sandeep Krishna, and Ala Trusina. Modeling the NF-$\varkappa$B mediated inflammatory response predicts cytokine waves in tissue. *BMC Systems Biology*, 5(1):115, July 2011. ISSN 1752-0509. doi:10.1186/1752-0509-5-115. URL https://doi.org/10.1186/1752-0509-5-115.

Tohru Yonekawa and Andrew Thorburn. Autophagy and Cell Death. *Essays Biochem*, 55: 105–117, 2013. ISSN 0071-1365. doi:10.1042/bse0550105. URL https://www.ncbi.nlm.nih.gov/pmc/articles/PMC3894632/.

Hyun Youk and Wendell A. Lim. Secreting and Sensing the Same Molecule Allows Cells to Achieve Versatile Social Behaviors. *Science*, 343(6171):1242782, February 2014. doi:10.1126/science.1242782. URL https://www.science.org/doi/10.1126/science.1242782. Publisher: American Association for the Advancement of Science.

Daniel E. Zak, Vincent C. Tam, and Alan Aderem. Systems-Level Analysis of Innate Immunity. *Annual Review of Immunology*, 32(1):547–577, 2014. doi:10.1146/annurev-immunol-032713-120254. URL https://doi.org/10.1146/annurev-immunol-032713-120254. _eprint: https://doi.org/10.1146/annurev-immunol-032713-120254.

Ce Zhang, Hsiung-Lin Tu, Gengjie Jia, Tanzila Mukhtar, Verdon Taylor, Andrey Rzhetsky, and Savaş Tay. Ultra-multiplexed analysis of single-cell dynamics reveals

logic rules in differentiation. *Sci Adv*, 5(4):eaav7959, April 2019. ISSN 2375-2548. doi:10.1126/sciadv.aav7959. URL https://www.ncbi.nlm.nih.gov/pmc/articles/PMC6447378/.

Chaolei Zhang, Chao Wang, Shan Zhao, and Zhilong Xiu. Role of c-di-gmp in improving stress resistance of alginate-chitosan microencapsulated bacillus subtilis cells in simulated digestive fluids. *Biotechnology Letters*, 2021. doi:10.1007/s10529-020-03055-0.

Qiuhong Zhang, Sanjana Gupta, David L. Schipper, Gabriel J. Kowalczyk, Allison E. Mancini, James R. Faeder, and Robin E. C. Lee. NF-κB Dynamics Discriminate between TNF Doses in Single Cells. *cels*, 5(6):638–645.e5, December 2017. ISSN 2405-4712. doi:10.1016/j.cels.2017.10.011. URL https://www.cell.com/cell-systems/abstract/S2405-4712(17)30448-9. Publisher: Elsevier.

Zhikuan Zhang, Umeharu Ohto, Takuma Shibata, Masato Taoka, Yoshio Yamauchi, Ryota Sato, Nikunj M. Shukla, Sunil A. David, Toshiaki Isobe, Kensuke Miyake, and Toshiyuki Shimizu. Structural Analyses of Toll-like Receptor 7 Reveal Detailed RNA Sequence Specificity and Recognition Mechanism of Agonistic Ligands. *Cell Reports*, 25(12):3371–3381.e5, December 2018. ISSN 2211-1247. doi:10.1016/j.celrep.2018.11.081. URL https://www.cell.com/cell-reports/abstract/S2211-1247(18)31872-2. Publisher: Elsevier.

Xu Zhou, Ruth A. Franklin, Miri Adler, Jeremy B. Jacox, Will Bailis, Justin A. Shyer, Richard A. Flavell, Avi Mayo, Uri Alon, and Ruslan Medzhitov. Circuit design features of a stable two-cell system. *Cell*, 172(4):744–757.e17, 2018. ISSN 0092-8674. doi:https://doi.org/10.1016/j.cell.2018.01.015. URL https://www.sciencedirect.com/science/article/pii/S0092867418300527.